CIVIL ENGINEERING STUDIES
Hydraulic Engineering Series No 105

ISSN: 0442-1744

Kalamazoo River In Situ Flume Bed Erosion Study

David M. Waterman[1]
Dimitrios Fytanidis[1]
Marcelo H. García[2]

[1]Graduate Research Assistant
[2]Professor and Director, Ven Te Chow Hydrosystems Laboratory

Ven Te Chow Hydrosystems Laboratory
Dept. of Civil and Envir. Engineering
University of Illinois
Urbana, Illinois

August 2015

Kalamazoo River In Situ Flume Bed Erosion Study

David M. Waterman[1]
Dimitrios Fytanidis[1]
Marcelo H. García[2]

[1]Graduate Research Assistant
[2]Professor and Director, Ven Te Chow Hydrosystems Laboratory

August 2015

EXECUTIVE SUMMARY

Field-based *in situ* flume experiments on the erodibility of Kalamazoo River riverbed sediments were performed from November 16-21, 2013 using a flume designed and fabricated by staff at the Ven Te Chow Hydrosystems Laboratory (VTCHL) at the University of Illinois in Urbana-Champaign. The goal of the field experiments was to quantify parameters utilized in cohesive sediment transport models; hydrodynamics and sediment transport models are being developed for the portion of the Kalamazoo River affected by the July 2010 Enbridge Line 6B pipeline release of diluted bitumen (dilbit). The areas of particular concern for the study were depositional portions of the river system with cohesive sediment that were known to have accumulated submerged oil.

Critical bed shear stresses (τ_c) were quantified and erosion rates (E) were determined as a function of the applied bed shear stress (τ_b). Erosion rates were ascertained by calculating sediment mass flux using the recorded time series of turbidity and flume discharge rates (Q_{flume}). The bed shear stresses in the erosion section of the flume were determined for the full range of Q_{flume} values using computational fluid dynamics (CFD) modeling.

The field experiments at five locations along the Kalamazoo River revealed that typical values of the critical bed shear stress (τ_c) were between 0.10 and 0.15 Pa. For fitting data to the erosion equation, the determination was made to only use those data points at each sample station where the cumulative sediment volume eroded (V_{er}) during a test was less than 1000 cm^3; points obtained when V_{er} > 1000 cm^3 were deemed to contain unacceptable error in the estimate of τ_b due to modified hydrodynamics in the erosion region of the flume relative to the initial bed modeled. The portions of the tests that satisfied the V_{er} criteria were associated with bed shear stresses less than 0.67 Pa. For such bed shear stresses, the maximum erosion rates (E) were found to be less than or equal to 5.8 x 10^{-6} m/s at each sample site for all data points that satisfied the V_{er} criteria. Applying the fitted erosion rate functions at each site to a common value of τ_b = 0.4 Pa yields values for E between 8.9 x 10^{-7} and 7.9 x 10^{-6} m/s. The erosion rate functions obtained from the current study should not be extended to τ_b values beyond the range quantified in the experiments. Variability in erosional behavior was discernable between closely-spaced sample stations.

Table of Contents

Chapter 1: INTRODUCTION

The July 2010 spill of crude bitumen diluted with natural gas condensate (dilbit) into Talmadge Creek and associated wetlands, a tributary of the Kalamazoo River, was the largest release of heavy crude oil into a freshwater inland waterbody in North American history. The release, reported to be 843,000 gallons by Enbridge Energy, occurred during a product change from Western Canadian Select to Cold Lake Blend while the Kalamazoo River was experiencing a flood with a 4 percent annual exceedance probability based on statistical analysis of the annual series of peak flows (Hoard et al., 2010). During transport the lighter diluent volatilized and a portion of the oil submerged beneath the water surface, presumably by adhering to sediment and organic matter. The submerged oil was subject to further transport, along with the remaining surface oil, until eventually settling into quiescent areas of the Kalamazoo River. An approximately 38-mile long reach of the Kalamazoo River between Marshall and Kalamazoo, MI was affected by the spill. One of the needs of the U.S. Environmental Protection Agency is to understand the fate and transport of submerged oil and oiled sediment and the river flow conditions under which the submerged oil and oiled sediment becomes resuspended, transported and re-deposited.

As part of a larger team of scientists studying the fate and transport of submerged oil and oiled sediment in freshwater riverine systems, the Ven Te Chow Hydrosystems Laboratory (VTCHL) at the University of Illinois at Urbana-Champaign (UIUC) is assisting in the development of sediment transport algorithms, performing laboratory and field experiments on oil-particle mixtures, and performing 2D- and 3D-numerical modeling of sub-reaches of the system to aid in the ongoing site operations. The study described in this document was implemented to help quantify the physical process of oiled sediment resuspension.

General formulations characterizing the critical bed shear stress (the minimum bed shear stress that results in particle mobilization) and sediment transport rates of coarse-grained non-cohesive sediment are available because the relevant forces that drive and resist sediment motion are reasonably well understood. Fine-grained sediments where inter-granular cohesive forces are the dominant factor dictating sediment motion are much less amenable to published generalized formulations based on index properties of the bulk sediment. This is due to unique site-specific (hydrodynamics, water chemistry, etc.) and history-specific (sediment deposition and consolidation) characteristics that alter the inter-granular cohesive forces. The use of site-specific empirical data is still heavily relied upon when erosive behavior of cohesive sediments needs to be ascertained.

The U.S. Army Corps of Engineers, a co-collaborator on the project, performed an onsite bed erosion study (Perkey et al., 2014) with the same objectives as the current study; specifically, to identify erosion parameters that can be implemented in a numerical hydrodynamic and sediment transport model to represent erosional characteristics of oiled sediment in depositional areas of the Kalamazoo River. The parameters that are most commonly quantified are the critical bed shear stress (τ_c), along with a coefficient of proportionality and an exponent that fit an equation that quantifies the erosion rate as a function of the applied bed shear stress (τ_b). The U.S. Army Corps of Engineers study used the Sedflume (McNeil et al., 1996), an apparatus that has been extensively used for this type of analysis. Testing with the Sedflume requires the collection of sediment cores, which are then transported to a mobile laboratory facility where the testing takes place by extruding the sediment from the core into the bottom of a flume containing flowing water whose hydrodynamic properties are closely controlled. Such analysis has the benefit of well-regulated hydrodynamics and the ability to quantify changing erosional behavior with depth; the latter factor is particularly important in riverine depostional environments that often have complex stratigraphy where each strata of the sediment may have considerably different properties.

An *in situ* flume such as the type developed for the current study operates by lowering a device to the bed or banks of the river and eroding sediment in place. Such systems have been implemented by Young (1977), Grissinger et al. (1981), Gust and Morris (1989), and Ravens and Gschwend (1999), among others, and in various environmental settings. An *in situ* flume has the advantages of involving less antecedent disturbance of the sediment being tested, as a core does not have to be extracted; it also can characterize a larger footprint of the bed, rather than being limited to the diameter of a sediment core. However, after τ_c is exceeded, the hydrodynamics inside the erosion chamber are less well-controlled, because the flow field is altered as the bed geometry changes during erosion; and a method does not currently exist to obtain meaningful information regarding variable erosion properties with depth. Due to the relative advantages and disadvantages of both the Sedflume and an *in situ* flume, the two methods provide complementary but different data, both types of which are useful for bounding the parameters of numerical models.

Chapter 2: METHODOLOGY

2.1 Field Experiments: Apparatus and Measuring Procedures

The *in situ* flume developed for this study operates by pumping water through a straight flume chamber, a portion of which is open at the bottom, thus subjecting the bed to erosive forces. Turbid water is sampled from the pipe downstream of the flume chamber to quantify the amount of bed material eroded. A schematic of the field setup is illustrated in Figure 1; photographs are shown in Figures 2 through 6.

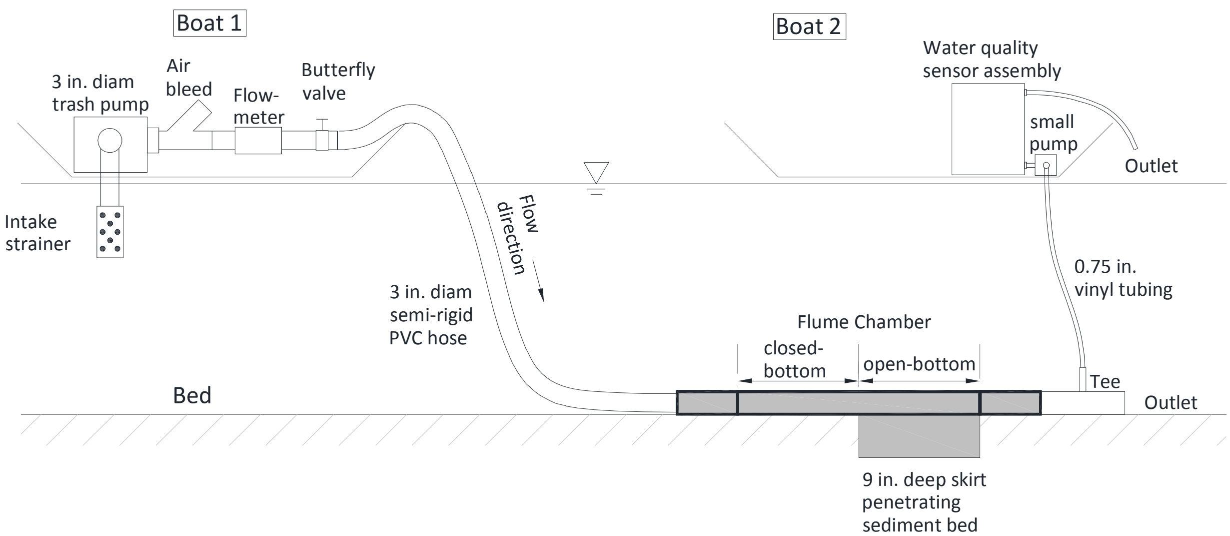

Figure 1: General schematic of *in situ* flume setup; profile view

Figure 2: The upstream Boat 1 consisting of the trash pump, air bleed assembly, flow-meter, and butterfly valve. Nicholas Moller of UIUC is standing in the foreground; Kalamazoo River, November 2013.

Figure 3: The flume chamber used in the Kalamazoo River experiments, November 2013. The sheet-metal skirt bounding the open-bottomed erosion segment is on the left, such that flow in this configuration would be from right to left; (note that the closed-bottom right side is supported in the photo by a concrete block).

Figure 4: A top view of the chamber while seated on the river bed in a shallow area, Kalamazoo River near Morrow Lake, November 2013. Two 35-lb free weights (or concrete blocks) were lowered onto the flume chamber to stabilize it on the bed.

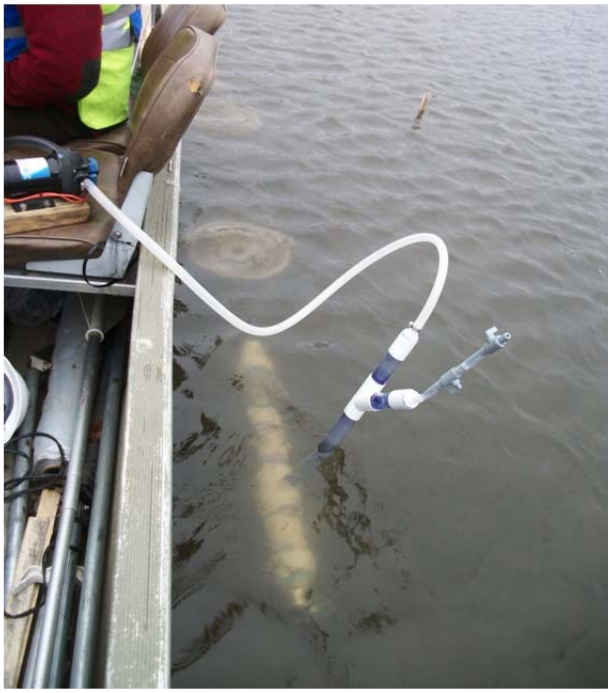

Figure 5: A view of the downstream end of the setup used in the Kalamazoo River, November 2013. The small pump on Boat 2 (left side of photo) draws water continuously from the sampling port. From the pump, the water is passed through the water quality sensor apparatus, which is shown on the following photo. The photo was provided by Rex Johnson (GRT/START).

Figure 6: The water quality sensor system provided by Paul Reneau of the USGS Wisconsin Water Science Center. Flow into the box passes in series through a YSI 6920 flow-through chamber and a Turner C6 flow-through chamber. Data is stored with a CR1000 data logger. At the outlet, the water can either be collected in a sample bottle or discharged back to the river.

The field equipment utilized in the study included the following: (2) 20-ft johnboats with jet motors and speed rail fittings for galvanized metal spuds to anchor the boats; 3-in. diameter Northstar trash pump with Honda GX240 engine (7.9 HP) rated at 352 gal/min at 88 ft total head; (2) 25-ft lengths of semi-rigid PVC suction hose with cam-lock fittings; metal strainer for intake; air-bleed assembly (wye with the angled arm reduced to 0.5-in. diameter ball valve and hose barb); 3-in. diameter McCrometer Ultra Mag flow-meter; 3-in. diameter butterfly valve; *in situ* flume chamber with cam-lock hose fittings; flume brackets with vertical extensions constructed of PVC-pipe to control and push down flume in deeper water; 3-in. x 1-in. tee for sampling port; Jabsco Par-max 4.0 pump; Turner C6 multiprobe assembly with turbidity, fluorometric dissolved organic-matter (FDOM), and crude-oil sensors within a Turner flow-through chamber; YSI 6920 multiprobe assembly with turbidity probe, conductivity / temperature probe, pH probe, and optical dissolved oxygen probe within a flow-through chamber; Campbell Scientific CR1000 data logger; laptop computer for visualizing water quality data; (3) 12V marine-cycle batteries; (2) 400W inverters; (4) concrete blocks; (2) 35-lb. free weight plates; 0.5L HDPE amber sample bottles; 1L glass amber sample bottles; 0.5L wide-mouth glass sample bottles; Wildco hand-push sediment core sampler with 20-in. long by 1.88-in. inside diameter clear plastic sleeves and extension handle; metal pan for sediment investigation; 6-ft. folding ruler for measuring water depth and scour hole topography; Trimble Pro XRS GPS used in real-time differential correction mode.

Due to the importance of the hydrodynamics within the flume chamber, greater detail is provided regarding the geometry and construction of the flume chamber. The inlet of the flume contains a short length of 3-in. diameter SCH 40 PVC pipe with a cam-lock fitting to allow quick connection to the semi-rigid PVC hose. The inlet end of the fiberglass flume chamber was formed around a 3-in. diameter socket x socket SCH 40 PVC coupling that transitions directly to the fiberglass flume shell. The flume chamber consists of a shell of fiberglass (two sides and the top) with a PVC bottom (except in the open-bottomed erosion segment).The fiberglass shell was constructed with an outward-facing bottom flange to allow connection to the bottom PVC piece using silicone caulk and threaded fasteners. Surface imperfections on the interior surface of the fiberglass were treated with Bondo filler to prevent seepage into the fiberglass structure; this yielded a rougher surface than iron or PVC pipe. The outer surface of the fiberglass shell was painted with Duratec polyester surface primer to provide greater durability.

The flume chamber consists of 4 separate flow segments: (a) a flow expansion segment; (b) a flow development segment; (c) an erosion segment; and (d) a flow contraction segment. Beginning at the joint with the 3-in. diameter PVC coupling, the entire flume chamber has a rectangular cross-section with constant 3.875-in. depth but variable width. The flow expansion segment is 12.125-in. long; it expands uniformly in width from 3.375 in. to 11.25 in.; the PVC bottom is covered with an adhesive-backed sandpaper (500 µm) to enhance the bed roughness. The flow development section is 24.0-in.

long; it has constant 11.25-in. width; the PVC bottom here is also covered with 500 µm sandpaper. The erosion segment is 24.0-in. long with constant 11.25-in. width; the bottom is open; the four sides of the erosion segment's bottom opening are bounded with 1.5-inch by 1.5-inch aluminum angles connected to the flange (sides) or the PVC bottom (upstream and downstream ends). The flange connects to a vertically-aligned sheet metal penetrating skirt that bounds the four sides of the erosion segment's bottom opening; the penetrating skirt originally extended 6-in. deep, but was retrofitted to 9-in. deep after the Site 2 test to allow more extensive erosion and higher pressures in the chamber before failure. The flow contraction segment is 12.125-inches long; it contracts uniformly in width from 11.25 in. to 3.375 in. The end of the contraction segment was formed around a PVC coupling identical to the inlet end of the flume. A schematic of the chamber geometry is shown in Figure 7.

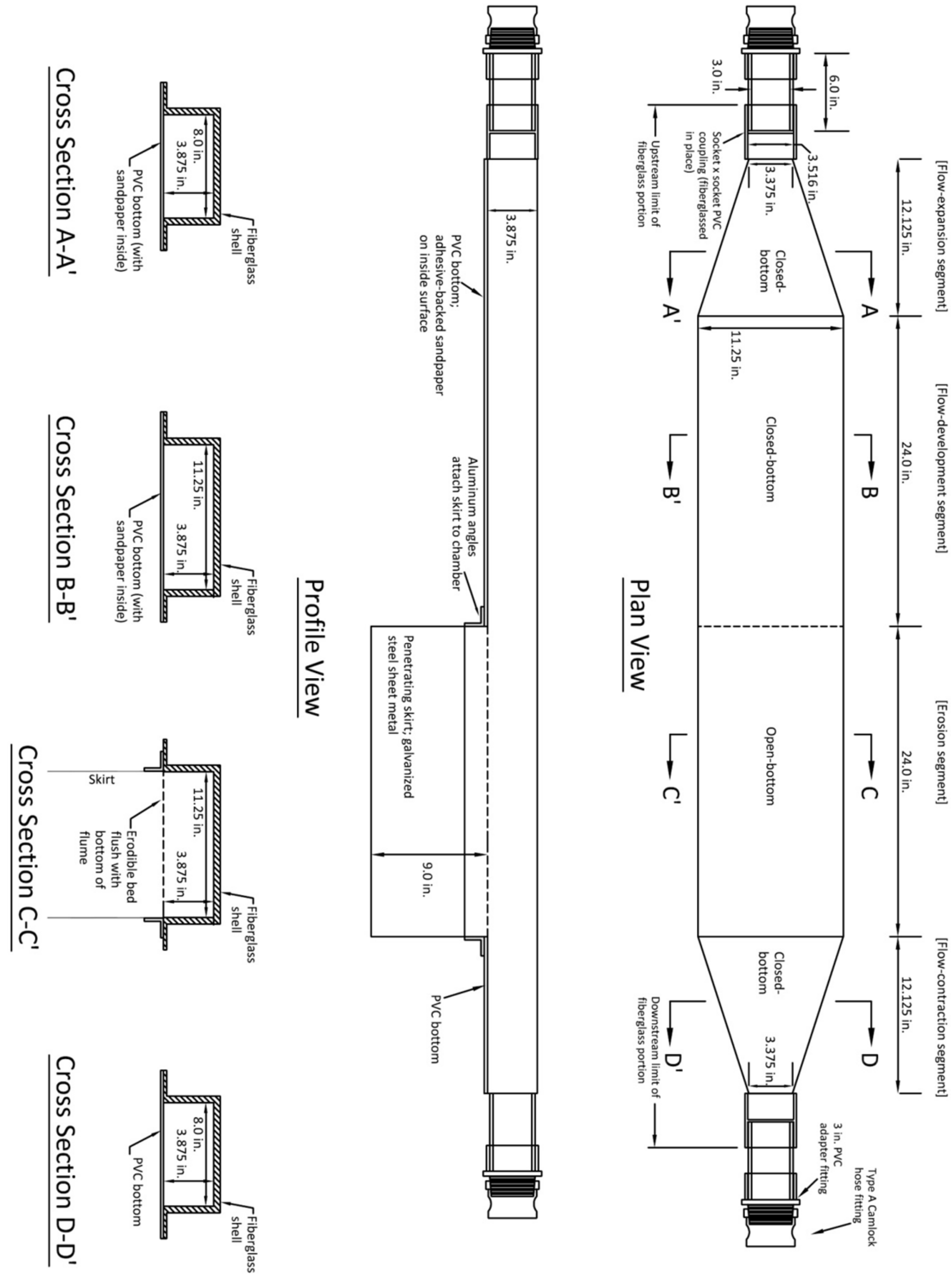

Figure 7: Schematic of the *in situ* flume chamber.

The four segments of the flume chamber have specific design objectives and involve a number of performance trade-offs. The ultimate goal is to have a fully developed, uniform flow (i.e, with the cross-sectional velocity distribution not changing in the longitudinal direction) that causes the bed to erode uniformly both in the transverse and longitudinal directions within the erosion segment. Such a condition is difficult to achieve when the conduit undergoes an abrupt geometric change such as from a small diameter circular cross-section to a wider rectangular cross section. The following list includes items (A), (B), and (C) that describes design objectives and trade-offs associated with the identified segments of the flume. In (A), the need for a cross-sectional geometry transition is described; in (B), the design objectives for the flow-expansion segment and flow development section are described; and in (C) the design objectives for the flow-contraction segment are described.

(A) The current design is a positive pressure system in which the flow is provided from the discharge end of the pump; a pressure gradient forces the flow through the chamber such that pressures are higher within the flume than hydrostatic pressures at the bed outside the flume. The alternative is a negative pressure system in which the flow is drawn through the flume from the suction end of the pump (e.g., Ravens and Gschwend, 1999) yielding lower pressure in the flume than the hydrostatic pressure at the bed outside the flume. A suction-flow system can largely eliminate the need for a rapid geometry transition, as the inlet side of the flume can be an open conduit with the same cross-sectional geometry as the flume chamber. A draw-back of such a system is that turbulence is created as flow accelerates into the inlet which can cause erosion in the river-bed that is drawn into the flume; it is not possible to discern which material eroded from the bed at the flume inlet and which material eroded from the erosion segment of the flume. Another draw-back is that with lower pressure within the flume chamber than the hydrostatic pressure outside the flume, groundwater pressure gradients can cause removal of bed material due to seepage forces that may be difficult to discern from erosion due to fluid shear stress. The positive pressure system also has the potential for such bed material loss in the opposite direction, but the resulting blow-out does not yield turbidity in the flume that can be confused for erosion; (it is observed as turbidity surfacing in the water column outside the flume). The choice of a positive-pressure system necessitates a geometric transition from the small diameter conduit dictated by the pump outlet to the larger cross-section desired for the erosion segment. The objective of a larger cross-section for the erosion segment is that side-wall effects are minimized and progressive erosion has less effect on chamber hydrodynamics when the original cross-sectional area is large relative to the added flow cross-sectional area caused by erosion.

(B) The flow-expansion segment is designed to more smoothly transition the velocity distribution between different cross-sectional geometries. Ideally the expansion segment would be sufficiently long and gradual to allow the flow to expand without separation from the wall, and such that the velocity distribution at the end of the expansion is very similar to the fully-developed velocity distribution to be obtained in the erosion segment. However, such a design requires a much longer expansion segment than is practicable for the purpose of an *in situ* flume. The longer the closed-bottom portions of the flume, the more difficult it is to find a flat enough location on the bed to allow the flume to be properly seated. The objective of the flow development segment is similar, to allow the velocity distribution to evolve in the longitudinal direction, ideally to a uniform condition before reaching the downstream end. Typically flow development requires approximately ten pipe diameters (or 40 hydraulic radii, where the hydraulic radius is the cross-sectional area divided by the wetted perimeter) following even a minor change in geometry; for more drastic changes in geometry, the required distance is longer. Forty hydraulic radii for the given conduit geometry is approximately 4.8-ft long. A longer flow expansion segment and flow development segment would have yielded a flume configuration very difficult to seat on the bed. Reducing the length of these segments was a practical necessity.

(C) The short flow-contraction segment is also designed to minimize the influence of the transition on the hydraulics within the erosion segment of the flume. An abrupt transition would cause undesirable flow recirculation regions and greater complexity to the bed shear stress field in the erosion segment. To smoothly contract the flow generally requires considerably less length than to smoothly expand the flow. A transition from the erosion segment cross-section to a smaller cross-section is required to accelerate the flow and ensure a representative sample of the suspended sediment can be obtained downstream of the erosion segment.

Field measurements were conducted in the following manner. The boat containing the *in situ* flume chamber and the water quality measurement system was positioned parallel to the desired flume alignment, with one edge of the boat over the sample location. The boat was anchored using metal spuds. After transferring one end of the semi-rigid PVC discharge hose from the second boat containing the pump to the anchored boat, the boat with the pump moved into position such that it was aligned with the desired flume alignment and at a distance such that a small amount of slack was maintained in the semi-rigid PVC hose. The pump boat was then anchored with metal spuds. The intake hose and strainer on the suction end of the pump was mounted in place as far as possible from the river bed; the strainer was fixed by tying off to the side of the boat or onto a metal fence post, depending on water depth. The pump was turned on and water was discharged through the semi-rigid PVC hose to fill the hose with water and evacuate air pockets within the hose. The pump was then turned off to allow connection of the discharge hose to the inlet side of the flume. The water depth over the sampling position was measured with a folding ruler. The flume was held in place over the sampling position, the discharge hose was connected to the inlet side of the flume, the flume was submerged just below the water surface, and water was pumped through the flume to evacuate any air pockets. The pump was again turned off to allow the flume to be seated on the bed. The flume was gently lowered until the penetrating skirt came into contact with the river bed. The penetrating skirt was then firmly pushed into the bed until the flat bottom upstream and downstream of the erosion section rested securely on the bed to ensure a flush fit against the sediment surface within the erosion segment. The water depth over the top surface of the flume was measured to compare against the depth measured prior to flume placement to ensure the flume was seated flush with the bed. Once the field staff was satisfied with the flume seating, concrete blocks or 35-lb. free weights were gently lowered onto the top surface of the flume and set in place to ensure the flume remained seated during testing.

To initiate the testing process, the butterfly valve just downstream of the pump was closed to the nearly shut position, and water began to be pumped through the flume at a flow rate low enough that it was not able to be registered by the flow-meter; note that the minimum flow rate able to achieve a stable flow-meter reading was approximately 0.3 L/s. While flowing at the sub-0.3 L/s flow rate, the water quality system was engaged by turning on the small pump and pumping through the water quality assembly. Turbidity measurements were observed in real time on the laptop computer. After turbidity readings stabilized, an ambient water sample was collected from the outlet of the water quality sensor system. The flow rate was then adjusted to 0.3 L/s and several minutes were allowed to pass to observe any turbidity response. Flow rate continued to be increased incrementally, while allowing real-time data to be observed for sufficient time at each increment to allow any potential erosion event to be observed, typically 3 to 5 minutes. The flow adjustment increments were generally small prior to the first observed erosion event to ensure the critical shear stress level was bounded by a narrow discharge increment. An erosion event was evident as a response in the real-time turbidity readings; eroded material was also generally visible passing through the clear tubing and flow-through chambers of the water quality sensor assembly. Water samples were collected at the outlet of the water quality apparatus at the discretion of the field staff. Erosion events were typically observed as large, fairly rapid increases in the turbidity signal, followed by a slow exponential decline to a stable level. During the portion of the tests involving active erosion, the flow rate was maintained constant until the stable turbidity level had been achieved, typically on the order of 10 to 15 minutes. The flow rate was incrementally increased as in the preceding manner until the system ultimately failed when flow undercut the bottom of the penetrating skirt due to a combination of excessive erosion in the erosion segment and the large pressure gradient between the interior of the flume and the ambient water outside the flume. Failure was generally observed as a jet of turbid water emanating from the sides of the flume; failure was sometimes preceded by bubbles emerging from the bed around the flume and floating to the surface.

Upon completion of the test, the pump was turned off, and the corners of the erosion segment were demarcated by inserting wooden lathe into the bed, which was possible when water depth was less than 3 feet. Sediment samples were then collected from the bed directly adjacent to the erosion segment of the flume using the hand-core sampler, which is illustrated in Figure 8. One core was collected and kept intact within the plastic core liner for analyses of grain size distribution and dry bulk density. (Cores were kept in a vertical upright position during all stages of transport and storage.) A second core was collected and extruded into a 0.5-L wide-mouth glass jar for hydrocarbon chemical analysis. The flume was then gently lifted from the bed onto the boat, and the hosing was disconnected. If the bed was not excessively disturbed during the unseating process, water depth measurements were made within the erosion segment for comparison against the pre-test measurement. This provided a qualitative estimate for the depth of material eroded and ensured that erosion was occurring as anticipated within the erosion segment. The spatial coordinates of the test sites were located with sub-meter accuracy by differential GPS before any features used to demarcate the flume positions were removed.

Figure 8: A view of a sediment core being collected using the hand-held core sampler. The core is captured within a plastic liner inside the steel core barrel. Zhenduo Zhu of UIUC is holding the handle of the core sampler and Rex Johnson of GRT/START is handling the core barrel. USEPA photo by Jacob Hassan.

2.2 Laboratory Methods and Procedures

The water samples in the amber HDPE bottles were collected to obtain suspended sediment concentration (SSC); this allows correlation between the field-measured turbidity measurements and SSC. The SSC analysis was performed at the USGS Illinois Water Science Center Laboratory. The samples were evaluated in accordance with ASTM method D3977-97, Test Method B (Filtration). This involves weighing the water-sediment mixture prior to filtration, and then passing the entire contents of the sample through a glass-fiber filter disc (1.5-μm openings) under vacuum; the sediment-laden filter is dried at 105°C and weighed to obtain the dry mass of sediment. Following the determination of SSC per the above procedure, the sediment-laden filter discs were subsequently placed in a muffle furnace at 550°C for 30 minutes per Method 2540 E of the American Water Works Association to volatilize the organic content of the samples; the samples were then weighed as above, with the difference indicating the organic portion of the sample. Equipment used included the following: Whatman 934-AH glass fiber filter discs (24-mm diameter); Coorstek 60051 Gooch crucibles; ELE International Soiltest Product Division stove; Neytech 85M muffle furnace; (2) 1L HDPE Erlenmeyer flasks with vacuum hose fittings and rubber stopper top to fit the crucibles; Welch model 2545B-01 vacuum pump; Nalgene desiccator chamber; Sartorius Research R200D scale.

The cores were analyzed for dry bulk density and grain size distribution at the Ven Te Chow Hydrosystems Laboratory. Results are shown in Appendix A. Procedures for the analyses were as follows. Water was decanted from the top of each core using a 25-mL transfer pipette with bulb. The depth from the sediment surface to the bottom of the core was measured with a ruler. The core was placed on a metal baking sheet and cut open in the longitudinal direction with a utility knife on opposite sides of the core; duct tape was used to secure the side of the core cut first to allow the core to be laid open. Photographs of the core were taken; one side of the core was evaluated for stratification based on grain size, organic matter, and other physical properties based on visual investigation and texture analysis by feel using small subsamples. The depth of each identified layer was measured. Aluminum baking pans were weighed before adding sediment. Each sediment layer was scooped into a separate baking pan using a spoon. All residual sediment from the spoon, the knife used to cut the core, the core liner, the baking sheet, and hands were washed into a separate aluminum pan using a laboratory wash-bottle with distilled water. The aluminum pans were labeled and placed in a 60°C drying oven for at least 12 hours. Each pan was weighed after drying. The sediment sample was then disaggregated with a pestle and dry-sieved with a 500-μm sieve to remove the large organic matter that was common in the samples. A hygroscopic moisture analysis sample comprising approximately 10% of the sample was then removed and placed in a pre-weighed aluminum sample dish. The hygroscopic moisture sample was placed in the drying oven at 110°C for 24 hours. The dried hygroscopic moisture sample was then weighed to determine the hygroscopic moisture correction per ASTM method D422-63 to be applied to the original sample mass. The dry mass of each layer and the residual was calculated in this manner for the bulk density calculation. The dry bulk density of the sample is calculated as the total dry mass of all layers and residual from the core divided by the total volume of the core. The volume of the core required an estimation of the depth sampled within the 20-in. long core sleeve (sampler); a sediment sample depth of 19 inches was approximated unless specific conditions noted in the field warranted a different value to be used. An estimated error of ±5% in the dry bulk density calculation is associated with the depth approximation.

The remaining content of each aluminum pan containing the 60°C-dried and disaggregated sediment was added to a stainless steel mixing cup with 0.5 L of distilled water. The slurry was mixed for 1 minute with a Gilson SA-10 mixer with mixing blade as specified in ASTM method D422-63. A 1-mL pipette was inserted into the cup immediately after mixing to sample the entire vertical depth of the sample. The aliquot was transferred to a beaker, which was then diluted with distilled water sufficiently to allow the grain size distribution to be obtained with a LISST-ST. The procedure for using the LISST-ST for grain size distribution is described later in this section. The remainder of the slurry in the stainless steel mixing cup was wet-sieved with a 74-µm sieve to determine the grain size distribution of the sand fraction per ASTM method D6913-04. The portion retained on the 74-µm sieve was placed in a labeled aluminum pan and transferred to a 110°C oven for at least 12 hours. The dried sample was then disaggregated with a pestle. The sample was transferred to a sieve sequence of 300-µm, 149-µm, 125-µm, and 74-µm sieves, and shaken on a mechanical shaker for 10 minutes. The portion captured on each sieve was transferred to a pre-weighed container and then weighed. The dry sieve analysis was used for the grain-size distribution of the portion ≥ 74 µm in diameter.

The LISST-ST, manufactured by Sequoia Scientific, Inc. (Bellevue, Wash.), operates on the principle of laser diffraction to determine the particle size distribution of a dilute mixture of suspended sediments. Per the current firmware installed on the instrument, the LISST provides a size distribution in 32 log-spaced size classes with bin midpoints ranging from 1.4 µm to 231 µm. The procedures for evaluating samples with the LISST were as follows. Each day that samples were evaluated, the LISST was calibrated by running a background scatter test using distilled water. After evacuating the calibration sample, the dilute mixture of suspended sediment was mixed vigorously in its container using a stirring rod, and then poured into the LISST measuring chamber. The LISST-ST was programmed to record three grain-size distributions of 20 measurements each, with each 20-measurement average requiring 5 seconds. After completing the analysis, the sample was evacuated from the LISST. The first of the three recorded grain size distributions (associated with the first 5-second measurement window) was utilized; the second and third distributions were only utilized as a means of confirming the reasonableness of the first recorded distribution. In a mixed grain size distribution of fines (silt and clay) and sand, obtaining a representative sample of the sand fraction within the small sampling volume of the LISST laser beam is very challenging due to the tendency of the sand to settle in the mixing container while it is being transferred into the LISST chamber. Because of this issue, only the size classes less than 74 µm from the LISST were utilized for the grain size distributions; i.e., in a cumulative percent finer analysis, the 100 percent value was associated with the 74-µm size class. These values were then incorporated into the overall grain size distribution by multiplying the percent finer than 74 µm from the LISST analysis by the known total percent finer than 74 µm from the sieve analysis.

2.3 Computational Fluid Dynamics (CFD) modeling

The three dimensional flow was simulated using the Finite or Control Volume (FVM) approach and the computational algorithms provided by the commercial Computational Fluid Dynamics (CFD) solver ANSYS Fluent (ANSYS, 2014). The applied solver solved the non-hydrostatic 3D Reynolds Averaged Navier-Stokes (RANS) equations for the case of steady, turbulent, incompressible and isothermal flow (ANSYS, 2014). The hydrodynamics equations are outlined in Appendix B.

Initially, the computational domain was designed using the Computer Aided Design (CAD) program ANSYS DesignModeler (DM). To simulate the flume experiment conditions, straight 15-inch-long parts were added in the computational domain. To reduce the computational cost of the simulation, half the domain was simulated, taking advantage of the inherent geometrical and hydraulic symmetry of the chamber. The final examined domain is shown in Figure 9. The geometry was imported to the mesh generator ANSYS Meshing. A predominant hexahedral "Cut cell" Cartesian computational grid was created. For the surface grid a hybrid hex-mixed-element type of grid was created in order to conform to the complex geometry of the scoured geometry scenarios. Also, local mesh refinement was applied to capture accurately the likely small features caused by the scouring mechanism. Finally, a mesh independent study was carried out to check the effect of the grid size value on the results. A coarse (Δx=0.1-0.8 cm), a medium (Δx=0.025-0.4 cm) and a fine (Δx=0.01-0.32cm) resolution grid were examined, and the differences in the velocity distribution, the wall shear stress distribution and turbulent characteristics of the flow were evaluated. The differences between the fine and the medium grid were found to be relatively small and thus the fine grid was used for the present analysis. The fine resolution mesh chosen consists of 780,878 cells for the original flat-bed geometry. Additional complexity associated with the eroded bed surfaces utilized in the quasi-morphodynamic analysis described in Appendix C increased the mesh to approximately 1,000,000 cells. A view of the examined grid for the initial flat bed geometry is shown in Figure 10.

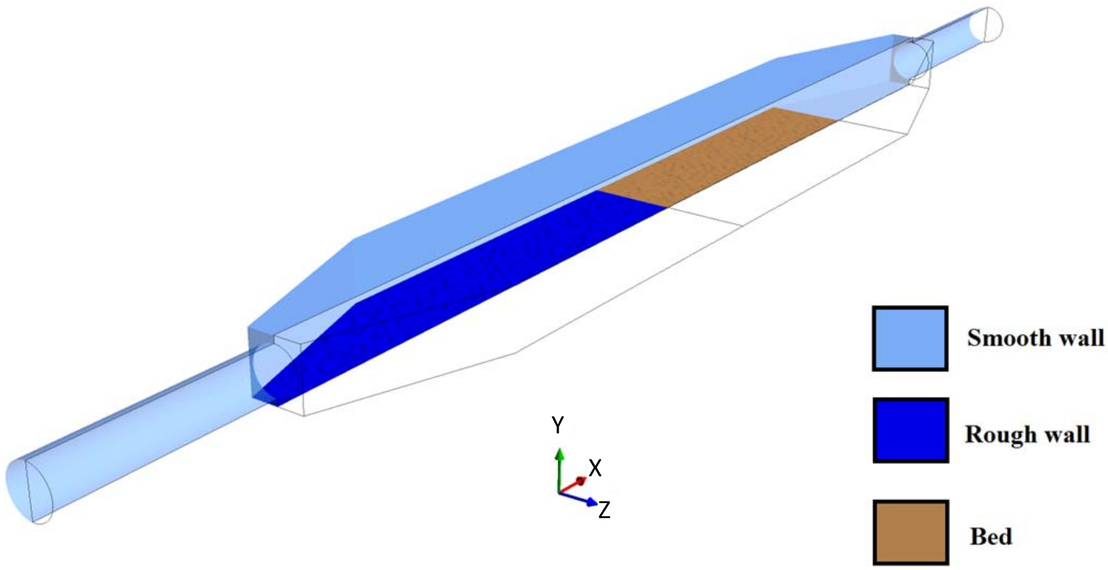

Figure 9: The computational domain of the examined flume chamber. The smooth wall roughness height (k_s) is 200 µm; the rough wall k_s is 500 µm; the bed k_s is 250 µm. Direction of flow is indicated by positive direction of X axis (toward upper right).

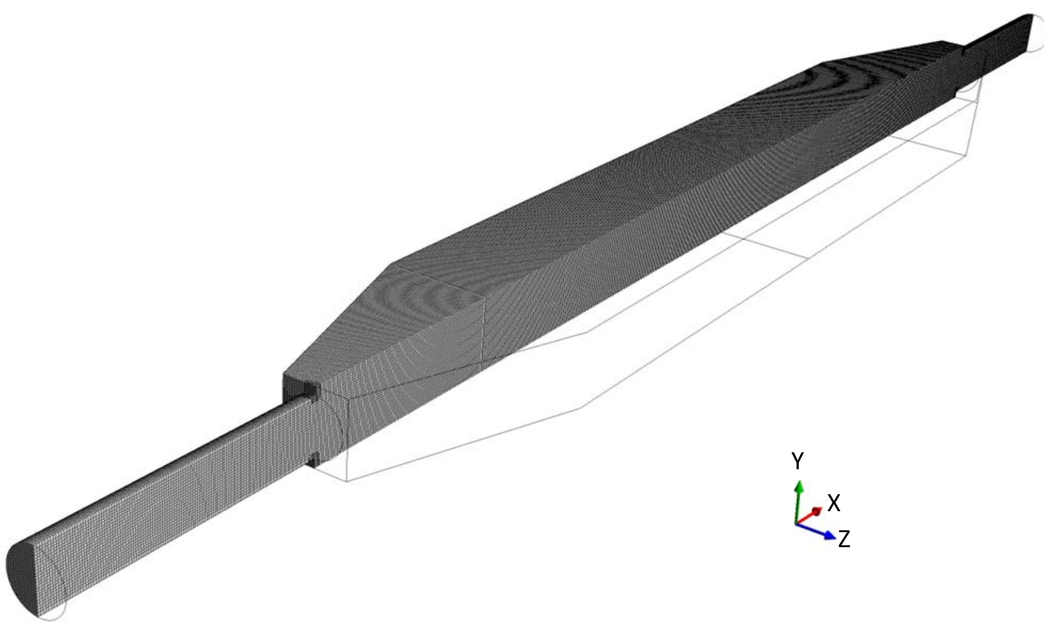

Figure 10: The computational grid for the initial condition of no bed erosion; the fine resolution grid size selected for modeling is shown (Δx=0.01-0.32 cm).

The roughness heights (k_s) for components of the computational domain were estimated as follows.

- The bed k_s was determined using the formulation of Engelund and Hansen (1967), developed for natural distributions of sand-bedded streams. In this formulation, $k_s = 2D_{65}$, where D_{65} is the grain diameter for which 65% of the mass of the sediment is finer. The value D_{65} = 125 µm is the average value of D_{65} from all the cores analyzed in Appendix A. This yields k_s = 250 µm.
- The rough wall k_s in the portion of the flume containing the sandpaper surface was established as the Nikuradse roughness height (i.e., the grain diameter of uniform sand grains); the grain size was estimated using a hand lens and grain-size template to yield an estimate of k_s = 500 µm.
- The smooth wall k_s was estimated through visual analysis of the inside of the fiberglass shell in comparison with standard values of roughness heights for typical pipe surfaces. Smooth finished fiberglass has a very small roughness height k_s = 5 µm; however, the surface imperfections and Bondo filler in the flume interior was considerably rougher than smooth fiberglass. The interior surface was visually estimated to have roughness between galvanized iron pipe (k_s = 150 µm) and concrete pipe (k_s = 300 µm); the estimate was k_s = 200 µm. Note that for the experimental flow Reynolds number (1000 to 60000) and the order of magnitude of relative roughness (.001), the friction factor is fairly insensitive to the roughness height.

The extracted computational grid was imported in the commercial multi-purpose solver ANSYS Fluent. For the turbulent flow hydrodynamics, the Reynolds Averaged Navier-Stokes (RANS) equations were solved combined with a standard k-ε turbulence model for the estimation of the Reynolds' stresses terms in the 3D RANS equations; note that k is the turbulent kinetic energy is ε is the dissipation rate of turbulent kinetic energy. Wall functions are used to solve the boundary shear stress. The solved set of equations is provided in Appendix B.

Chapter 3: APPROACH FOR FIELD DATA ANALYSIS

The goal of the experiments is to parameterize numerical sediment transport models developed for the Kalamazoo River. The critical bed shear stress and the erosion rate as a function of the bed shear stress are the most important aspects to quantify.

3.1 Critical Bed Shear Stress (τ_c) determination

The critical bed shear stress (τ_c) is the minimum bed shear stress (τ_b) that initiates discernible mobilization of bed material. During field experiments, as the flow rate pumped through the flume (Q_{flume}) is increased, a threshold is crossed whereby the previous Q_{flume} interval does not erode sediment and the subsequent Q_{flume} interval erodes sediment, as indicated by an increase in turbidity measurements above the ambient turbidity levels. The value of τ_c is bounded by the characteristic τ_b associated with these two experimental flow rates. However, identifying the characteristic τ_b associated with each flow rate is complicated by the fact that bed shear stresses in the flume are not measured directly.

The most common method to quantify bed shear stresses within the erosion segment of *in situ* devices has been to assume a uniform flow field and obtain a correlation between the mean velocity and the mean bed shear stress. This correlation can be obtained through log-law fits of measured velocity profiles during calibration or through assignment of a friction factor (e.g., Ravens and Gschwend, 1999):

$$\tau_b = \rho \frac{f}{8} U^2 \tag{1}$$

where f is the dimensionless friction factor and U is the cross-sectional average velocity. Spatial variability still exists in the bed shear stresses even in fully-developed uniform flow in rectangular cross-sections due to side-wall effects and development of secondary flow cells; in rectangular conduits with width-to-depth ratios greater than 2.0, greater than 80% of the bottom boundary surface area typically experiences a bed shear stress within 20% of the maximum value that exists along the centerline (Knight and Patel, 1985). Variability is generally neglected, under the judgment that it constitutes acceptable error in estimates of τ_b; more detailed analyses are not warranted when other uncertainties such as spatial variability of the bed conditions are expected to yield errors in excess of the τ_b estimate. However, in flumes with more complicated flow patterns (e.g., Waterman et al., 2011), such variability in the bed shear stress cannot be neglected without introducing considerable error. This is particularly important in flow that is not fully-developed (i.e., the cross-sectional velocity distribution changes in the longitudinal direction), which is shown to be the case within the erosion section of the current flume.

To address the more complex hydrodynamics of the current flume, CFD modeling is used. This allows more reliable estimates of τ_c than can be obtained by selecting an average value per conventional methods used with flumes where the flow is more reasonably represented as fully-developed uniform flow. Prior to τ_c being exceeded, the bed within the erosion segment of the *in situ* flume is approximately flat and flush with the closed-bottom portions of the flume immediately upstream and downstream of the erosion segment. The results of the CFD simulations for the initial bed under the full range of experimental flow rates are illustrated in Figures 11 through 23; these figures are plan views of the bed shear stresses in the erosion segment only. They are plotted using the same color legend (logarithmic scale) for all figures to highlight the relative differences in τ_b associated with the various experimental flow rates.

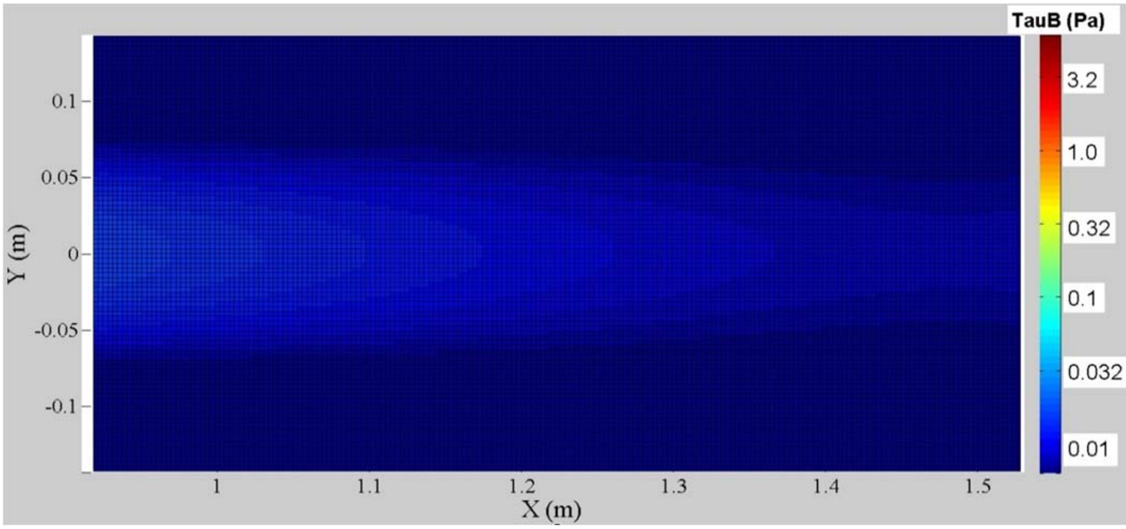

Figure 11: Bed shear stress distribution for Q_{flume} = 0.5 L/s

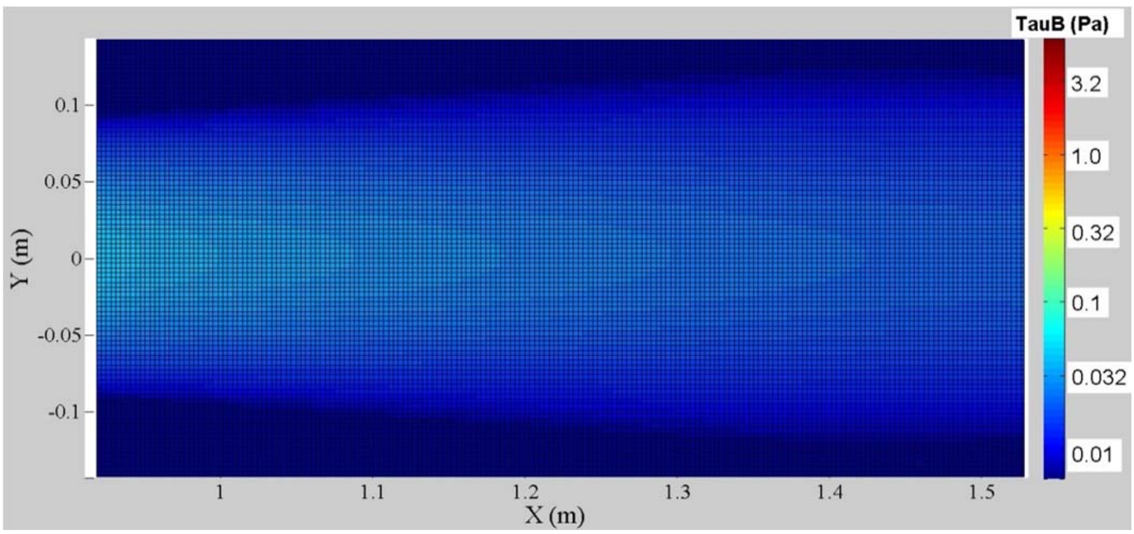

Figure 12: Bed shear stress distribution for Q_{flume} = 1.0 L/s

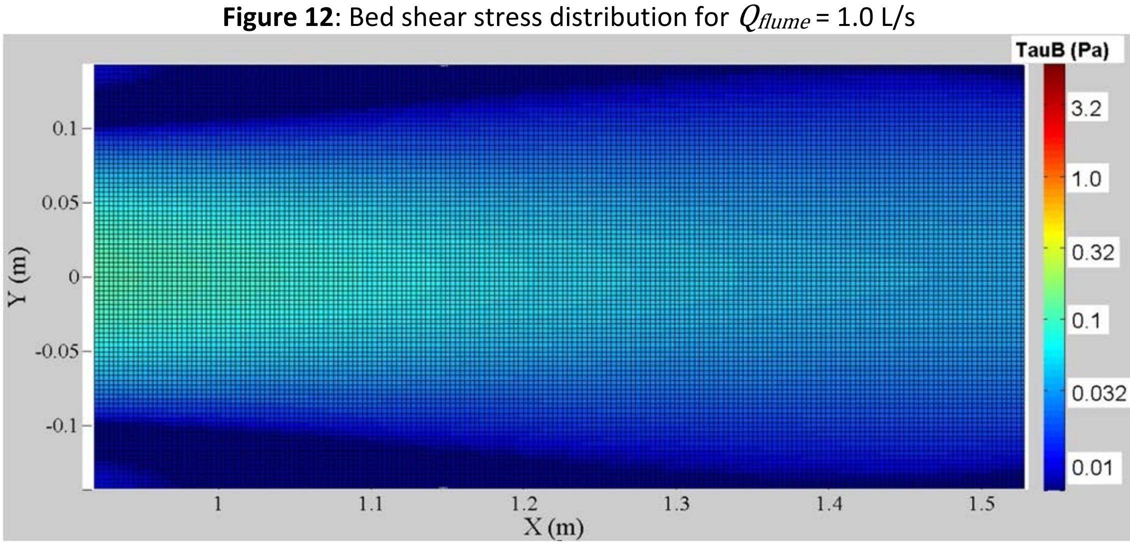

Figure 13: Bed shear stress distribution for Q_{flume} = 1.5 L/s

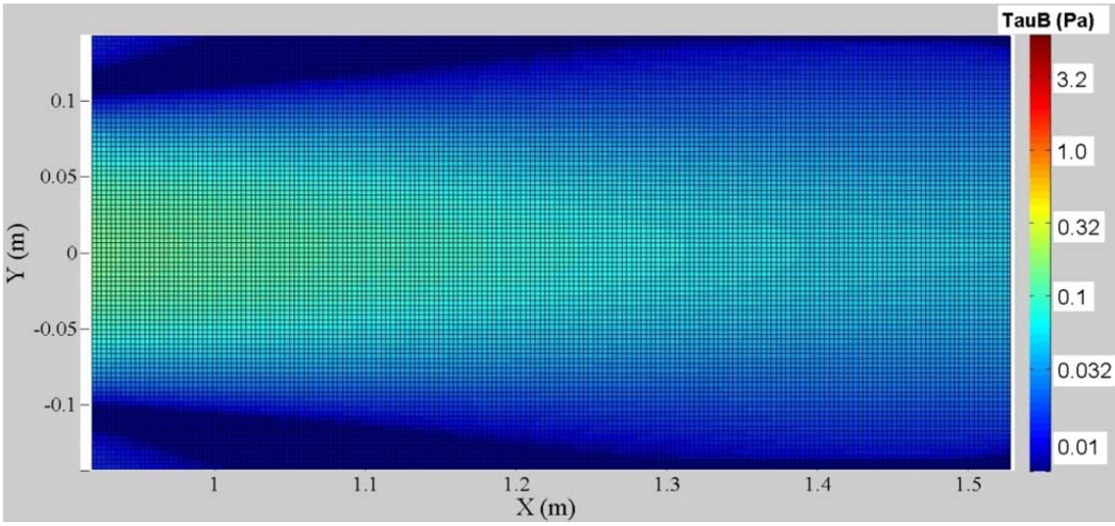

Figure 14: Bed shear stress distribution for Q_{flume} = 1.75 L/s

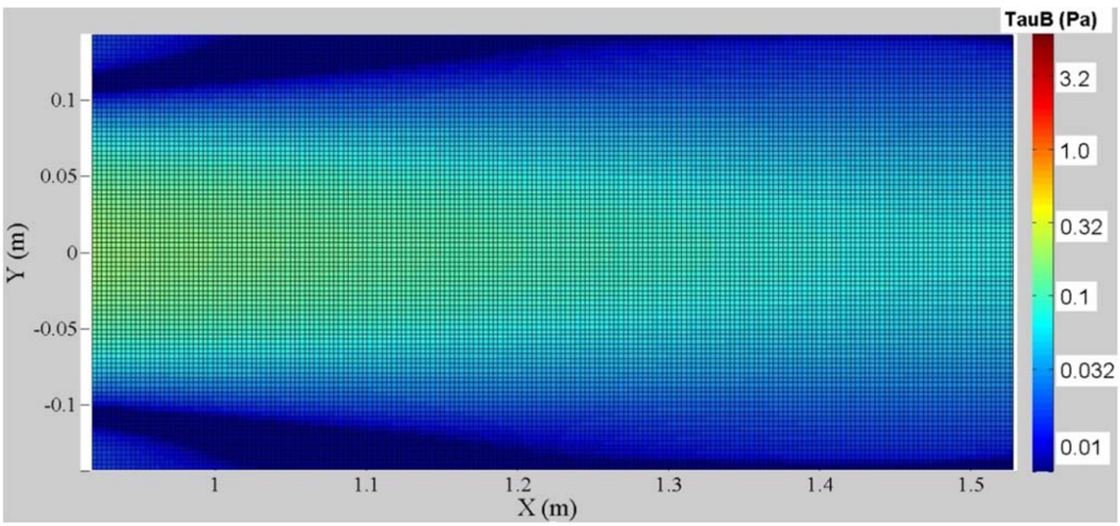

Figure 15: Bed shear stress distribution for Q_{flume} = 2.0 L/s

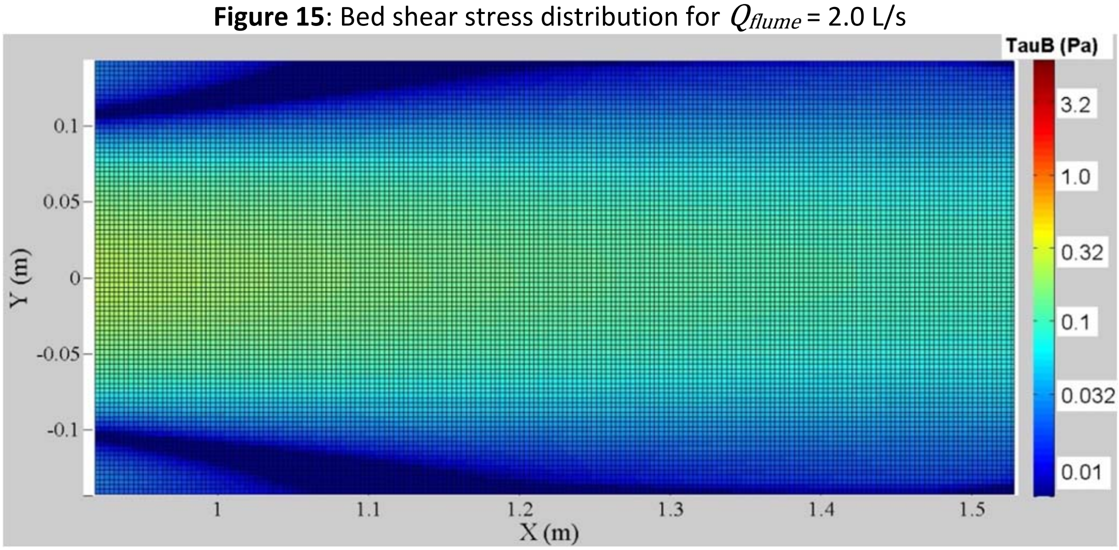

Figure 16: Bed shear stress distribution for Q_{flume} = 2.5 L/s

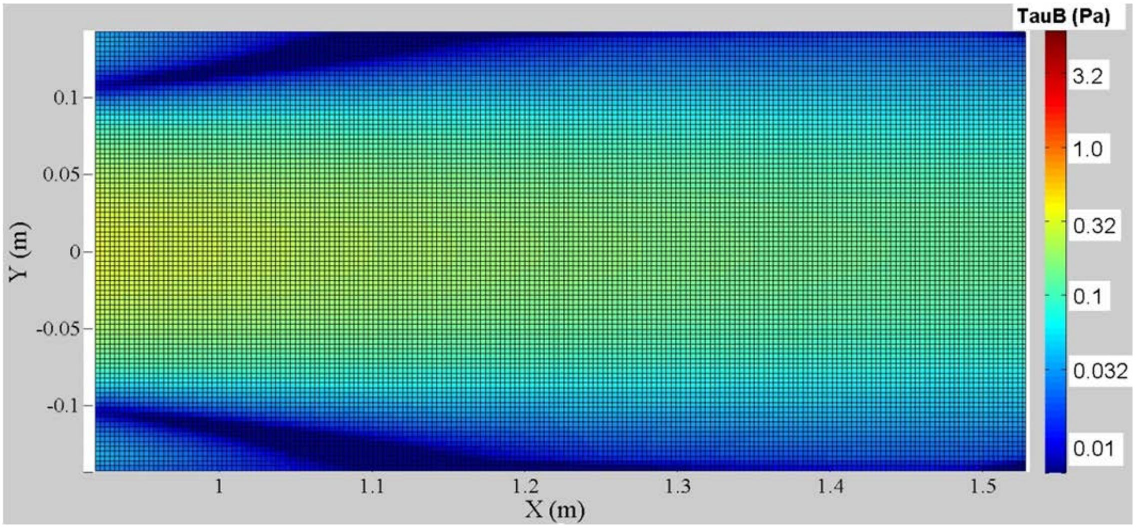

Figure 17: Bed shear stress distribution for Q_{flume} = 3.0 L/s

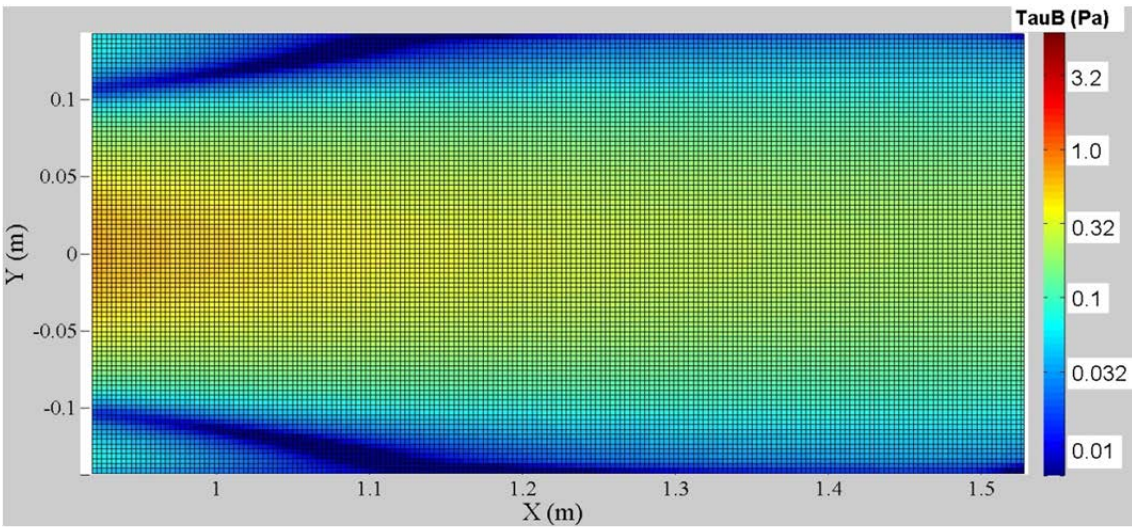

Figure 18: Bed shear stress distribution for Q_{flume} = 4.0 L/s

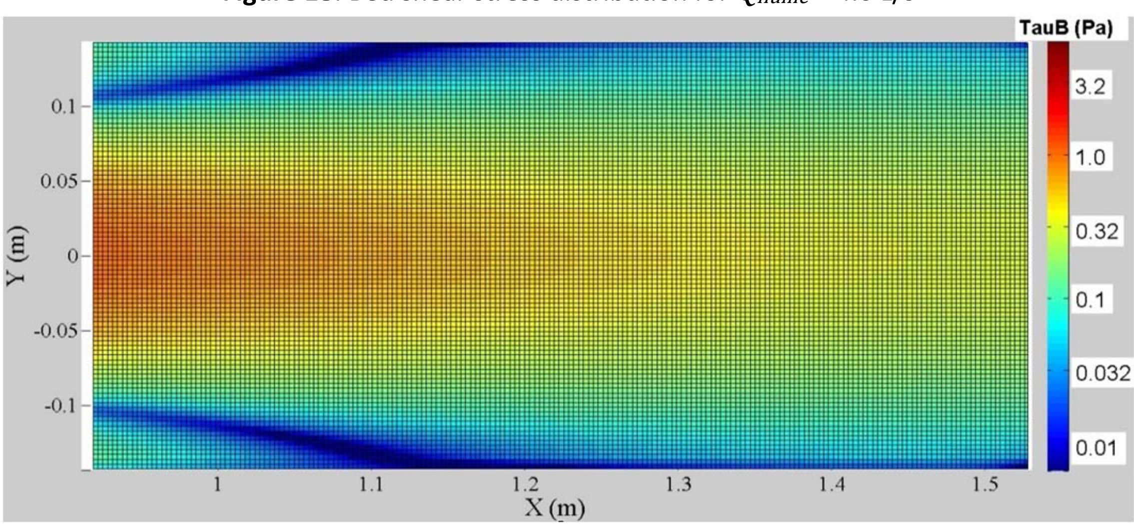

Figure 19: Bed shear stress distribution for Q_{flume} = 5.0 L/s

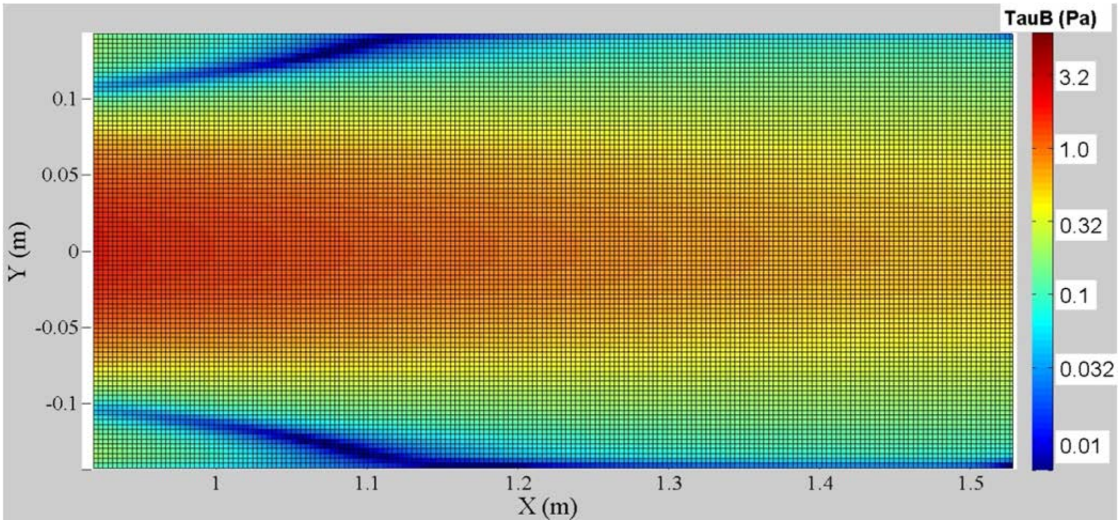

Figure 20: Bed shear stress distribution for Q_{flume} = 6.5 L/s

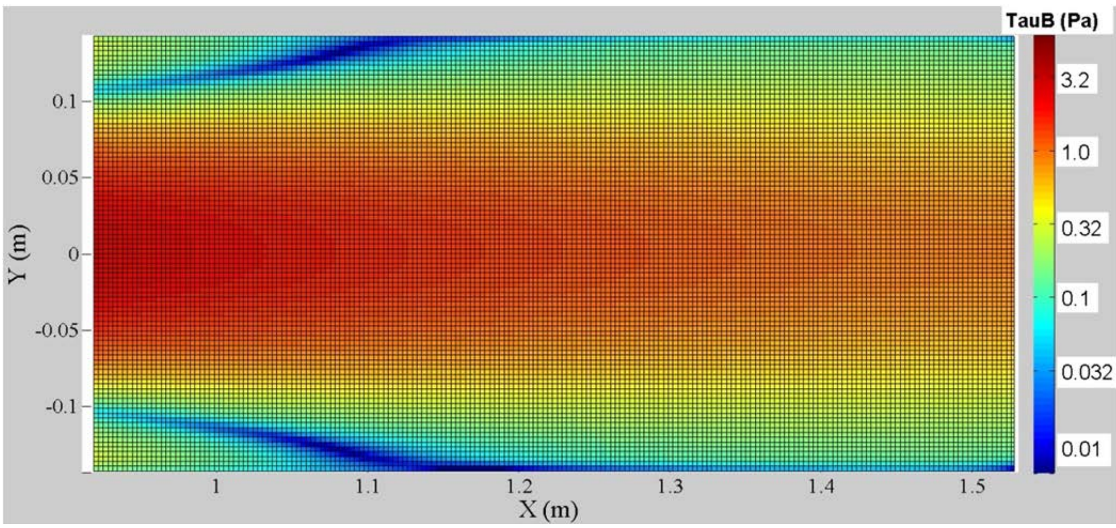

Figure 21: Bed shear stress distribution for Q_{flume} = 8.0 L/s

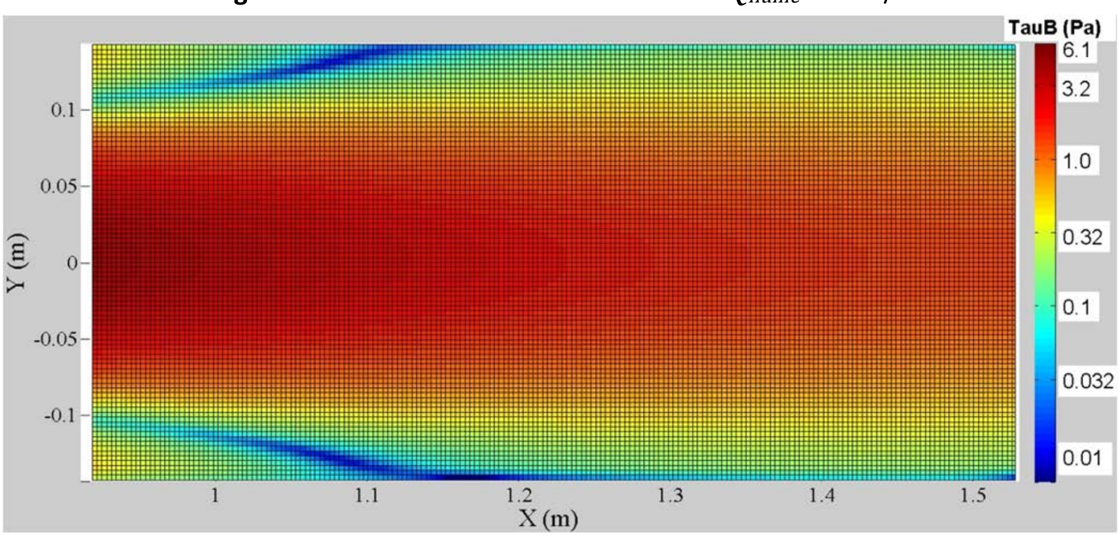

Figure 22: Bed shear stress distribution for Q_{flume} = 10.0 L/s

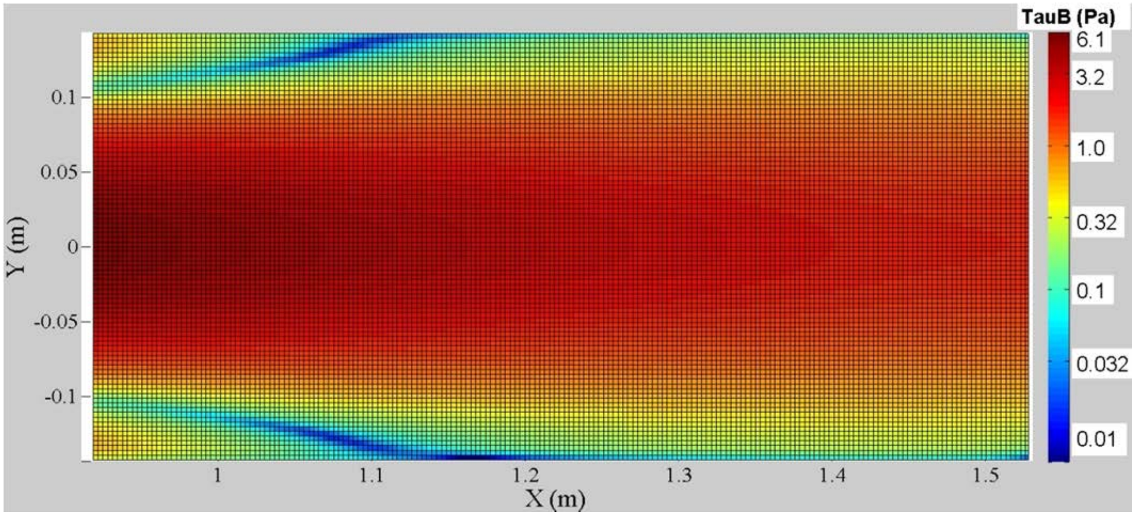

Figure 23: Bed shear stress distribution for Q_{flume} = 11.5 L/s

To better illustrate the bed shear stress variability for a single flow rate, a linear color scale that includes only the range of bed shear stresses experienced for the single flow rate is provided in Figure 24.

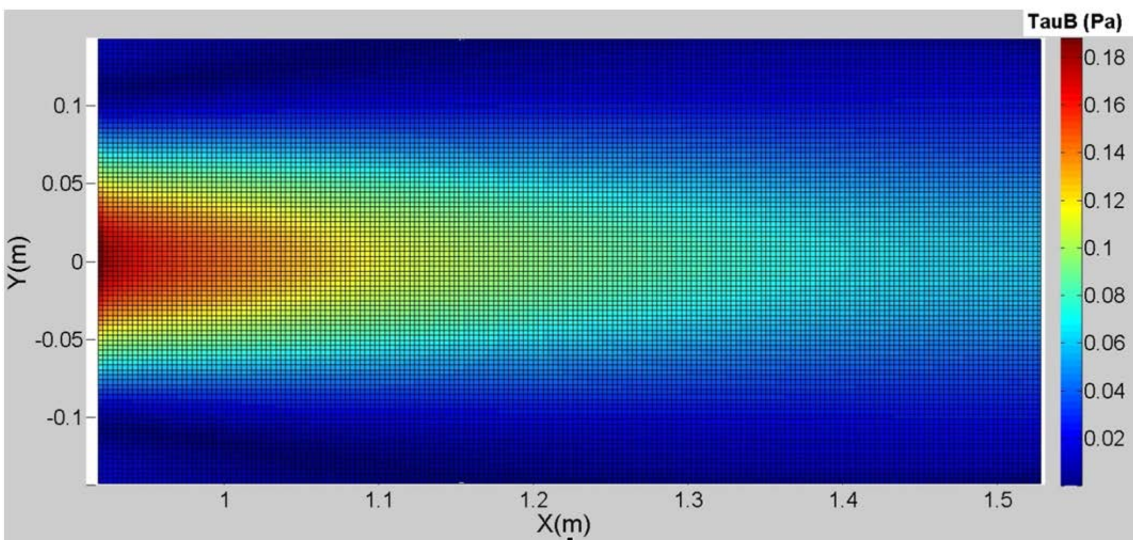

Figure 24: Bed shear stress distribution for Q_{flume} = 2.0 L/s

The CFD results reveal that the flow is not fully developed upon entering the erosion segment and that a distribution of τ_b over the sediment bed exists; the key aspect of the analysis of τ_c is to identify the most appropriate value of τ_b associated with the experimental flow rates. The method implemented in the current study is to compare the full distributions of τ_b associated with the Q_{flume} values on both sides of the threshold where bed mobilization is initiated. This is illustrated in Figure 25, an example that shows the threshold between Q_{flume} = 1.75 L/s (no erosion) and Q_{flume} = 2.0 L/s (erosion); these bounding Q_{flume}

values commonly defined the transition between no erosion and discernible erosion among the various field sampling sites in the Kalamazoo River study area.

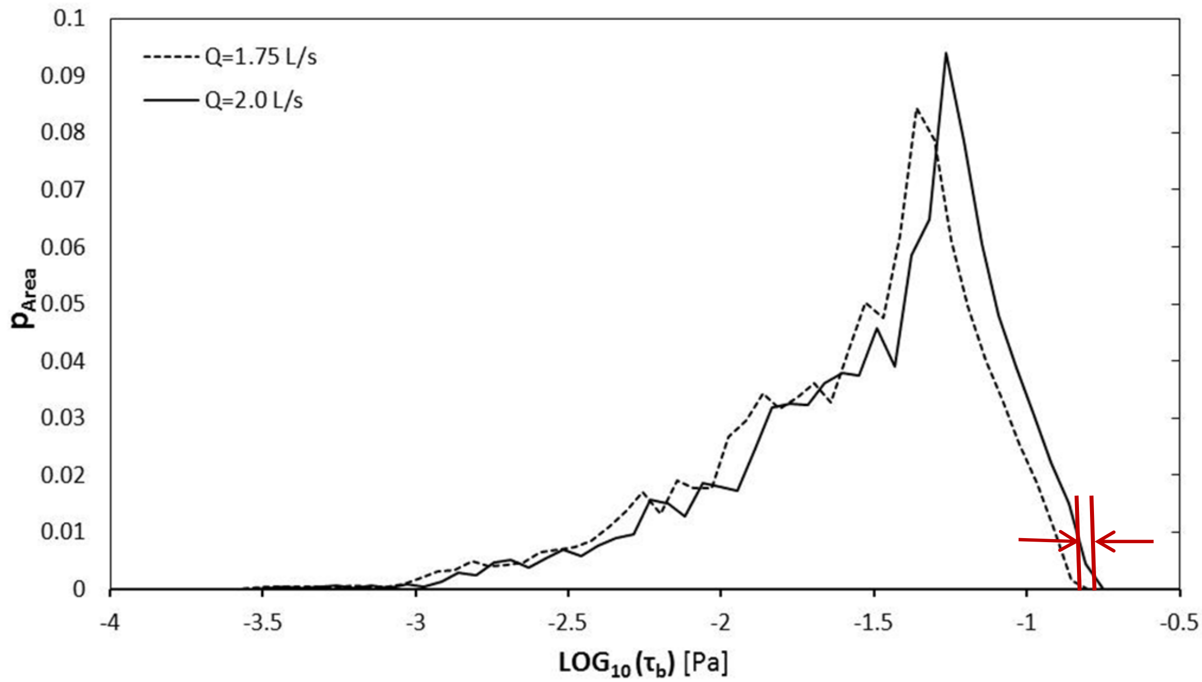

Figure 25: Illustration of method for determining critical bed shear stress

In Figure 25, p_{Area} is the percentage of the bed area within a given shear stress bin as determined from the CFD results; summing p_{Area} over all the bins equals 1. The distributions are based on 51 equally spaced intervals of LOG$_{10}$(τ_b) that span the full range of τ_b for that particular value of Q_{flume}.

The most straight-forward determination of a characteristic τ_b for each flow rate would be an area-weighted average of the τ_b distribution. However, the area-weighted average is not necessarily the most suitable value to quantify the initiation of erosion, as illustrated using the provided example where the initiation of erosion occurs in the transition between Q_{flume} = 1.75 L/s and Q_{flume} = 2.0 L/s. In the case of Q_{flume} = 2.0 L/s, the area-weighted average τ_b is 0.049 Pa; however, over 20% of the surface area for Q_{flume} = 1.75 L/s (in which no erosion occurred) experiences $\tau_b \geq$ 0.049 Pa. Clearly, 0.049 Pa cannot be the characteristic τ_b to quantify the initiation of erosion; if 0.049 Pa was the critical bed shear stress, erosion would have been observed at Q_{flume} = 1.75 L/s. The only logically consistent means of identifying a characteristic τ_b to quantify the initiation of motion is to consider the high end of the τ_b distribution for Q_{flume} = 2.0 L/s in the portion that exceeds the maximum value of τ_b for Q_{flume} = 1.75 L/s. For the example shown in Fig. 25, the critical shear stress must be greater than the highest value of τ_b

associated with Q_{flume} = 1.75 L/s and less than or equal to the highest value of τ_b associated with Q_{flume} = 2.0 L/s; in other words, within the region indicated with the red arrows in Fig. 25. The value of τ_c is estimated as being the area-weighted average τ_b in that portion of the higher curve between the two arrows shown in Figure 25.

3.2 Quantifying Erosion Rates

Graphs are desired with the erosion rate (E) as the dependent variable and bed shear stress (τ_b) as the independent variable. The functional form most commonly used to describe the erosion rate in cohesive sediments is per the Ariathurai-Partheniades equation (Ariathurai, 1974):

$$E = k_d(\tau_b - \tau_c)^a \tag{2a}$$

where k_d is a dimensioned erodibility coefficient; a is an exponent; and τ_c is the critical bed shear stress (force per unit area) that initiates sediment entrainment from the bed. McAnally and Mehta (2001) provide a history of the development of this equation along with the rationale to support the common usage of a = 1 (i.e., a linear relationship). The erosion rate E can be expressed in units of mass per unit area per unit time or volume per unit area per unit time (which is equivalent to depth eroded per unit time); the coefficient of proportionality is dimensioned accordingly. Using the volumetric-unit form of E has the benefit of providing a direct comparison to the results of the USACOE Sedflume study (Perkey et al., 2014).

An alternate formulation to Eq. (2a) is that of Lick (2009):

$$E = A\tau_b^n \qquad [\text{for } \tau_b > \tau_c] \tag{2b}$$

where A is a dimensioned erodibility coefficient; and n is an exponent that is commonly greater than 1. The experiments and analysis of Fukuda and Lick (1980) suggest the exponent in this type of erosion formulation is greater than 1 for values of τ_b slightly greater than τ_c, and the exponent is approximately equal to 1 for higher values of τ_b. Thus Eq. (2b) may be most applicable for low τ_b / τ_c and Eq. (2a) for high τ_b / τ_c.

Determining erosion rate E from the field data:

Some transformations are required to obtain erosion rates E from the field data. The first is to obtain an estimate of suspended sediment mass concentration (C_{sed}) from the time series of turbidity measured in NTU (nephelometric turbidity units). This is achieved by obtaining a correlation between C_{sed} determined from water samples collected in the field during the experiments and the associated turbidity measured while the sample was being collected. The correlation thus obtained is shown in Figure 26.

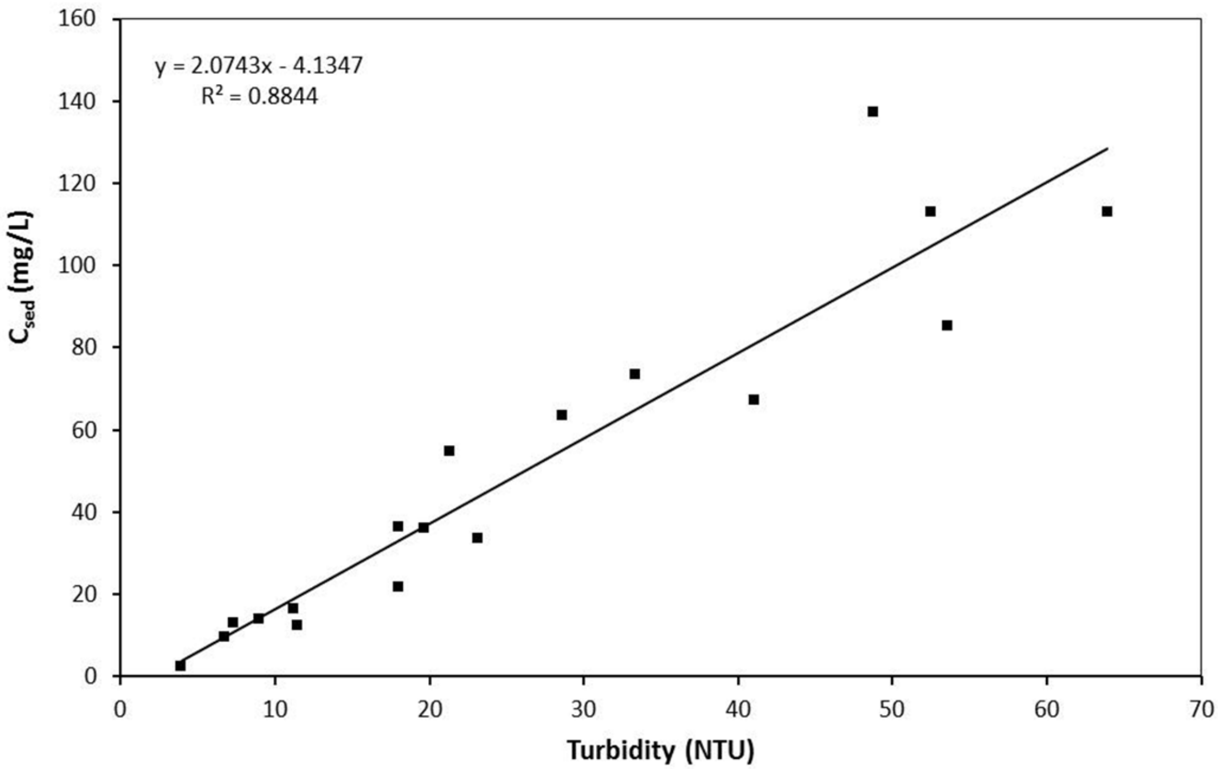

Figure 26: Correlation between turbidity measurements and suspended sediment concentrations

Using the linear relation illustrated in Figure 26, all turbidity measurements are transformed into a value of C_{sed}. To obtain the concentration of eroded sediment, the ambient concentration of suspended sediment which is pumped into the flume must be subtracted.

$$C_{sed,er} = C_{sed} - C_{sed,amb} \tag{3}$$

where $C_{sed,er}$ is the mass concentration of eroded sediment and $C_{sed,amb}$ is the ambient mass concentration of suspended sediment which was measured during the initial part of the experiment at each sample site. The mass of eroded suspended sediment per unit time (Q_{sed}) discharged from the flume chamber is calculated as:

$$Q_{sed} = Q_{flume} C_{sed,er} \tag{4}$$

The total mass of sediment eroded (M_{sed}) during any time interval t_1 to t_2 is obtained by integration:

$$M_{sed} = \int_{t1}^{t2} Q_{sed} dt \tag{5}$$

The mass of eroded sediment within the time interval t_1 to t_2 is converted to a volume of eroded bed (V_{er}) using the dry bulk density of the sediment ($\rho_{sed,bulk}$):

$$V_{er} = \frac{M_{sed}}{\rho_{sed,bulk}} \tag{6}$$

Values of $\rho_{sed,bulk}$ for the eroded surface sediments were estimated from soil cores sampled and measured by the U.S. Army Corps of Engineers (Perkey et al., 2014) at the same sample locations as the current study. (Soil cores were collected during the current study, but the method of bulk density measurement did not allow determination of variation of bulk density with depth after consolidation of the sediments within the core sample tube; see Appendix A for a description of the current study sediment cores.) Values of saturated bulk density (ρ_{sat}) were reported by the U.S. Army Corps of Engineers (USACOE); the ρ_{sat} values used in the current analysis were from the uppermost measurement (<2 cm depth) from the core associated with the sample site; the rationale for using only the uppermost sample is described in section 3.3. The dry bulk density is obtained from the reported wet bulk density under fully saturated conditions using the following equation:

$$\rho_{sed,bulk} = \frac{(\rho_{sat} - 1)}{(\rho_{sed} - 1)} \rho_{sed} \tag{7}$$

where ρ_{sed} is the solid particle density and ρ_{sat} is the saturated wet bulk density. Note that ρ_{sed} is assumed equal to 2.65 g/cm^3 by Perkey et al. (2014); for consistency, that value is also used in the current study.

To obtain the erosion depth (D_{er}) in the time interval t_1 to t_2, the erosion area (A_{er}) is required, which depends on the bed shear stress distribution:

$$D_{er} = \frac{V_{er}}{A_{er}} \quad (8)$$

The most fundamentally sound approach to establish A_{er} is to evaluate the full bed shear distribution to identify the surface area that experiences $\tau_b > \tau_c$ for the given Q_{flume}. To avoid compounding error associated with the estimation of τ_c, in addition to the uncertainties associated with the τ_b distribution for modified bed geometries after erosion has been initiated, the assumption is made that the entire bed surface area erodes; in other words, A_{er} is treated as a constant equal to 1742 cm^3. This approach is consistent with past analyses of *in situ* flume data (e.g., Ravens and Gschwend, 1999). This assumption tends to reduce the value of D_{er} and the subsequently calculated E. The error introduced is expected to be greatest for low flow rates where the CFD simulations suggest that a smaller fraction of the bed experiences $\tau_b > \tau_c$. The erosion rate (E) is then calculated as:

$$E = \frac{D_{er}}{t_2 - t_1} \quad (9)$$

Per the current analysis, a single value of E was calculated for each Q_{flume} interval; i.e., the integration to obtain M_{sed} per Eq. (5) was calculated such that t_1 was the beginning of the Q_{flume} interval and t_2 was the end of the Q_{flume} interval. This yields an average erosion rate over the interval. This is illustrated in Figure 27.

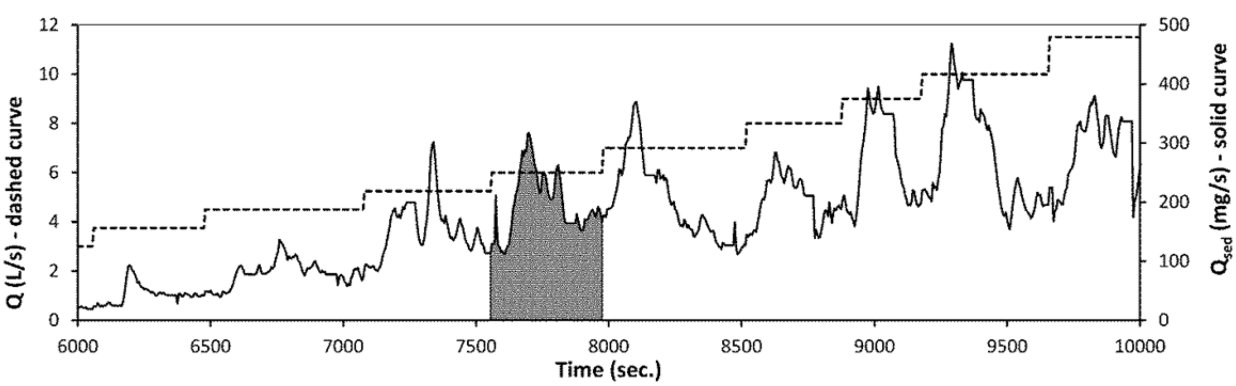

Figure 27: Integration of Q_{sed} over time for a single discharge interval yields a single value M_{sed} for that discharge interval; the example integration region is shaded.

Determining τ_b associated with the field data:

A characteristic value of the bed shear stress (τ_b) must be associated with each experimental flow rate (Q_{flume}) to fit the field data according to the erosion rate formulations. The τ_b distribution can be obtained from the CFD modeling results illustrated in Figures 11 through 24 provided that changes in the bed geometry during erosion do not alter the hydrodynamics sufficiently to alter the τ_b distribution excessively. This is an assumption that has been made in all past analyses of *in situ* flume data; the assumption is made in this analysis that CFD simulations using the initial bed geometry are valid throughout the duration of each experiment. (Section 3.3 discusses the limitations of this assumption.)

A single characteristic value of τ_b to represent the distribution is required for plotting to fit an erosion rate formulation. Maintaining consistency with the assumption of constant A_{er}, the variable $\tau_{b,R}$ is calculated as the area-weighted average τ_b over the entire bed surface area within the flume erosion segment:

$$\tau_{b,R} = \frac{1}{A_{er}} \int \tau_b dA \tag{10}$$

The subscript "R" indicates the representative value.

3.3 Limits on the Unchanging Bed Geometry Assumption

As indicated in subsection 3.2, the CFD results associated with the initial bed geometry are used to quantify the bed shear stresses, regardless of the magnitude of bed erosion. However, as the bed erodes, the hydrodynamics within the erosion segment of the flume is altered. Thus, the error in the $\tau_{b,R}$ estimate increases with increasing sediment mass eroded during the experiments. Establishing an upper limit on the acceptable error warrants consideration.

To make reasonable error estimates, the first case considered is that of uniform, fully-developed flow in an infinitely long rectangular cross-section; this is an idealized condition of uniform erosion that allows for the simplest possible analysis. During erosion, the mean velocity decreases with increasing cross-sectional area:

$$U = \frac{Q_{flume}}{BH} \tag{11}$$

where U is the mean velocity, B is the flume width (a constant equal to 11.25 inches), and H is the cross-section depth, which changes during erosion. Assuming that the bed friction factor f maintains a constant value during the erosion process, the bed shear stress under a constant value of Q_{flume} can be expressed relative to the initial un-eroded bed condition as:

$$\frac{\tau_b}{\tau_{b,0}} = \frac{\rho\frac{f}{8}U^2}{\rho\frac{f}{8}U_0^2} = \left(\frac{H_0}{H}\right)^2 \tag{12}$$

where the subscript "0" indicates the initial condition of un-eroded bed geometry. For assessment of error, the case under consideration is that τ_b is the actual value and $\tau_{b,0}$ is the inferred value associated with the initial bed geometry condition; using the definition of relative error:

$$\delta\tau_b = \frac{\tau_{b,0}}{\tau_b} - 1 = \left(\frac{H}{H_0}\right)^2 - 1 \tag{13}$$

The acceptable amount of relative error is dependent on the application. For the current application in which an order of magnitude difference in the erosion rate E as a function of τ_b between different testing methods is commonly considered acceptable, a relative error of 0.5 for τ_b is probably justifiable. When applied to the geometry of the current flume, Eq. (13) yields an erosion depth equal to 0.87 in. (2.21 cm) and a total eroded volume equal to 3850 cm^3 to achieve $\delta\tau_b = 0.5$.

The above simplified analysis provides a reference condition for the more complex situation in which the erosion is not uniform. In the case of an ideal flume of finite length with uniform, fully-developed flow entering the erosion segment, any uniform erosion during the initial erosion period yields an abrupt drop at the erosion segment entrance, a zone of vertical recirculation, and a downstream region of evolving velocity distribution (i.e., a flow development region); the downstream end will experience a similar transition in the opposite orientation. Such hydrodynamic complexity yields a non-uniform shear stress distribution and subsequent non-uniform erosion, even for the ideal flume considered. Accounting for the case of co-evolving geometry and hydrodynamics is not readily resolvable; full morphodynamic simulations are not practicable when the properties of the bed are unknown and may vary over small spatial scales. The issue is further complicated by the more complex hydrodynamics associated with the current flume.

A quasi-morphodynamic approach was developed as an alternative approach for data analysis; it was later abandoned due to the inherent uncertainties of the approach in the absence of additional field instrumentation to verify bed geometry changes during the erosion process. Nevertheless, the approach does provide reasonable approximations of bed geometry changes during the erosion process along with the resulting altered bed shear stress distributions. Although the quasi-morphodynamic approach was abandoned for the detailed data analysis, the results are utilized as a means of qualitative comparison against the idealized solution for error embodied in Eqs. (19) through (21). The quasi-morphodynamic approach is fully described in Appendix C. The results pertaining to the error analysis are summarized in Figure 28.

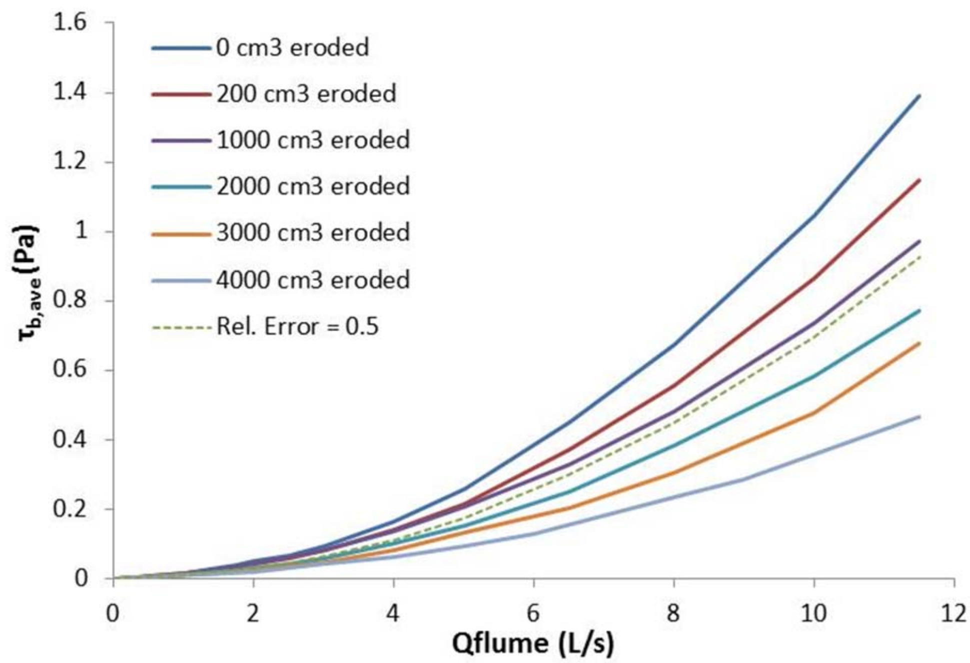

Figure 28: Alteration of the bed shear stress distribution as the volume of erosion increases using the quasi-morphodynamic simulations.

The value of τ_b plotted on Figure 28 is the area-weighted average over the entire bed of the erosion segment of the flume. The dashed line represents the 0.5 relative error using τ_b calculated under the initial geometry condition as the inferred value. The quasi-morphodynamic solution suggests that the 0.5 relative error is exceeded when the volume eroded is between 1000 cm^3 and 2000 cm^3. This is considerably less than the 3850 cm^3 calculated using the ideal solution for uniform erosion.

Although the quasi-morphodynamic solution can only be considered an approximation, it does represent a more conservative estimate of relative error than the ideal uniform erosion solution. The conservative assumption is implemented herein that only the data points obtained under field conditions with $V_{er} \leq 1000$ cm^3 have valid (within a reasonable degree of error) estimates of τ_b using the initial bed geometry CFD results. All other data points obtained where the cumulative $V_{er} > 1000$ cm^3 are plotted using different symbols and are not included in the curve-fitting to parameterize the erosion rate formulation; a means of providing valid estimates of τ_b under such conditions do not currently exist in the published literature.

For estimates of dry bulk density used in the V_{er} calculation (Eq. 6), only the uppermost bulk density measurement from the associated sediment core reported in Perkey et al. (2014) is used. The uppermost measurements were taken at depths that varied between 1.13 and 1.45-cm below the sediment surface for the five sample stations evaluated in the current study; the measurements at the next shallowest depth were taken between 5.55 and 6.75-cm below the sediment surface. A 1000 cm^3 net erosion volume represents a 0.57-cm mean erosion depth over the entire surface area of the erosion segment of the flume. Field observations revealed that the erosion is quite non-uniform, and so some portions of the surface area are eroded more deeply than 0.57 cm when $V_{er} = 1000\ \mathrm{cm}^3$. However, using values taken from 5.55 to 6.75-cm depth below the surface cannot be justified with the available data regarding geometry modification during erosion. Thus the uppermost measurement reported by Perkey et al. (2014) is considered to best represent the bulk density of the eroded volume up to $V_{er} = 1000\ \mathrm{cm}^3$.

Chapter 4: EXPERIMENTAL RESULTS AND ANALYSIS

Experiments were performed at six sample stations in the Kalamazoo River during the period of November 14 to November 21, 2013. The sample sites are illustrated on Figure 29 and additional details are provided in Table 1. On November 14-15, field experimentation involved trouble-shooting, modifying the equipment, and establishing specific methods to obtain the highest quality data. Sample Site 1 was investigated during this time period; the limited data obtained during the initial trouble-shooting experiments was deemed unusable. The location of Sample Site 1 is shown on Figure 29, but no additional data pertaining to that site is included. Valid data were obtained from Sample Sites 2 through 6; those data are evaluated in this section.

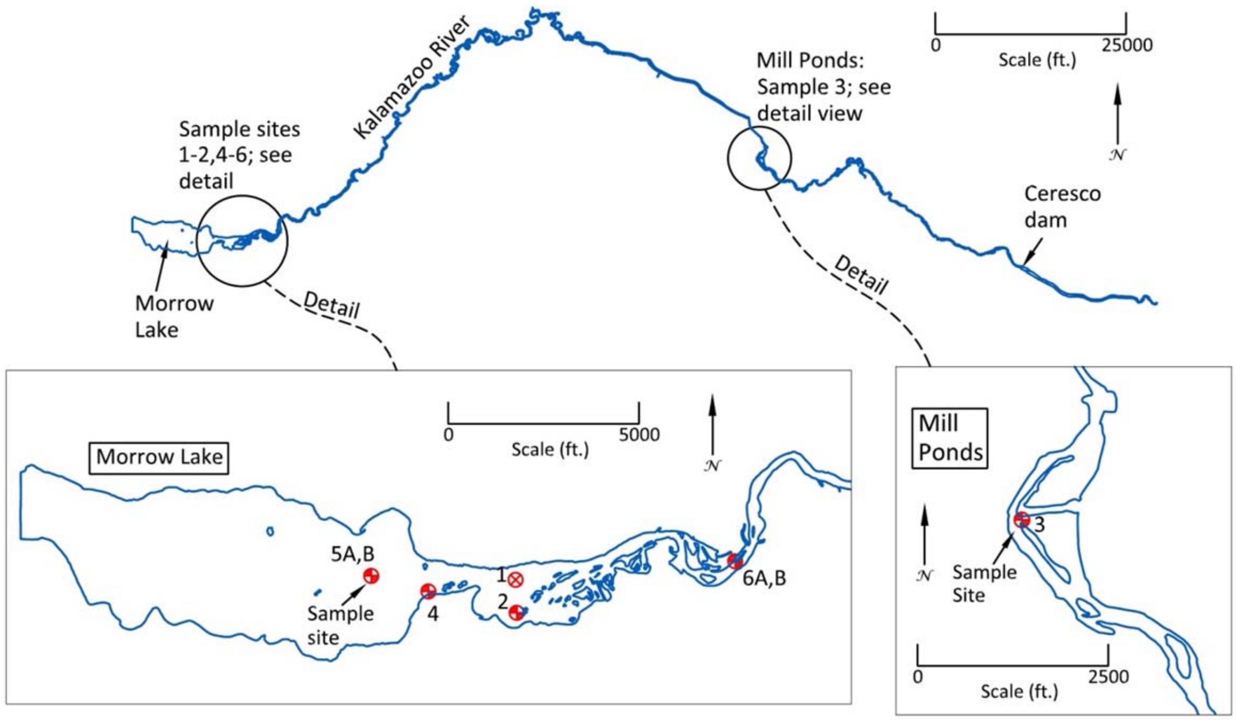

Figure 29: Plan view showing the locations of the field experiment sites; Site 1 is shown with a different symbol to indicate that no usable data were obtained at that site.

Table 1: Locations of the field experiment sites

ID	Latitude	Longitude	Date sampled
Site 2	42.274395	-85.443324	11/16/13
Site 3	42.308067	-85.188859	11/18/13
Site 4	42.275865	-85.451878	11/19/13
Site 5A	42.276923	-85.457439	11/20/13
Site 5B	42.276951	-85.457420	11/20/13
Site 6A	42.278309	-85.422245	11/21/13
Site 6B	42.278307	-85.422219	11/21/13

In the following data analysis, curve fitting is only performed in accordance with Eq. (2b). An attempt was not made to fit the data to Eq. (2a) due to the low values of $\tau_{b,R}$ calculated from the area-weighted average over the entire bed, which presumably incorporates areas where $\tau_b < \tau_c$. This yields some data points early in the tests with $\tau_{b,R} < \tau_c$, yielding negative values of the independent variable.

Site 2:

The field data showing the time series of flow rates and turbidity at Site 2 are shown in Figure 30.

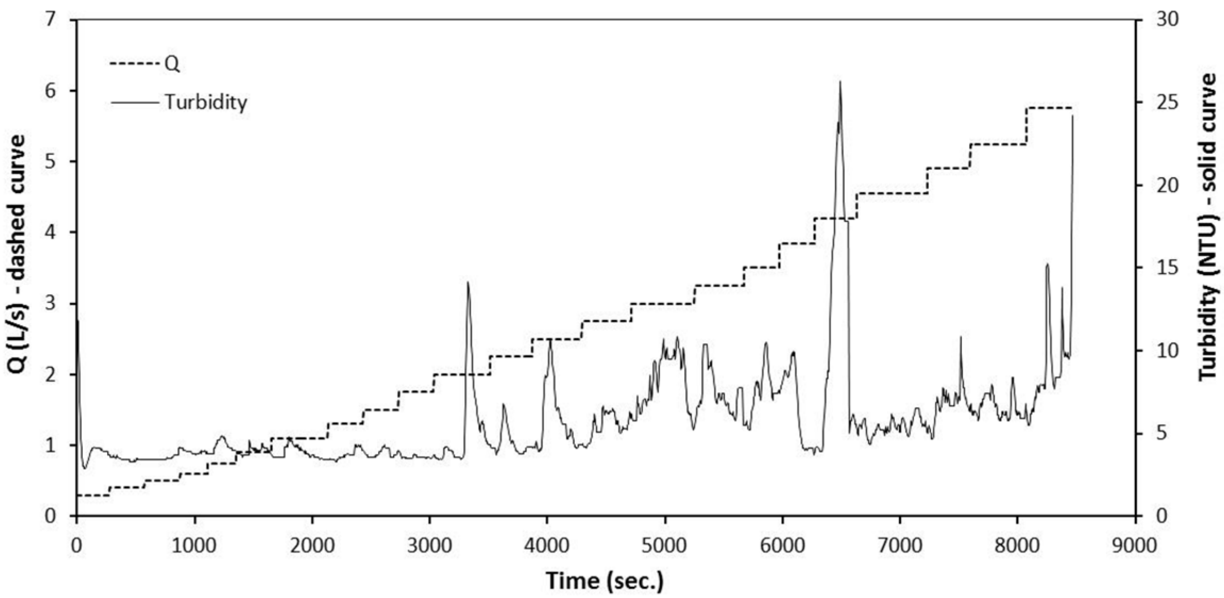

Figure 30: Field data from Site 2

For Site 2, the threshold between no erosion and erosion was crossed in the discharge interval between Q_{flume} = 1.75 L/s and Q_{flume} = 2.0 L/s; this yields a τ_c of 0.14 Pa. The total sediment mass eroded was 143.2 g. This site corresponds to “SF-4alt” in Perkey et al. (2014), where the saturated bulk density at 1.45-cm depth was reported as 1.27 g/cm^3. Per Eq. (7), this yields $\rho_{sed,bulk}$ = 0.43 g/cm^3. Using this value with Eq. (6), only 333 cm^3 was eroded throughout the entire test, and thus the entire data set is within $V_{er} \leq 1000\ \text{cm}^3$.

During the erosion portion of the test, one suspended sediment sample was collected at Q_{flume} = 2.5 L/s; 32.3% of the sediment mass from that sample volatilized at 550°C.

At Site 2, the flow rates were increased at small intervals to prevent early blow-out around the edges of the penetrating skirt, which was a problematic issue during early field trials at Site 1. Due to the fact that a relatively small mass of sediment was eroded during this field trial, the influence of bed geometry modifications on the resulting hydrodynamics can be expected to be relatively small compared to other sample sites. Note that this test was performed with the flume equipped with the original 6-inch penetrating skirt; all other tests at the remainder of the sample stations were performed with a retrofitted 9-inch penetrating skirt. The shallower skirt allowed blow-out around the bottom of the skirt to occur after less total sediment mass had been eroded as compared to the other test sites. The analyzed results are shown on Figure 31.

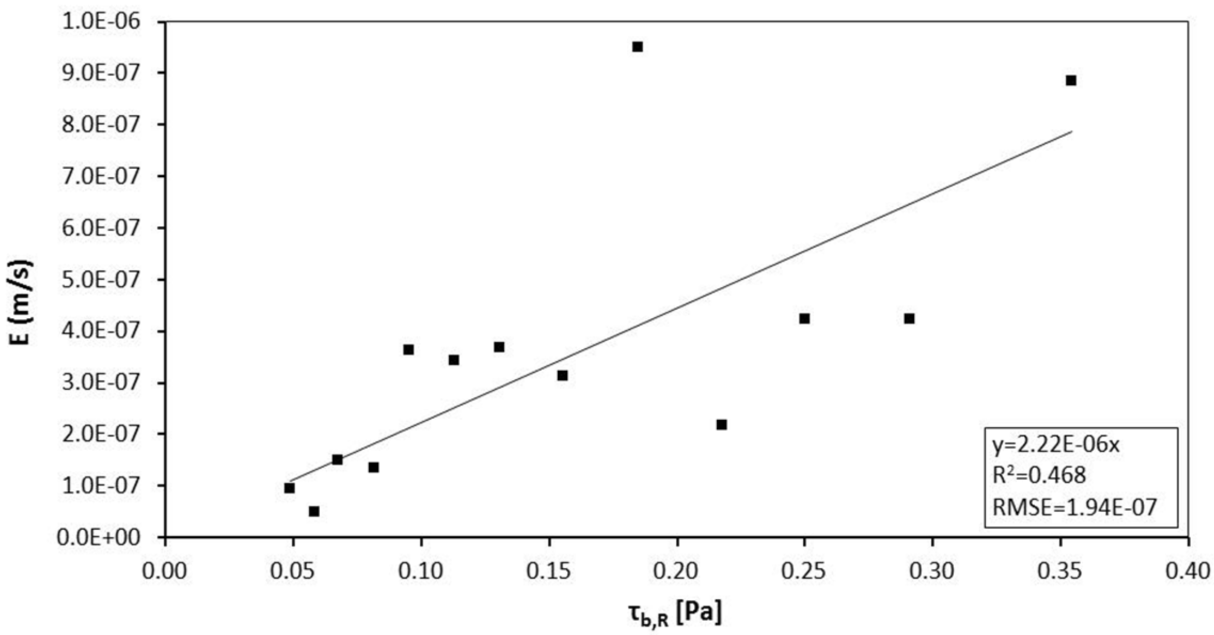

Figure 31: Analysis of field data from Site 2

In Figure 31 and most of the associated figures from the other sample sites, the points early in the test have $\tau_{b,R}$ less than the determined value of τ_c. This is associated with the different value of the relevant boundary shear stress in the τ_c determination (the upper end of the τ_b distribution) compared to that of the erosion rate determination (area-weighted average of the τ_b distribution).

In Figure 31, beyond the data point with $\tau_{b,R}$ = 0.185 Pa, it appears that more erosion-resistant sediments were exposed; it would be possible to fit a coherent curve to the points up to and including $\tau_{b,R}$ = 0.185 Pa, and a second curve to the points with $\tau_{b,R}$ = 0.185 Pa. Such curves would have steeper slopes than the curve fit to the entirety of the data set shown. The best-fit curve according to the minimum root mean square error (RMSE) yielded an exponent of 0.82; that curve had an RMSE of 1.91E-07. An exponent <1 is not encountered in the literature and it appears to be an artifact of the different erodibilities encountered; the exponent was consequently set to 1.0, which yielded only a slightly higher RMSE (1.94E-07) than the original fitted curve.

Site 3:

The field data showing the time series of flow rates and turbidity at Site 3 are shown in Figure 32.

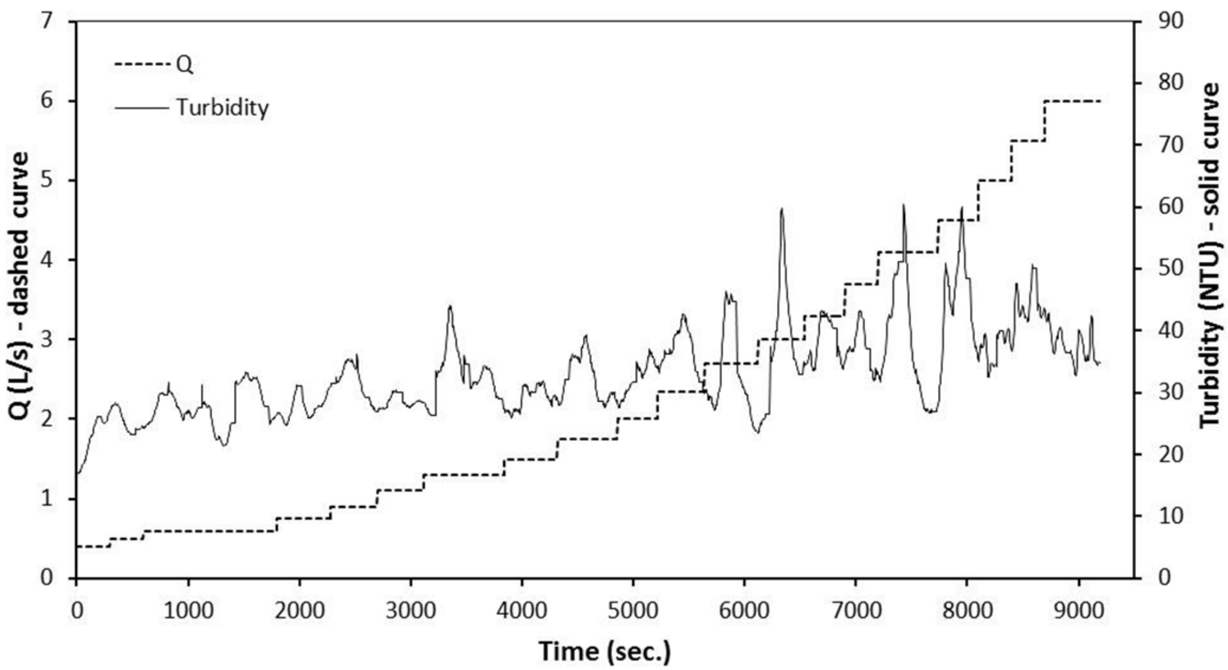

Figure 32: Field data from Site 3

At the Mill Ponds site on the day of sampling, the lowest discharge tested (0.4 L/s) generated a turbidity response. It should be noted that the first four discharge intervals (from 0.4 L/s through 0.75 L/s) yielded only 11.1 grams of eroded sediment. Onsite conditions associated with a severe weather event may have been responsible for the presence of readily entrained loose material at the sediment surface on the day of sampling; this is discussed in greater detail following the figures that describe the data analysis. The maximum τ_b within the τ_b distribution for 0.4 L/s is less than 0.01 Pa. Defining τ_c at this site is not possible with the available data as no lower bound was obtained associated with no entrainment; thus, τ_c can only be identified as being <0.01 Pa, rather than assigning a specific value.

During the erosion portion of the test, four suspended sediment samples were collected:

- At Q_{flume} = 0.3 L/s, 26.9% of the sediment mass volatilized at 550°C
- At Q_{flume} = 2.35 L/s, 27.8% of the sediment mass volatilized at 550°C

- At Q_{flume} = 2.7 L/s, 29.4% of the sediment mass volatilized at 550 °C
- At Q_{flume} = 4.1 L/s, 27.3% of the sediment mass volatilized at 550 °C

The total sediment mass eroded was 588.7 grams. This site corresponds to "SF-1" in Perkey et al. (2014), where the saturated bulk density at 1.28-cm depth was reported as 1.15 g/cm^3. Per Eq. (7), this yields $\rho_{sed,bulk}$ = 0.24 g/cm^3. Using this value with Eq. (6), the total volume eroded during the experiment was 2440 cm^3. The cumulative V_{er} exceeded 1000 cm^3 during the interval with Q_{flume} = 3.7 L/s. Data obtained for Q_{flume} > 3.7 L/s are plotted, but were not utilized in the curve-fitting due to the uncertainty in the $\tau_{b,R}$ estimate as described in section 3.3.

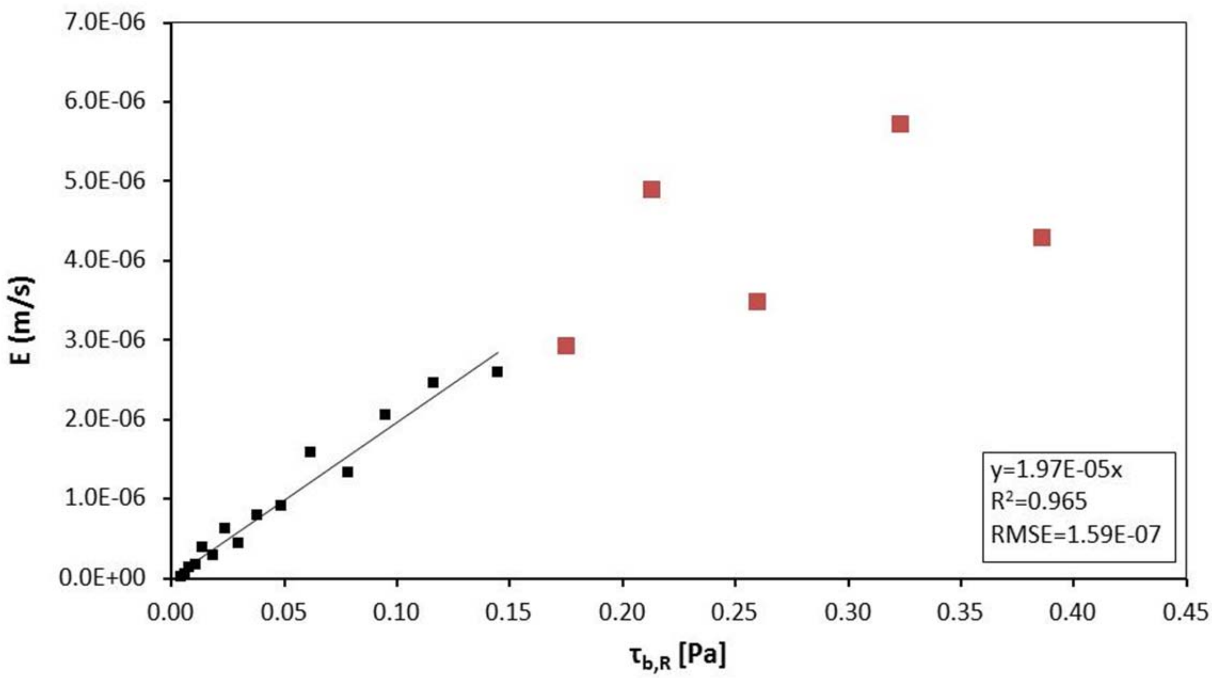

Figure 33: Analysis of field data from Site 3. The red data points are from the portion of the test where V_{er} > 1000 cm^3.

The best-fit curve according to the minimum root mean square error (RMSE) yielded an exponent of 0.94; that curve had an RMSE of 1.56E-07. As described for Site 2, an exponent <1 is not encountered in the literature and suggests an experimental artifact, which in this case is most likely the progressive over-estimation of $\tau_{b,R}$ upon bed geometry modification during erosion. The exponent was consequently set to 1.0, which yielded only a slightly higher RMSE (1.59E-07) than the original fitted curve. The flattening of the erosion rates at larger values of $\tau_{b,R}$ is a clear signature of the over-estimation of $\tau_{b,R}$ due to modified hydrodynamics in the later stages of the test where substantial sediment volume had been eroded.

The unique conditions that may have been responsible for τ_c not being readily defined at this site warrant additional discussion. Site 3 was sampled on 11/18/13. The Kalamazoo, Mich., National Weather Service station recorded 1.21 inches of precipitation on 11/17/13; peak wind gusts of 63 mph and 41 mph were recorded on 11/17/13 and 11/18/13, respectively. The USGS Kalamazoo River at Marshall gauge station (the first gauge station upstream of the Mill Ponds) recorded a moderate response associated with this precipitation event, peaking at a discharge less than 500 cfs on 11/18/13. Morrow Lake and delta area were inaccessible by boat on November 18 due to the strong winds. Although considerably more sheltered than Morrow Lake, wave action within the depositional Mill Ponds setting, in conjunction with the higher discharge, had resulted in relatively high ambient suspended sediment concentration ($C_{sed,amb}$ = 43.9 mg/L) at the test site. This may have been due to re-entrainment of shallow sediment associated with wave action and/or advection of suspended sediment transported by the main channel into the depositional area. (Note that ambient suspended sediment concentrations were much greater than those observed at any of the other sites on the dates of their sampling; the next highest $C_{sed,amb}$ was 12.9 mg/L at Site 5 in upper Morrow Lake.) It is quite possible that the small mass of sediment eroded during the early portion of the test was loose sediment that had been entrained and re-deposited in association with the ongoing weather event.

Site 4:

The field data showing the time series of flow rates and turbidity at Site 4 are shown in Figure 34.

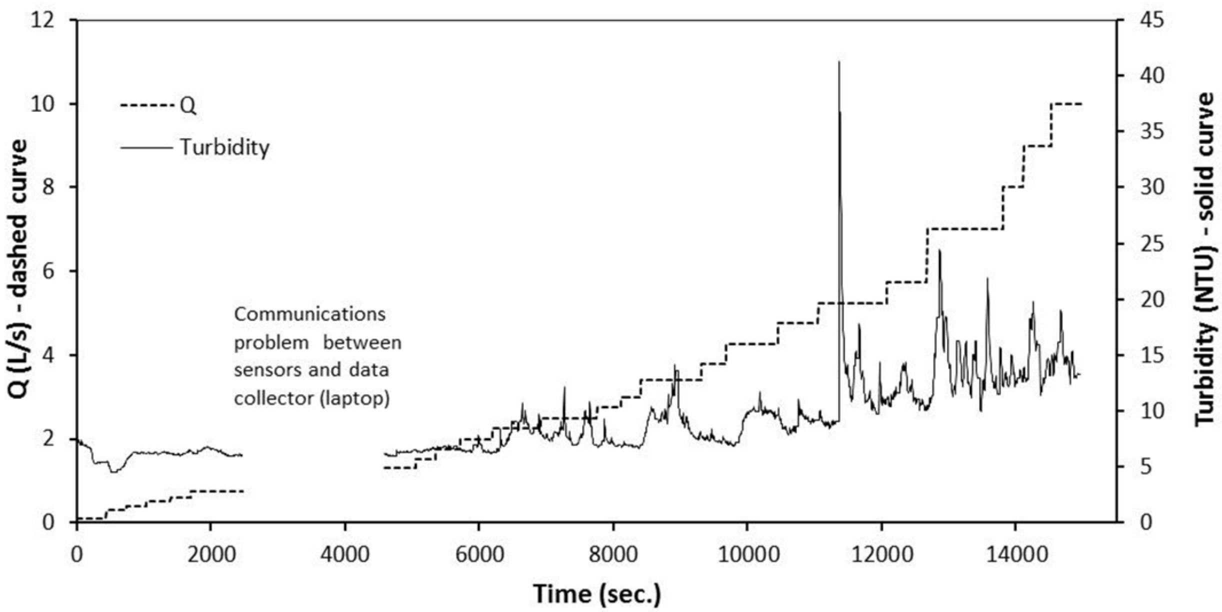

Figure 34: Field data from Site 4

The threshold between no erosion and erosion was crossed in the discharge interval between Q_{flume} = 1.75 L/s and Q_{flume} = 2.0 L/s; the analysis procedure yielded a τ_c of 0.14 Pa. The total sediment mass eroded throughout the test was 489.3 g. This site corresponds to "SF-5" in Perkey et al. (2014), where the saturated bulk density at 1.13-cm depth was reported as 1.16 g/cm^3. Per Eq. (7), this yields $\rho_{sed,bulk}$ = 0.26 g/cm^3. Using this value with Eq. (6), the total volume eroded during the experiment was 1900 cm^3. The cumulative V_{er} exceeded 1000 cm^3 during the interval with Q_{flume} = 7 L/s. Data obtained for Q_{flume} > 7 L/s are plotted, but were not utilized in the curve-fitting due to the uncertainty in the $\tau_{b,R}$ estimate as described in section 3.3.

During the erosion portion of the test, three suspended sediment samples were collected:

- At Q_{flume} = 2.25 L/s, 37.2% of the sediment mass volatilized at 550°C
- At Q_{flume} = 3.4 L/s, 48.9% of the sediment mass volatilized at 550°C
- At Q_{flume} = 9 L/s, 29.6% of the sediment mass volatilized at 550°C

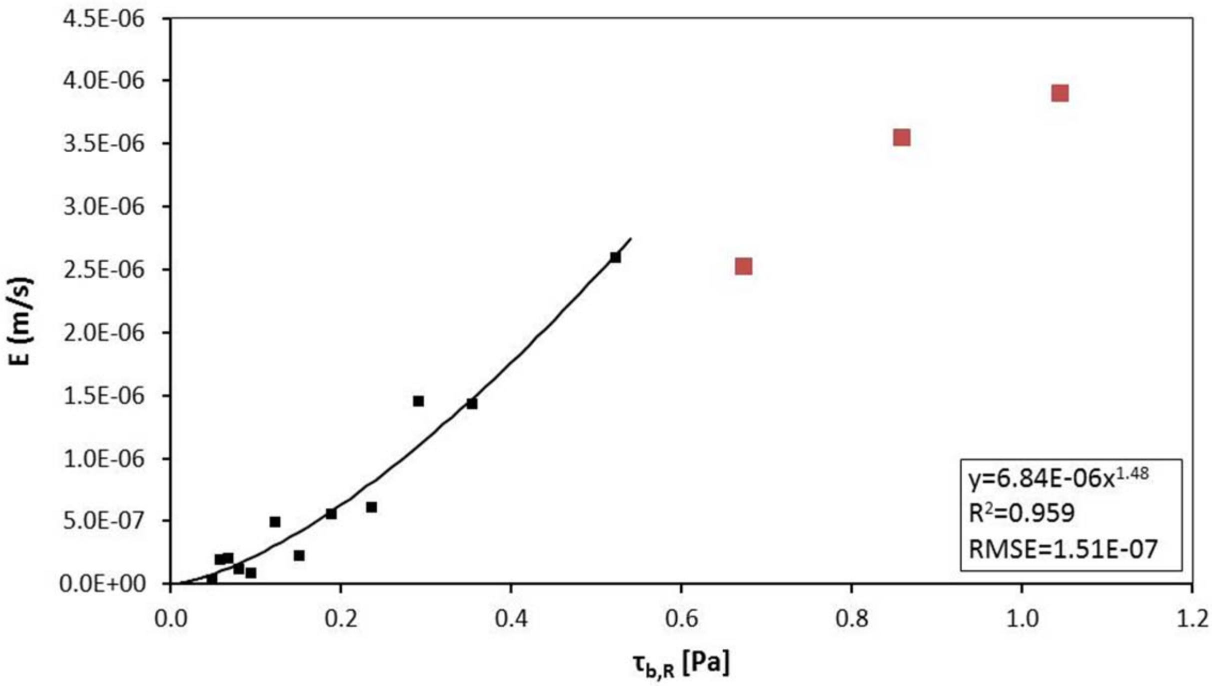

Figure 35: Analysis of field data from Site 4

Similar to Site 3, the flattening of the erosion rates at larger values of $\tau_{b,R}$ on Figure 35 is a signature of the over-estimation of $\tau_{b,R}$ after substantial sediment volume had been eroded.

Site 5A:

Two flume setups were implemented at Site 5; the distance separating Site 5A from Site 5B was approximately 10 feet. The intent of performing two experiments in close proximity was to determine variability at relatively small spatial scales. The field data showing the time series of flow rates and turbidity at Site 5A are shown in Figure 36.

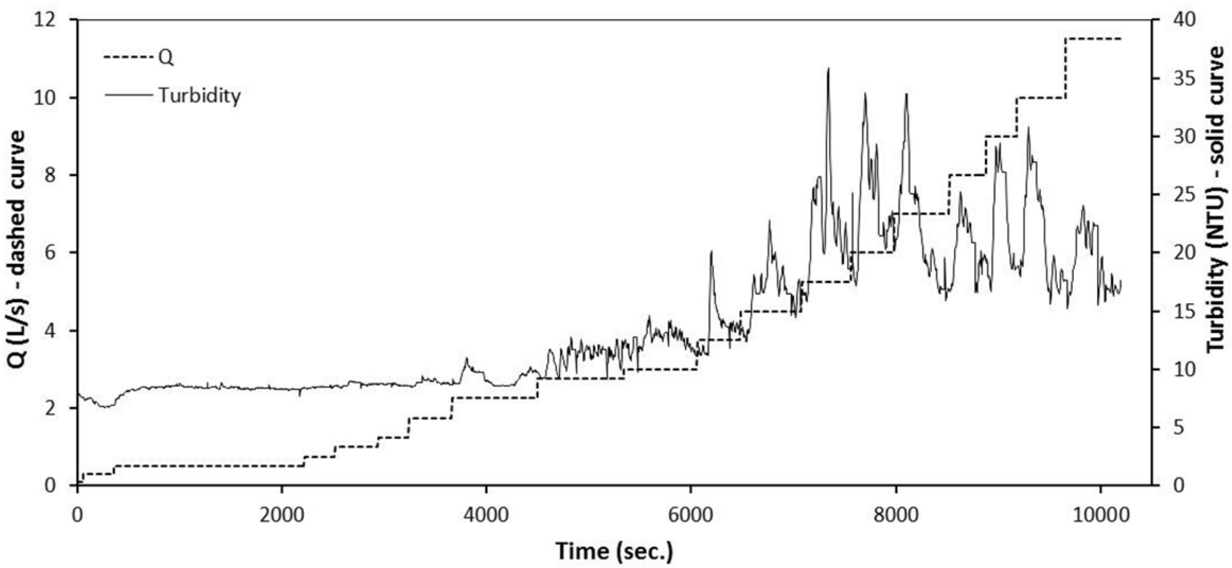

Figure 36: Field data from Site 5A

Based on the turbidity measurements, the threshold between no erosion and erosion was crossed in the discharge interval between Q_{flume} = 1.75 L/s and Q_{flume} = 2.25 L/s; the analysis procedure yielded a τ_c of 0.15 Pa. The total sediment mass eroded throughout the test was 796.5 g. This site corresponds to "SF-7" in Perkey et al. (2014), where the saturated bulk density at 1.25-cm depth was reported as 1.20 g/cm^3. Per Eq. (7), this yields $\rho_{sed,bulk}$ = 0.32 g/cm^3. Using this value with Eq. (6), the total volume eroded during the experiment was 2480 cm^3. The cumulative V_{er} exceeded 1000 cm^3 during the interval with Q_{flume} = 7 L/s. Data obtained for Q_{flume} > 7 L/s are plotted, but were not utilized in the curve-fitting due to the uncertainty in the $\tau_{b,R}$ estimate as described in section 3.3.

During the erosion portion of the test, four suspended sediment samples were collected:

- At Q_{flume} = 3.75 L/s, 40.1% of the sediment mass volatilized at 550°C
- At Q_{flume} = 4.5 L/s, 37.2% of the sediment mass volatilized at 550°C
- At Q_{flume} = 5.25 L/s, 33.6% of the sediment mass volatilized at 550°C
- At Q_{flume} = 7.0 L/s, 23.7% of the sediment mass volatilized at 550°C

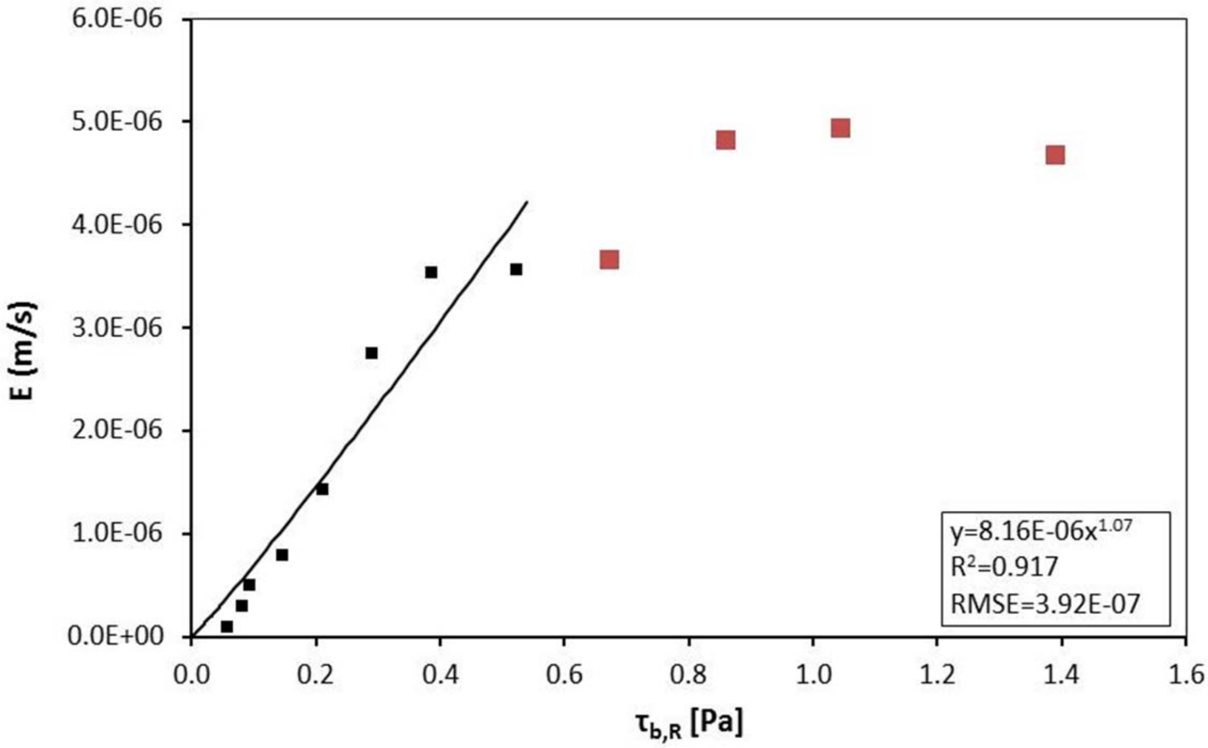

Figure 37: Analysis of field data from Site 5A

Site 5B:

The field data showing the time series of flow rates and turbidity at Site 5B are shown in Figure 38.

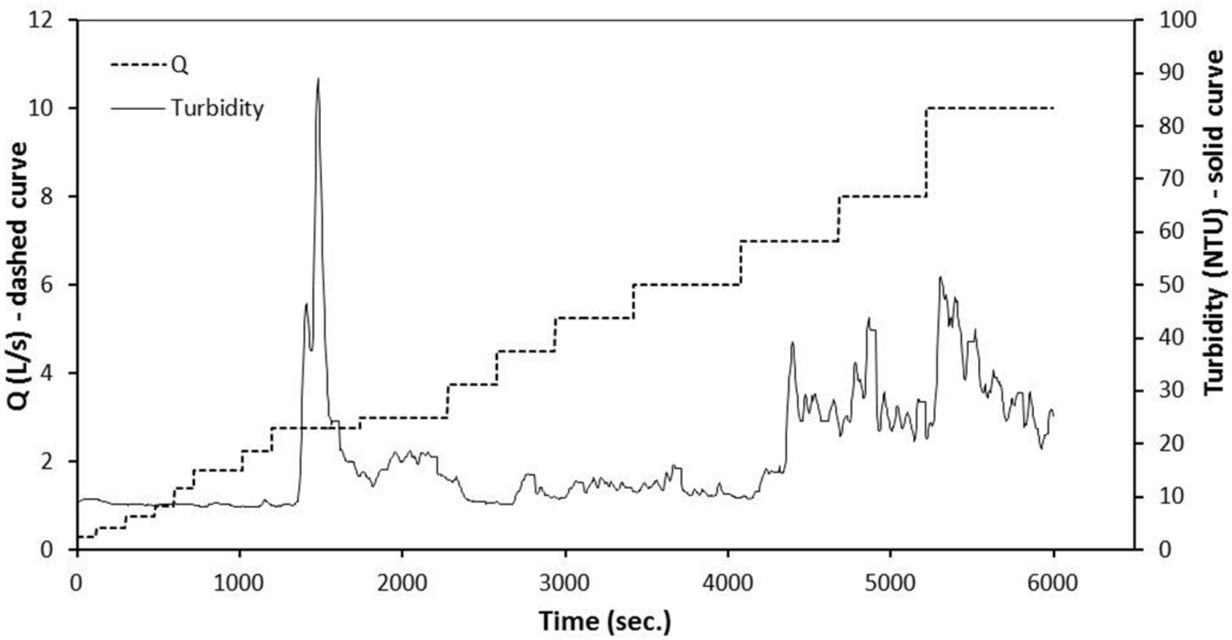

Figure 38: Field data from Site 5B

As in the previous setup at Site 5 (Site 5A), the threshold between no erosion and erosion was crossed in the discharge interval between Q_{flume} = 1.75 L/s and Q_{flume} = 2.25 L/s; the analysis procedure yielded a τ_c of 0.15 Pa. The total sediment mass eroded throughout the test was 793.4 g. This site corresponds to "SF-7" in Perkey et al. (2014), where the saturated bulk density at 1.25-cm depth was reported as 1.20 g/cm^3. Per Eq. (7), this yields $\rho_{sed,bulk}$ = 0.32 g/cm^3. Using this value with Eq. (6), the total volume eroded during the experiment was 2470 cm^3. The cumulative V_{er} exceeded 1000 cm^3 during the interval with Q_{flume} = 8 L/s. Data obtained for Q_{flume} > 8 L/s are plotted, but were not utilized in the curve-fitting due to the uncertainty in the $\tau_{b,R}$ estimate as described in section 3.3.

During the erosion portion of the test, two suspended sediment samples were collected:

- At Q_{flume} = 7.0 L/s, 24.5% of the sediment mass volatilized at 550°C
- At Q_{flume} = 10.0 L/s, 23.9% of the sediment mass volatilized at 550°C

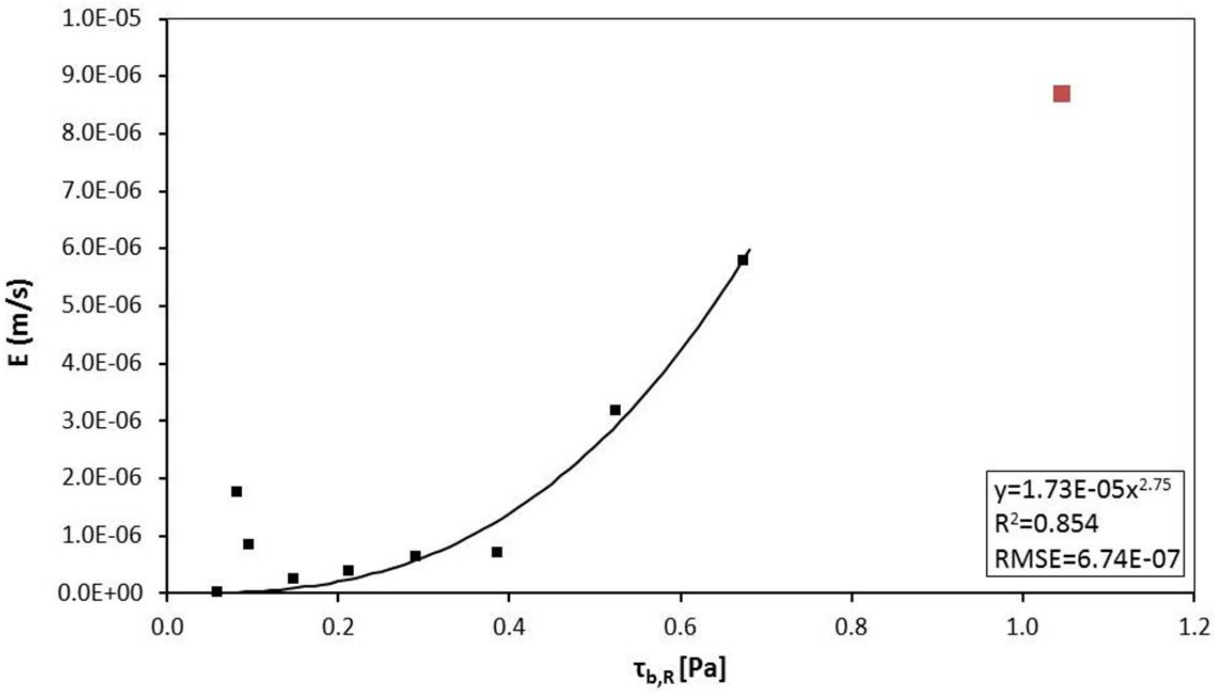

Figure 39: Analysis of field data from Site 5B

As evident from the turbidity signal, a large erosion event occurred early in the experiment. After the discharge of 2.75 L/s and 3.0 L/s eroded approximately 78 grams of sediment, little sediment was eroded for the discharges between 3.75 and 6.0 L/s. Substantial erosion was again activated upon reaching a flow rate of 7 L/s. This sequence suggests a loose, highly mobile layer at the surface was eroded and a more resistant layer underneath was exposed. Note that the erosion rate of 3.2 x 10^{-6} m/s at $\tau_{b,R}$ = 0.52 Pa at Site 5B is very similar to the erosion rate of 3.6 x 10^{-6} m/s at $\tau_{b,R}$ = 0.52 Pa at Site 5A, even though the shapes of the best-fit curves are considerably different.

Site 6A:

Similar to the techniques implemented at Site 5, two flume setups were implemented at Site 6; the distance separating Site 5A from Site 5B was approximately 8 feet. The field data showing the time series of flow rates and turbidity at Site 6 are shown in Figure 40.

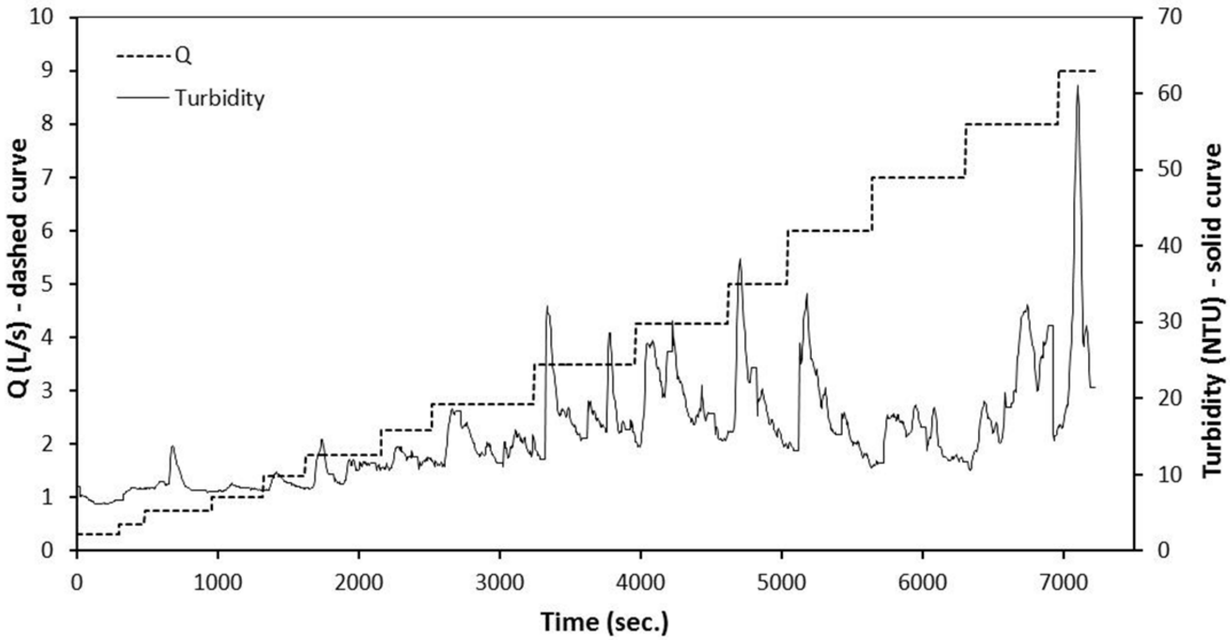

Figure 40: Field data from Site 6A

The threshold between no erosion and erosion was achieved at very low bed shear stresses, in the discharge interval between Q_{flume} = 0.5 L/s and Q_{flume} = 0.75 L/s; this yields a τ_c of 0.02 Pa. This low value may have been associated with a layer of unconsolidated highly organic "fluff" at the surface, although that was not field-verified in adjacent core samples collected at the site; regardless, with this experimental system, only one value of τ_c can be ascertained. The total sediment mass eroded was 593.3 g. This site corresponds to "SF-9" in Perkey et al. (2014), where the saturated bulk density at 1.20-cm depth was reported as 1.16 g/cm^3. Per Eq. (7), this yields $\rho_{sed,bulk}$ = 0.26 g/cm^3. Using this value with Eq. (6), the total volume eroded during the experiment was 2300 cm^3. The cumulative V_{er} exceeded 1000 cm^3 during the interval with Q_{flume} = 6 L/s. Data obtained for Q_{flume} > 6 L/s are plotted, but were not utilized in the curve-fitting due to the uncertainty in the $\tau_{b,R}$ estimate as described in section 3.3.

During the erosion portion of the test, two suspended sediment samples were collected:

- At Q_{flume} = 3.5 L/s, 31.1% of the sediment mass volatilized at 550 °C
- At Q_{flume} = 6.0 L/s, 22.5% of the sediment mass volatilized at 550 °C

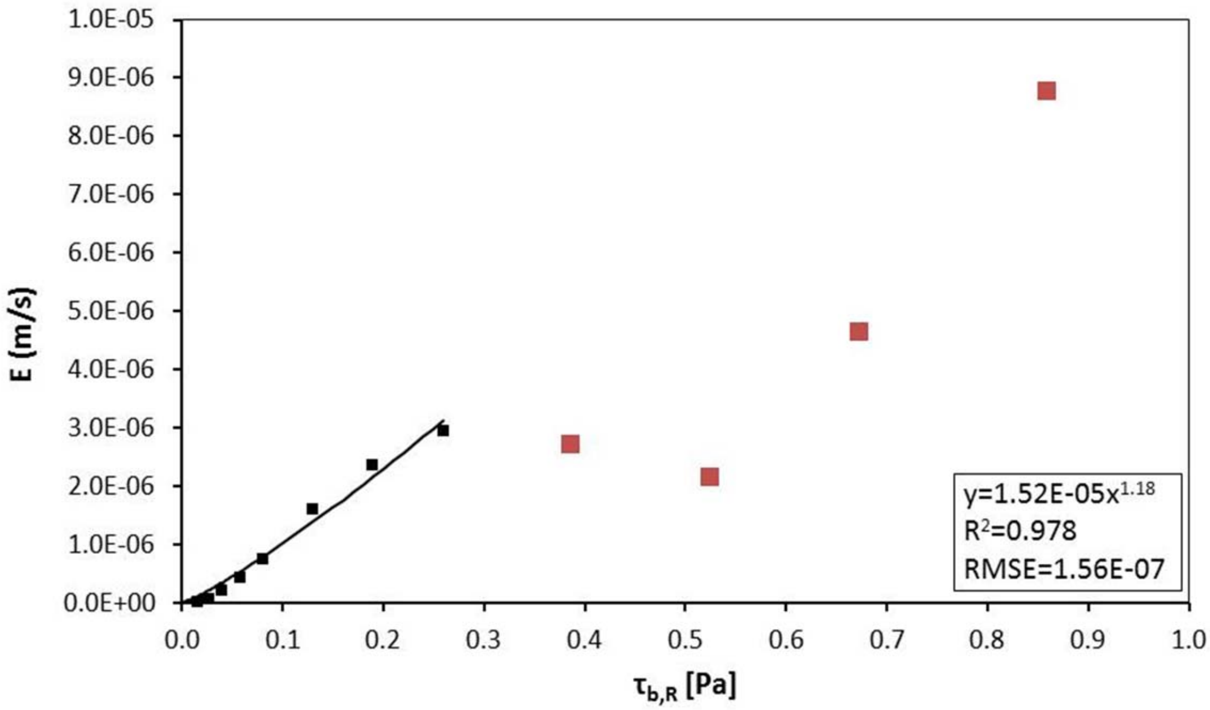

Figure 41: Analysis of field data from Site 6A

Site 6B:

The field data showing the time series of flow rates and turbidity at Site 6B are shown in Figure 42.

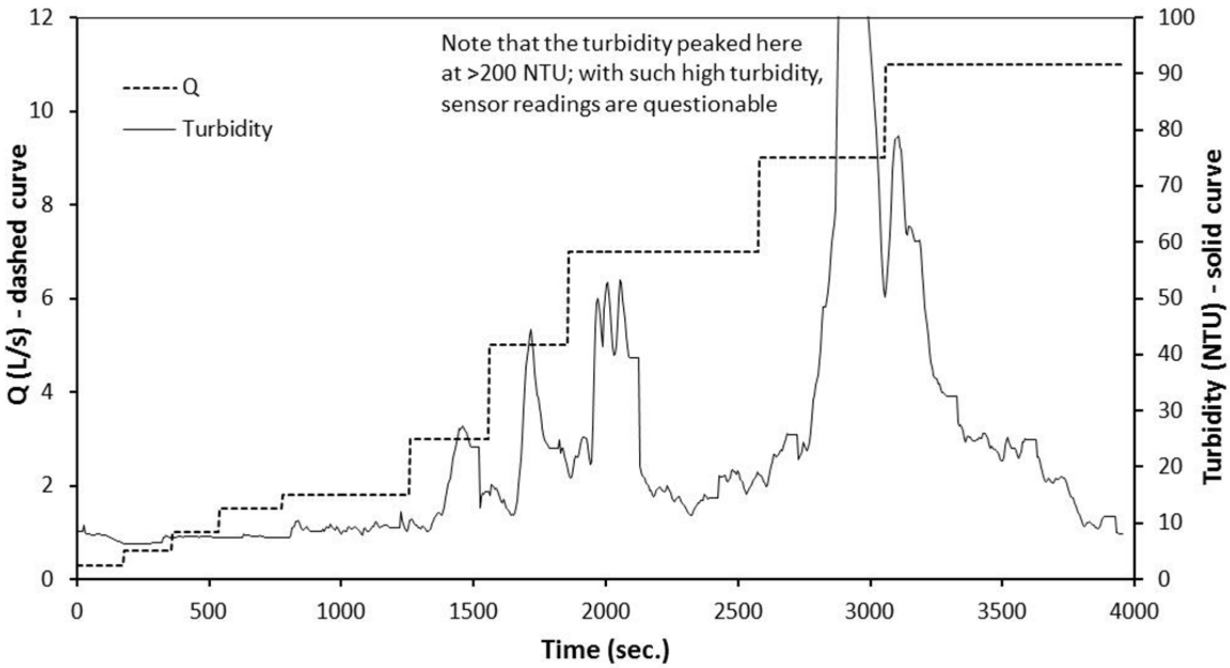

Figure 42: Field data from Site 6B

The threshold between no erosion and erosion was crossed in the discharge interval between Q_{flume} = 1.5 L/s and Q_{flume} = 1.8 L/s; this yields a τ_c of 0.11 Pa. The total sediment mass eroded was 1210 g. This site corresponds to "SF-9" in Perkey et al. (2014), where the saturated bulk density at 1.20-cm depth was reported as 1.16 g/cm^3. Per Eq. (7), this yields $\rho_{sed,bulk}$ = 0.26 g/cm^3. Using this value with Eq. (6), the total volume eroded during the experiment was 4700 cm^3. The cumulative V_{er} exceeded 1000 cm^3 during the interval with Q_{flume} = 7 L/s. Data obtained for Q_{flume} > 7 L/s are plotted, but were not utilized in the curve-fitting due to the uncertainty in the $\tau_{b,R}$ estimate as described in section 3.3.

During the erosion portion of the test, one suspended sediment sample was collected:

- At Q_{flume} = 6.0 L/s, 22.1% of the sediment mass volatilized at 550°C

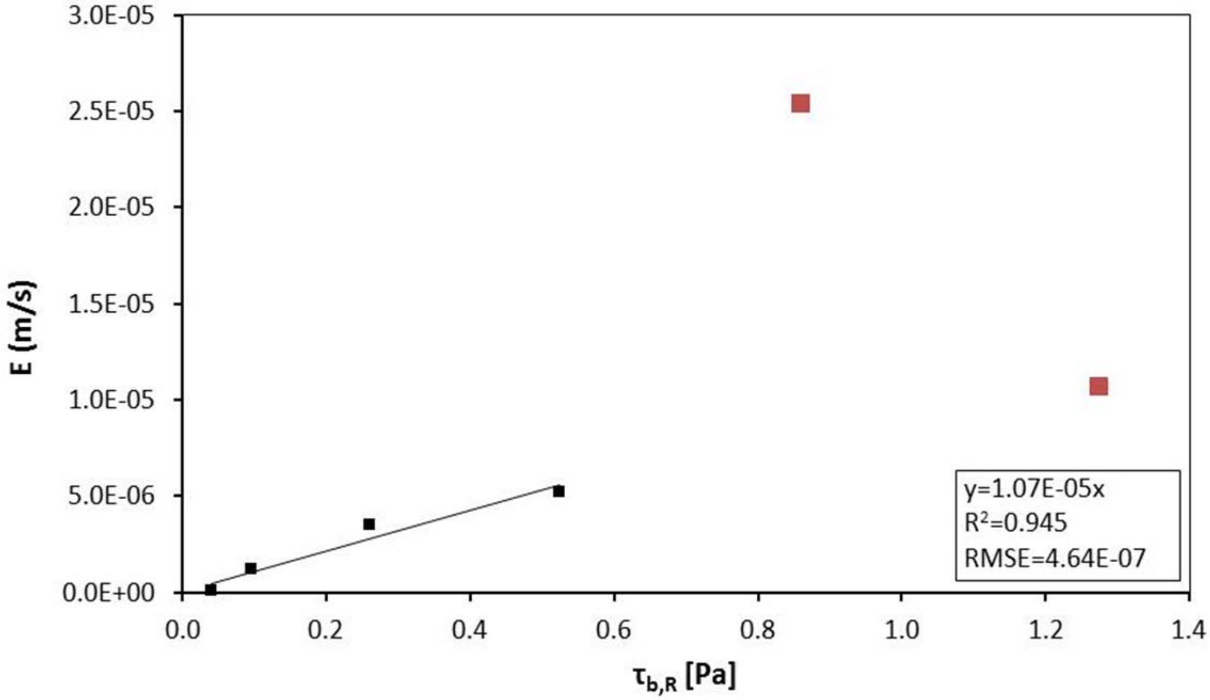

Figure 43: Analysis of field data from Site 6B

The best-fit curve according to the minimum root mean square error (RMSE) yielded an exponent of 0.83; that curve had an RMSE of 3.81E-07. As described for Site 2, an exponent <1 is not encountered in the literature and suggests an experimental artifact, which in this case is most likely the progressive over-estimation of $\tau_{b,R}$ once the bed geometry is modified during erosion. The exponent was consequently set to 1.0, which yielded only a slightly higher RMSE (1.59E-07) than the original fitted curve.

Results Synopsis:

In Appendix D, the raw data illustrated in the figures for all of the sample sites is summarized in tabular format. The following Table 2 summarizes the most important properties and erodibility parameters determined from the field data analysis. The variables D_{16}, D_{50}, and D_{84} indicate the grain size from a sediment core such that 16, 50, and 84 percent of the sediment mass, respectively, have grain-size finer than the identified value. When more than one layer was identified in the core, the values reported in the table indicate the upper-most layer. All other variables in Table 2 have been previously defined.

Table 2: Summary of Experimental Results

Site ID	D_{16} (µm)	D_{50} (µm)	D_{84} (µm)	% Organic (range) ①	$\rho_{sed,bulk}$ (g/cm^3) ②	$\rho_{sed,bulk}$ (g/cm^3) ③	τ_c (Pa)	A ④	n ⑤
2	33	90	250	32.3	0.21	0.43	0.14	2.22×10^{-6}	1
3	8	33	86	26.9 - 29.4	0.12	0.24	<0.01	1.97×10^{-5}	1
4‡	34 22	108 62	268 165	29.6 - 48.9	0.30 0.22	0.26	0.14	6.84×10^{-6}	1.48
5A	x	x	x	23.7 - 40.1	x	0.32	0.15	8.16×10^{-6}	1.07
5B	29	79	185	23.9 - 24.5	0.28	0.32	0.15	1.73×10^{-5}	2.75
6A	74	135	229	22.5 - 31.1	0.63	0.26	0.02	1.52×10^{-5}	1.18
6B	51	129	235	22.1	0.30	0.26	0.11	1.07×10^{-5}	1

①: The % organic matter was analyzed from suspended sediment samples collected during the erosion test. The reported value is not intended to represent the percent organic matter of the entire core; it only represents the percent organic matter from the near-surface layer that eroded.

②: The first $\rho_{sed,bulk}$ reported is the dry bulk density calculated from measurement of the entire core sample (approximately 19-in. deep) collected by UIUC. The near-surface bulk density is expected to be lower than the mean value represented by the reported measurement.

③: The second $\rho_{sed,bulk}$ reported is calculated using Eq. (6) based on the wet bulk density (ρ_{sat}) from the uppermost sample of the associated core reported by the USACOE (Perkey et al., 2014).

④: A is the coefficient of proportionality in Eq. (2b): $E = A\tau_b^n$. Because n varies, A is dimensionally inconsistent. The reported value of A is based on E expressed in m/s and τ_b expressed in Pa.

⑤: n values were specified as equal to 1 when curve-fitting yielded $n < 1$.

‡ : Two cores were obtained and analyzed from Site 4 as reported in Appendix A; the first value in the table is from the core collected on the day of in situ flume testing; the second value reported is from the core collected on the previous day during reconnaissance.

Chapter 5: SUMMARY

Field tests were implemented with an *in situ* flume on the Kalamazoo River in November 2013. Critical bed shear stresses (τ_c) were quantified and erosion rates (E) were determined as a function of the applied bed shear stress (τ_b). Erosion rates were ascertained by calculating sediment mass flux using the recorded time series of turbidity and flume discharge rates (Q_{flume}). The bed shear stresses in the erosion section of the flume were determined for the full range of Q_{flume} values using computational fluid dynamics (CFD) modeling.

The field tests revealed that typical values of the critical bed shear stress (τ_c) were between 0.10 and 0.15 Pa. Such values are typical of an unconsolidated sediment bed; the low dry bulk densities measured from the sediment cores provided additional evidence of unconsolidated conditions within the soft-sediment depositional areas. The sediment was generally dominated by the coarse silt and fine sand components and contained abundant organic matter. Following initiation of erosion, the data was fitted to the erosion equation (2b), consistent with Perkey et al. (2014). For curve-fitting to the erosion equation, the area-weighted average bed shear stress within the flume erosion section ($\tau_{b,R}$) was used, and the assumption was made that the entire bed area of the flume erosion section experienced erosion; this is consistent with accepted methods of past *in situ* flume analyses such as in Ravens and Gschwend (1999). The determination was made that unacceptable error in the $\tau_{b,R}$ estimate was obtained when the cumulative eroded sediment volume (V_{er}) exceeded 1000 cm^3 at a sample station; the error is associated with modifications to the hydrodynamics not taken into account when applying the CFD model using the initial bed geometry. As such, only the points obtained with cumulative V_{er} < 1000 cm^3 were utilized in the curve-fitting to parameterize the erosion equation. The data points deemed valid involved τ_b values between 0 and 0.67 Pa, although some sample sites exceeded the V_{er} = 1000 cm^3 threshold well before achieving τ_b = 0.67 Pa.

Erosion rates (E) were less than or equal to 5.8 x 10^{-6} m/s at each sample site for all data points with V_{er} < 1000 cm^3. Applying the fitted erosion rate functions at each site to a common value of τ_b = 0.4 Pa (a τ_b value tested on each of the cores in Perkey et al. (2014)) yields values for E between 8.9 x 10^{-7} and 7.9 x 10^{-6} m/s. The erosion rate functions obtained from the current study should not be extended to τ_b values much beyond the range of the field-tested $\tau_{b,R}$. Discernible variability was observed in erosional behavior at closely spaced sample stations as observed at Site 5 in Morrow Lake and Site 6 further upstream from the delta.

ACKNOWLEDGMENTS

The staff at the University of Illinois Ven Te Chow Hydrosystems Laboratory (VTCHL) would like to thank Jacob Hassan of EPA, Rex Johnson of GRT, and Faith Fitzpatrick of the USGS Wisconsin Water Science Center for project funding, logistical support, and coordination (respectively). Specifically, Rex Johnson of GRT/START is acknowledged for assistance with all aspects of the field work and for providing guidance based on detailed site-specific knowledge of the Kalamazoo River and the ongoing Enbridge field operations. Paul Reneau of the USGS Wisconsin Water Science Center provided the water quality sampling system, instructions for its proper usage, and assistance in trouble-shooting the in situ flume during the initial portion of the field testing.

The following staff and students of the VenTe Chow Hydrosystems Laboratory provided much appreciated assistance during various phases of this project. Andrew Waratuke, lab manager of VTCHL, constructed the flume and provided assistance during the design stage. Zhenduo Zhu and Nicholas Moller assisted with the entire field sampling effort, which included extensive after-hours work in modifying and retrofitting the flume. The field work would not have been successful without their diligent and skillful efforts.

REFERENCES

ANSYS, Inc. (2014), *ANSYS Fluent 14.5 Documentation Manual*, available on-line: http://www.ansys.com

Ariathurai, C. R. (1974). A finite element model for sediment transport in estuaries. Ph.D. Thesis, University of California, Davis.

Engelund, F., and Hansen, E. (1967). *A Monograph on Sediment Transport in Alluvial Streams*. Teknisk Vorlag, Copenhagen, Denmark, 1967.

Garcia, M.H., (2008). "Sediment Transport and Morphodynamics", Chapter 2 ASCE Manual of Practice 110, *Sedimentation Engineering: Processes, Measurements, Modeling and Practice*. Garcia, M.H. (ed). American Society of Civil Engineers. Reston, VA.

Grissinger, E. H., Little, W. C., and Murphey, J. B. (1981).Erodibility of streambank materials of low cohesion.*Transactions of the ASAE [American Society of Agricultural Engineers]*, 24.

Gust, G. and Morris, M. J. (1989).Erosion thresholds and entrainment rates of undisturbed in situ sediments.*Journal of Coastal Research*, 87-99.

Hoard, C.J., Fowler, K.K., Kim, M.H., Menke, C.D., Morlock, S.E., Peppler, M.C., Rachol, C.M., and Whitehead, C.M. (2010). Flood-inundation maps for a 15-mile reach of the Kalamazoo River from Marshall to Battle Creek, Michigan. *U.S. Geological Survey Scientific Investigations Map 3135*: 6 p. pamphlet, 6 sheets, scale 1:100,000.

Knight, D.W., and Patel, H.S. (1985). Boundary shear in smooth rectangular ducts. *Journal of Hydraulic Engineering*, 111(1), 29-47.

Lick, W. (2009). *Sediment and contaminant transport in surface waters*. CRC Press, Boca Raton, FL.

McAnally, W. H. and Mehta, A. J. (2001). "Preface", *Coastal and estuarine fine sediment processes (Vol. 3)*. McAnally, W. H. and Mehta, A. J. (eds). Gulf Professional Publishing.

McNeil, J., Taylor, C., and Lick, W. (1996). Measurements of erosion of undisturbed bottom sediments with depth, *Journal of Hydraulic Engineering*, 122(6), 316-324.

Patankar, S.V. (1980), *Numerical Heat Transfer and Fluid Flow*, Taylor-Francis.

Perkey, D.W., Smith, S.J., and Kirklin, T. (2014).*Cohesive Sediment Erosion Field Study: Kalamazoo River, Kalamazoo, Michigan. DRAFT DOCUMENT, dated March 17, 2014.* US Army Engineer Research and Development Center, Coastal and Hydraulics Laboratory, Vicksburg, Mississippi.

Ravens, T. M.and Gschwend, P. M. (1999). Flume measurements of sediment erodibility in Boston Harbor. *Journal of Hydraulic Engineering*, 125(10), 998-1005.

Rodi, W. (1980). *Turbulence Models and Their Application in Hydraulics*. State-of-the-Art Paper, International Association of Hydraulic Research, Delft, The Netherlands.

Sequoia Scientific. *LISST-ST Particle Size Analyzer User's Manual*, Version 2.1.

Waterman, D.M., Waratuke, A.R., Motta, D., Cataño-Lopera, Y.A., Zhang, H., and García, M. H. (2011). In situ characterization of resuspended-sediment oxygen demand in Bubbly Creek, Chicago, Illinois. *Journal of Environmental Engineering*, 137(8), 717-730.

Young, R.A. (1977). Seaflume: A device for in-situ studies of threshold erosion velocity and erosional behavior of undisturbed marine muds. *Marine Geology*, 23, M11-M18.

APPENDICES

Appendix A (Core Analysis from *In Situ* Flume sampling)

Appendix B (Flow Equations and Wall Functions in the ANSYS Fluent CFD Model)

Appendix C (Quasi-Morphodynamic Approach for Data Analysis)

Appendix D (Field Data in Tabular Format)

Appendix A

Core Analysis from *In Situ* Flume sampling

Core Summary – In Situ Flume Site 2

Notes:

Core liner is 20.0 inches long; in all cases, it is estimated that approximately 19” was penetrated into the sediment.

After sampling, the sediment settled to the lower 10.25 inches of the liner; the water was decanted from the top, and the top of the core was cut off; the remainder is what is shown in the photo. The ruler end (0”) is at the bottom of the core.

Only 2 layers were readily discernible; distinguished mainly by the degree of consolidation; both have mucky silt loam texture; lots of undecomposed organic debris in both layers, but slightly moreso in the upper layer.

During grain size analysis, the majority of the material >= 250 µm were pieces of organic material; the portion <= 149 µm was predominantly mineral sediment grains.

Grain size distributions:

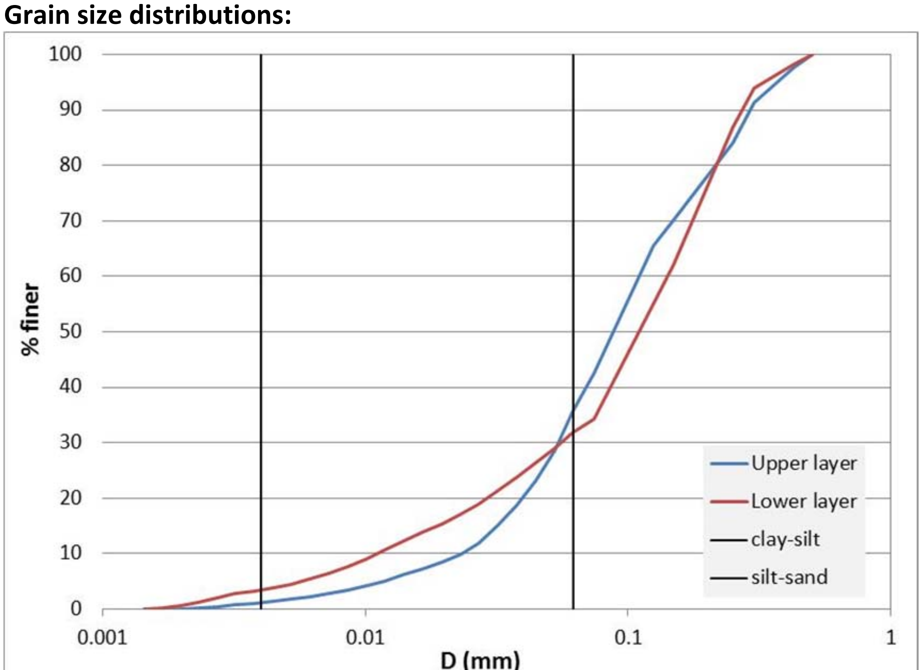

Dry Bulk Density Information:

Upper layer: 45.8 grams
Lower layer: 126.0 grams
Residue: 9.5 grams

Total dry mass: 181.3 grams
Sediment volume: 855 cm^3

Bulk density = 0.212 g/cm^3

Porosity ≈ 0.920

Core Summary – In Situ Flume Site 3

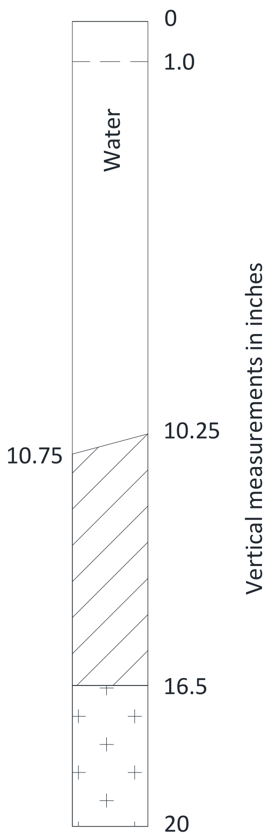

Notes:

Core liner is 20.0 inches long; in all cases, it is estimated that approximately 19” was penetrated into the sediment.

Water was decanted from the upper part of the core and the top of the core then cut off; the bottom of the core is at the bottom of the photo (20”).

Two layers were weakly discernible. The upper layer (10.5 to 16.5”) is mucky silt loam with lots of undecomposed organic debris. The lower layer (16.5 to 20”) is of the same texture but is a little more consolidated. Both layers are very soupy.

During sieve analysis, a lot of the material retained on the 125µm sieve and larger were pieces of organic material

Grain size distributions:

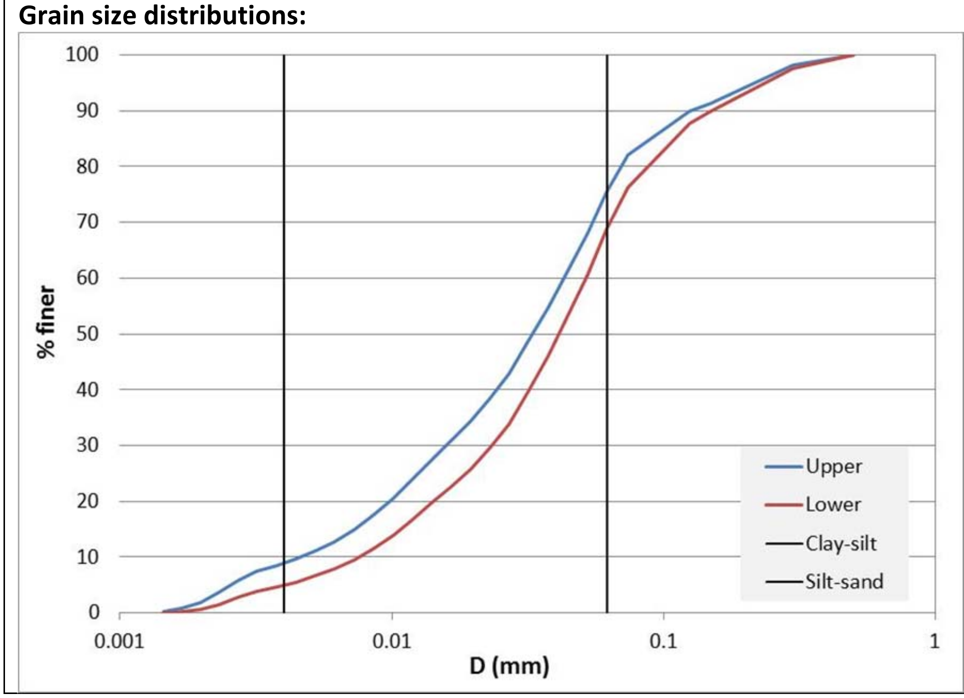

Dry Bulk Density Information:

Upper layer: 66.5 g
Lower layer: 35.7 g
Residue: 4.2 g

Total dry mass: 106.4 g
Sediment volume: 855 cm^3

Bulk density = 0.124 g/cm^3

Porosity ≈ 0.953

Core Summary – In Situ Flume Site 4 (day of sampling)

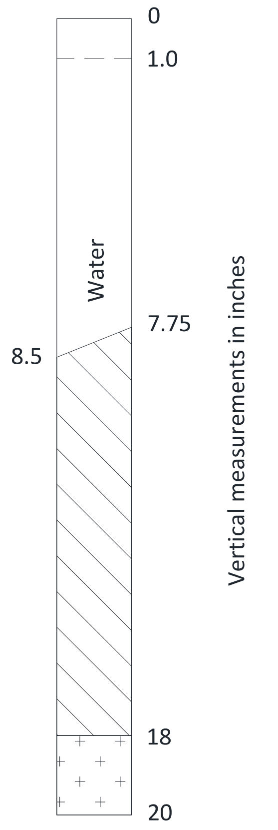

Notes:

Core liner is 20.0 inches long; in all cases, it is estimated that approximately 19” was penetrated into the sediment.

Water was decanted from the upper part of the core and the top of the core then cut off; the bottom of the core is at the bottom of the photo (20”).

Two layers were discernible; the upper layer (8 to 18”) is mucky silt loam with lots of undecomposed organic debris; the lower layer (18 to 20”) is fairly stiff silty clay loam

Grain size distributions:

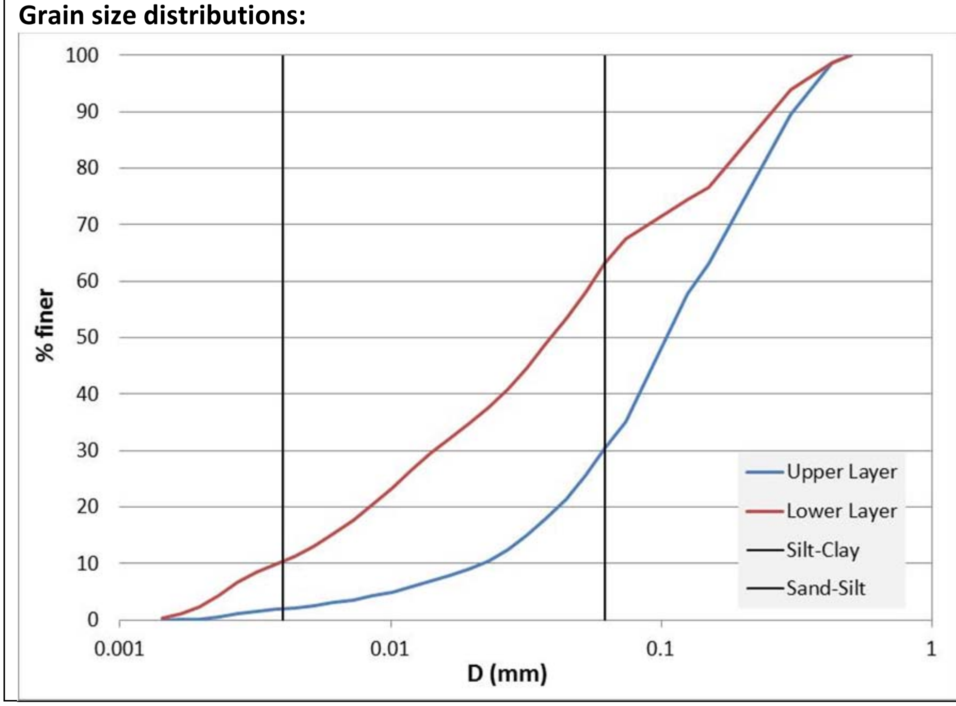

Dry Bulk Density Information:

Upper layer: 186.6 g
Lower layer: 62.9 g
Residue: 10.8 g

Total dry mass: 260.3 g
Sediment volume: 855 cm^3

Bulk density =0.304 g/cm^3

Porosity ≈ 0.885

Core Summary – In Situ Flume Site 4 (recon)

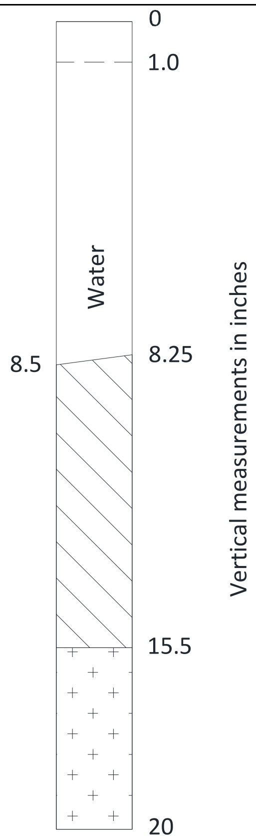

Notes:

Core liner is 20.0 inches long; in all cases, it is estimated that approximately 19" was penetrated into the sediment.

Water was decanted from the upper part of the core and the top of the core then cut off; the bottom of the core is at the bottom of the photo (20").

Two layers were discernible; the upper layer (8.25 to 15.5") is mucky silt loam with lots of undecomposed organic debris; the lower layer (15.5" to 20") is of similar texture but noticeably more consolidated

Grain size distributions:

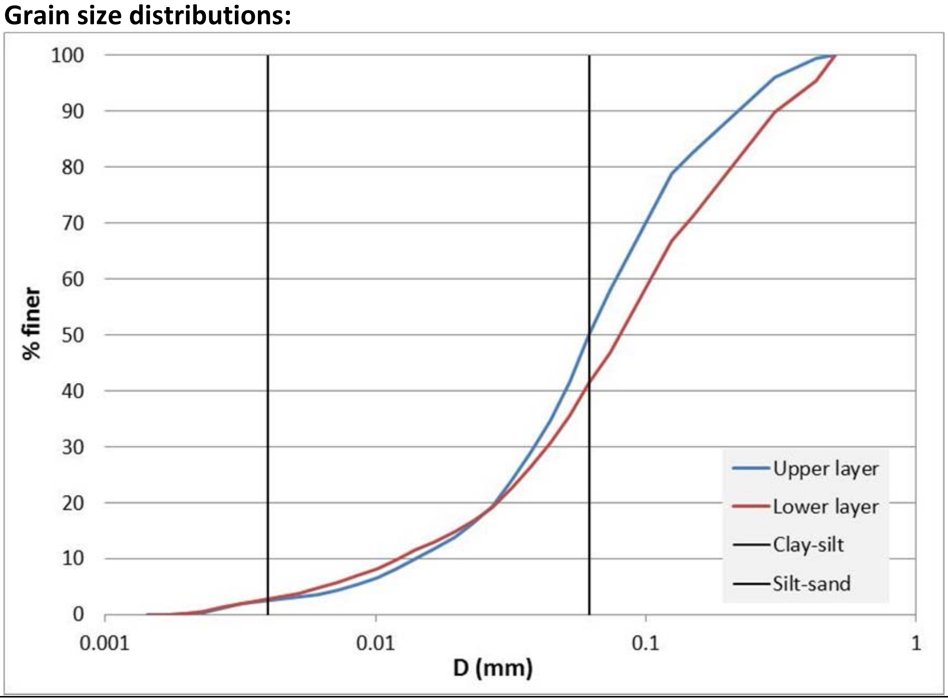

Dry Bulk Density Information:

Upper layer: 87.8 g
Lower layer: 96.7 g
Residue: 5.3 g

Total dry mass: 189.8
Sediment volume: 855 cm^3

Bulk density = 0.222 g/cm^3

Porosity ≈ 0.916

Core Summary – In Situ Flume Site 5B

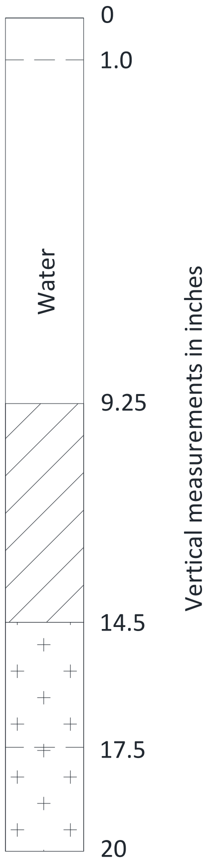

Notes:

Core liner is 20.0 inches long; in all cases, it is estimated that approximately 19” was penetrated into the sediment.

Water was decanted from the upper part of the core and the top of the core then cut off; the bottom of the core is at the bottom of the photo (20”).

Two layers were discernible. The upper layer (9.25 to 14.5”) is mucky silt loam with minimal discernible sand component. The lower layer (14.5 to 20”) is similar to the upper layer, but is more consolidated; it feels like the clay increases with depth, and the bottom of the layer has substantial sand component.

Grain size distributions:

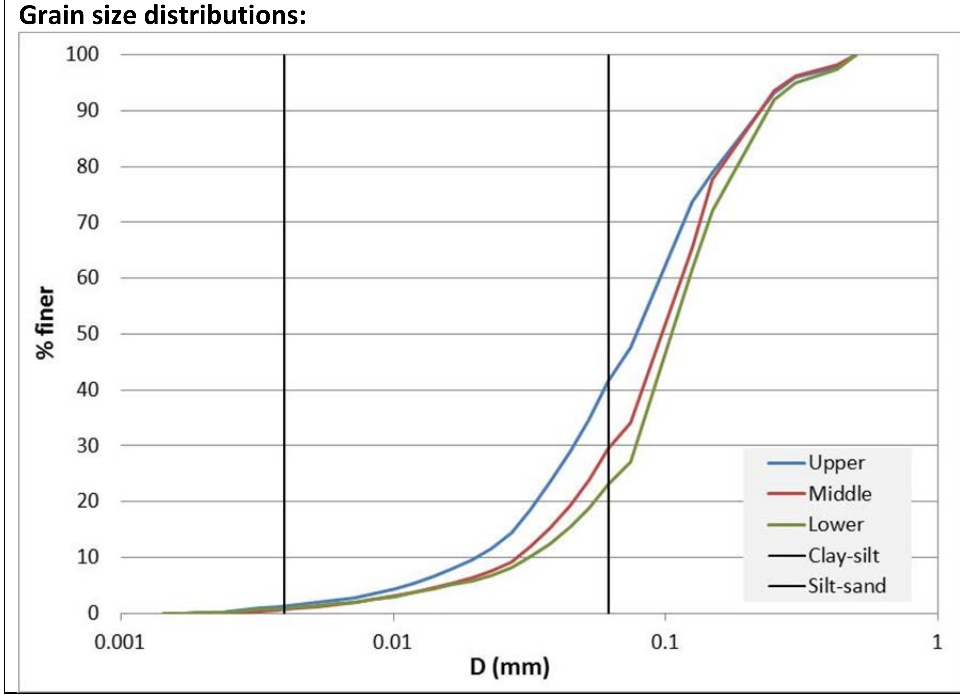

Dry Bulk Density Information:

Upper layer: 76.1 g
Middle layer: 60.2 g
Lower layer: 91.4 g
Residue: 12.6 g

Total dry mass: 240.3 g
Sediment volume: 855 cm^3

Bulk density = 0.281 g/cm^3

Porosity ≈ 0.893

Core Summary – In Situ Flume Site 6

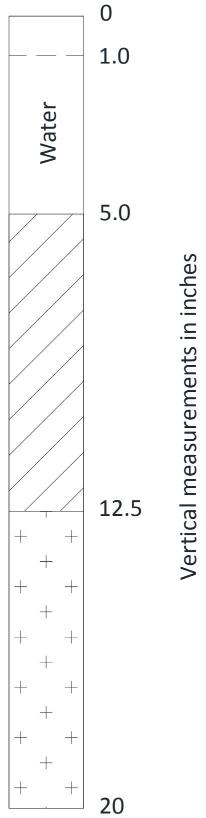

Notes:

Core liner is 20.0 inches long; in all cases, it is estimated that approximately 19” was penetrated into the sediment.

Water was decanted from the upper part of the core and the top of the core then cut off; the bottom of the core is at the bottom of the photo (20”).

Two layers were discernible. The upper layer (5 to 12.5”) is slightly sticky, mucky silt loam with seams of pure sand. The lower layer (12.5 to 20”) is mucky loam; sand feels coarser; some gravel (5 -12mm) at the base of the layer.

Grain size distributions:

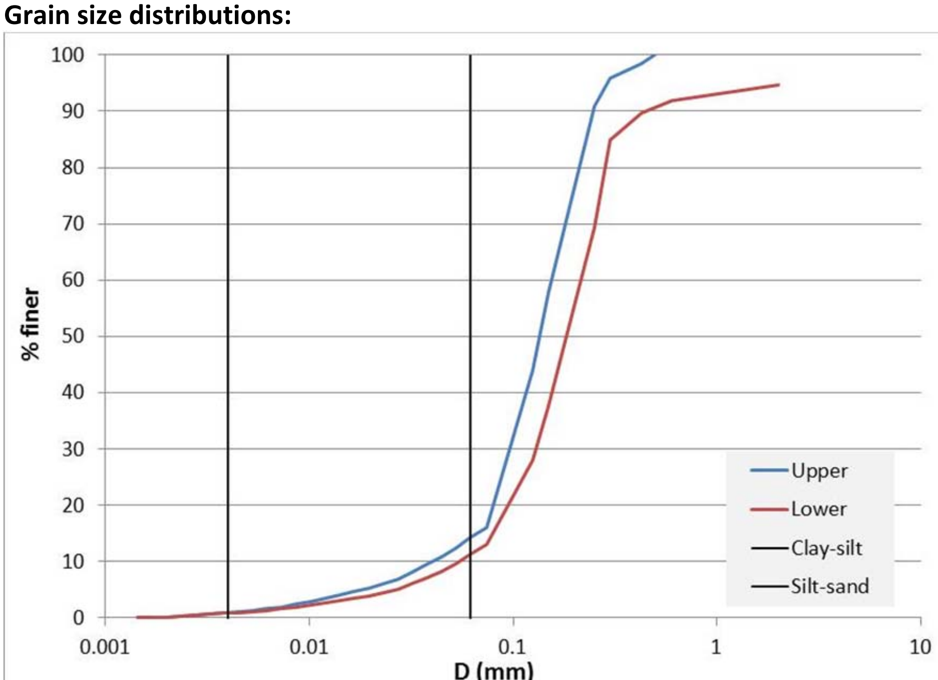

Dry Bulk Density Information:

Upper layer: 169.7 g
Lower layer: 341.1 g
Residue: 27.4 g

Total dry mass: 538.2 g
Sediment volume: 855 cm^3

Bulk density = 0.629 g/cm^3

Porosity ≈ 0.762

Core Summary – In Situ Flume Site 6B

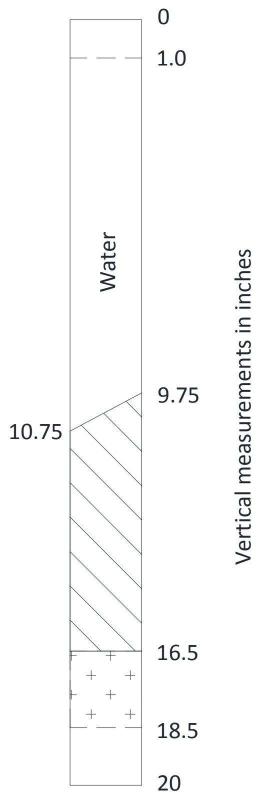

Notes:
Core liner is 20.0 inches long; in all cases, it is estimated that approximately 19” was penetrated into the sediment. In this case, we also used a bottom core-catcher; therefore approximately the bottom 1.5 inches of sediment was not retreived with the core – ie, left outside the catcher.

After sampling, the sediment settled to the lower 10.25 inches of the liner; the water was decanted from the top, and the top of the core was cut off; the remainder is what is shown in the photo. The bottom of the core is at the bottom of the photo.

Only 2 layers were discernible; the upper layer is mucky loam; lots of undecomposed organic matter; the lower layer was characterized as mucky loam to sandy loam; higher percent sand than above.

During grain size distribution, the portion >= 250 µm was predominantly organic debris; the portion <= 149 µm was predominantly mineral sediment grains

Grain size distributions:

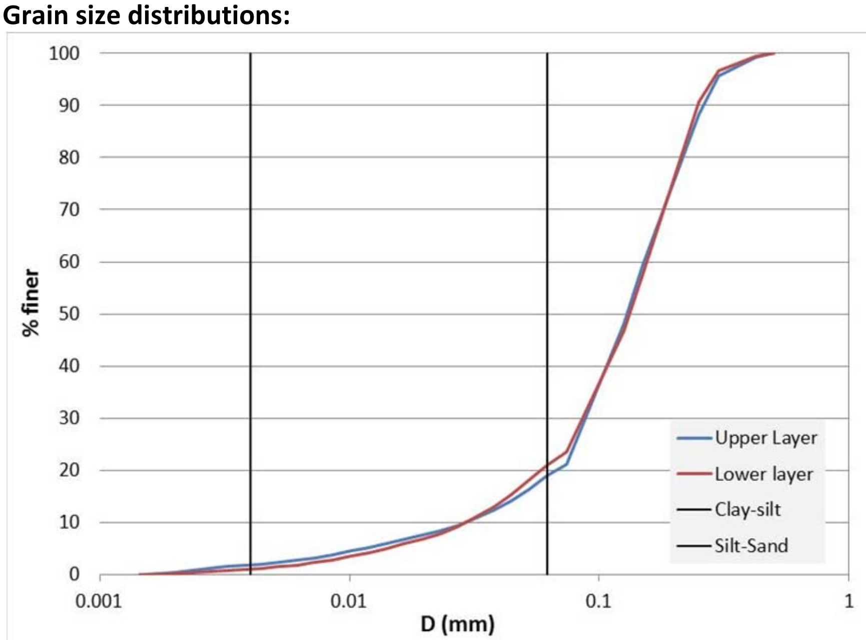

Dry Bulk Density Information:
Upper layer: 144.2 g
Lower layer: 71.3 g
Residue: 23.7 g

Total dry mass: 239.2 grams
Sediment volume: 788 cm^3

Bulk density = 0.304 g/cm^3

Porosity ≈ 0.885

Appendix B

Flow Equations and Wall Functions in the ANSYS Fluent CFD Model

Flow Equations:

For the turbulent flow the following RANS equations were solved (ANSYS, 2014), where Eq. (B1) is the continuity equation and Eq. (B2) is the momentum equation:

$$\frac{\partial(\rho u_i)}{\partial x_i} = 0 \tag{B1}$$

$$\frac{\partial(\rho u_i u_j)}{\partial x_j} = -\frac{\partial p}{\partial x_i} + \frac{\partial}{\partial x_j}\left[\mu\left(\frac{\partial u_i}{\partial x_j} + \frac{\partial u_j}{\partial x_i} - \frac{2}{3}\delta_{ij}\frac{\partial u_i}{\partial x_i}\right)\right] + \frac{\partial}{\partial x_j}\left(-\rho\overline{u_i^{'}u_j^{'}}\right) + \rho g_i \tag{B2}$$

Where i = 1 to 3 and j = 1 to 3 are index notation where 1 represents the X direction, 2 represents the Y direction, and 3 represents the Z direction; index notation allows Eq. (B1) and Eq. (B2) to be expressed in this concise form instead of the resulting three separate equations for Eq. (B1) and nine separate equations for Eq. (B2) when expanded and written in terms of the X, Y, and Z coordinates; ρ is the density [kg/m^3], u_i is the mean velocity component parallel to the i coordinate [m/sec], p is the pressure [Pa], μ is the molecular/dynamic viscosity [Pa sec], δ_{ij} is the Kronecker's delta, $\rho\overline{u_i^{'}u_j^{'}}$ is the Reynolds' stress term and g_i is the gravity acceleration component parallel to the i coordinate [m/sec^2].

For the closure of the set of equations, the Reynolds' stresses were approximated using the standard two-equation k-ε turbulence model (ANSYS, 2014). According to the standard k-ε model both turbulence kinetic energy (k) and its dissipation rate (ε) were simulated using two semi-empirical transport equations. The turbulence kinetic energy was calculated using the following transport equation:

$$\frac{\partial(\rho k u_i)}{\partial x_i} = \frac{\partial}{\partial x_i}\left[(\mu + \frac{\mu_t}{\sigma_k})\frac{\partial k}{\partial x_i}\right] + G_k + \rho\varepsilon \tag{B3}$$

where G_k is the turbulence kinetic energy production due to the mean velocity gradients, μ_t is the turbulent (or eddy) viscosity, σ_k is the turbulent Prandtl number for k and ε is the turbulence kinetic energy rate of dissipation calculated using the following transport equation:

$$\frac{\partial(\rho\varepsilon u_i)}{\partial x_i}=\frac{\partial}{\partial x_i}\left[(\mu+\frac{\mu_t}{\sigma_\varepsilon})\frac{\partial\varepsilon}{\partial x_i}\right]+C_{1\varepsilon}G_k-C_{2\varepsilon}\rho\frac{\varepsilon^2}{k} \tag{B4}$$

where $C_{1\varepsilon}$ and $C_{2\varepsilon}$ are constants and σ_ε is the turbulent Prandtl number for ε.

The turbulence kinetic energy production (G_k) can be defined as:

$$G_k=-\rho\overline{u_i^{'}u_j^{'}}\frac{\partial u_j}{\partial x_i} \tag{B5}$$

In order to estimate the turbulence kinetic energy production (G_k) in a manner consistent with the Boussinesq hypothesis (Rodi, 1980), the following formula can be used:

$$G_k=\mu_t S^2 \tag{B6}$$

where S is the modulus of the mean strain rate tensor calculated as:

$$S\equiv\sqrt{2S_{ij}S_{ij}} \tag{B7a}$$

$$S_{ij}=\frac{1}{2}\left(\frac{\partial u_i}{\partial x_j}+\frac{\partial u_j}{\partial x_i}\right) \tag{B7b}$$

The turbulent viscosity μ_t can be calculated using the following equation:

$$\mu_t=\rho C_\mu\frac{k^2}{\varepsilon} \tag{B8}$$

where C_μ is a constant.

For the solution of the momentum and pressure terms, second order schemes were used for the spatial discretization. For the turbulent quantities, a first order scheme was applied. Finally, the velocity-pressure coupling was achieved using the SIMPLE algorithm (Patankar 1980). Convergence criterion for all the partial differential equations was set to 10^{-6}.

Wall Functions:

Boundary shear stresses are incorporated in the numerical solution through the use of wall functions applied to the grid cells that have one or more faces defined by the wall. For the present ANSYS Fluent simulation, the "standard wall function" approach was used. The wall function approach does not resolve the viscosity-affected viscous sublayer and buffer layer near the wall. This region is modeled using a semi-empirical formula in order to bridge the wall with the fully-turbulent region. The choice of "wall functions" approach reduces the computational resource demands in most high-Reynolds-number flows, as it does not actually resolve the viscous sublayer in which the variables change rapidly.

The ANSYS Fluent standard wall function approach implements the law-of-the-wall in the following form:

$$U^* = \frac{1}{\kappa}\ln(E_0 y^*) \qquad \text{(B9)}$$

where κ is the von Kármán constant (0.4187), E_0 is an empirical constant (=9.793); U^* and y^* are defined as:

$$U^* \equiv \frac{U_P C_\mu^{1/4} k_P^{1/2}}{\tau_b/\rho} \qquad \text{(B10)}$$

$$y^* \equiv \frac{y_P C_\mu^{1/4} k_P^{1/2}}{\mu/\rho} \qquad \text{(B11)}$$

where U_P is the mean velocity of the fluid at point P; k_P is the turbulence kinetic energy at point P; y_P is the distance from point *P* to the wall; and τ_b is the boundary shear stress.

The aforementioned law for the mean velocity is adopted by the ANSYS Fluent solver when $y^* \geq 11.225$. When $y^* < 11.225$ at the wall adjacent cells due to lower grid resolution close to the wall, ANSYS Fluent uses the following laminar stress-strain relationship:

$$U^* = y^* \qquad \text{(B12)}$$

The ANSYS Fluent solver modifies the standard law-of-the-wall for the mean velocity when wall roughness is taken into consideration. Thus the modified law-of-the-wall becomes:

$$U^* = \frac{1}{\kappa}\ln(E_0 y^*) - \Delta B \qquad \text{(B13)}$$

The variable ΔB is a wall roughness modification; its value depends on the non-dimensional roughness height K_s^+ defined as:

$$K_s^+ \equiv \frac{k_s C_\mu^{1/4} k_P^{1/2}}{\mu/\rho} \tag{B14}$$

where k_s is the roughness height. The three different categories for K_s^+ and the corresponding forms for ΔB are as follows:

- Case I: hydrodynamically smooth wall ($K_s^+ \leq 2.25$)

  $$\Delta B = 0$$

- Case II: transition-region wall ($2.25 < K_s^+ \leq 90.0$)

  $$\Delta \text{B} = \frac{1}{\kappa} \ln \left[\frac{K_s^+ - 2.25}{87.75} + C_s K_s^+ \right] \times \sin \left\{ 0.4258 \left(\ln K_s^+ - 0.811 \right) \right\}$$

  where $C_s = 0.5$ is a constant related to the type of the roughness.

- Case III: fully rough wall ($K_s^+ > 90.0$):

  $$\Delta \text{B} = \frac{1}{\kappa} \ln \left(1 + C_s K_s^+ \right)$$

For the first layer of the computational mesh (wall-adjacent cells) the production of the turbulent kinetic energy (G_k) and its dissipation rate (ε) are calculated with the assumption of local equilibrium using the following equations:

$$G_k \approx \tau_b \frac{\partial U}{\partial y} = \tau_b \frac{\tau_b}{\kappa \rho y_P C_\mu^{1/4} k_P^{1/2}} \tag{B15}$$

$$\varepsilon_P = \frac{C_\mu^{3/4} k_P^{3/2}}{\kappa y_P} \tag{B16}$$

The turbulent energy dissipation rate (ε) equation is not solved in the wall-adjacent cells; instead Eq. (B16) is used.

Appendix C

Quasi-Morphodynamic Approach for Data Analysis

Following initial review of the *in situ* flume analysis by project collaborators, the quasi-morphodynamic approach was abandoned in the detailed data analysis; in the absence of additional instrumentation that could verify changing bed morphology during the experiments, the method was deemed to involve excessive uncertainties. However, the results of the quasi-morphodynamic analysis have been used as a means of generating conservative estimates of error in the determination of bed shear stress described in Chapter 3.3 of the report; therefore the approach is described in this appendix.

The bed shear stress field associated with a given Q_{flume} is dependent on the bed geometry. A full morphodynamic model that couples hydrodynamics, sediment transport and changing bed geometry would require a sophisticated numerical model and known values of the parameters in the erosion rate formulation to evaluate bed deformation. However, the parameters are not known; determination of the parameters is the primary purpose of an *in situ* flume study. Therefore a quasi-morphodynamic approach was implemented. In this approach, the condition of the bed geometry is estimated at relevant conditions of specified cumulative sediment volumetric erosion: 0 cm^3 (initial flat geometry), 200 cm^3, 500 cm^3, 1000 cm^3, 2000 cm^3, 3000 cm^3, 4000 cm^3, 5000 cm^3, 6000 cm^3, and 7000 cm^3. Subsequently, when determining the appropriate bed geometry to use in the determination of the bed shear stress field, the cumulative volume of erosion from the system must be evaluated.

The bed configuration at each given condition of eroded volume is dependent on the specific history of flow and bed shear stress that achieved that eroded volume. For example, the bed geometry at 4000 cm^3 eroded would be different if a single Q_{flume} equal to 8 L/s was applied continuously from the starting initial flat-bed condition as compared to an incremental increase of flows from 0.5 L/s up to 8 L/s. Such complexities of history cannot be resolved without a full morphodynamic model applied to each individual test, which is neither possible nor practicable. The approach used to establish the representative bed geometries considers a representative sequence of flows to achieve specified conditions of mass loss. The approach is described as follows:

(1) A representative sediment dry bulk density is obtained from the field data. In the following analysis, that value is 0.1 g/cm^3. (Note that this estimate was implemented as a representative value based on the field core samples reported Appendix A, where a bulk density over the entire sample depth was taken and the surface bulk density was assumed to be approximately half that calculated from the entire core. Following review by project collaborators, the decision was made to use the more depth-resolute bulk density values from the core samples evaluated by Perkey et al. (2014) for the detailed data analysis included in the body of the report. After the

quasi-morphodynamic approach was abandoned, the analysis was consequently not repeated using the modified estimates for the representative bulk density.)

(2) The results of all the field tests are evaluated to determine the Q_{flume} that yielded 20 grams of cumulative sediment mass loss ($Q_{flume,20}$); this represents 200 cm^3 eroded volume. The median value from all test sites is selected as the representative value.

(3) The CFD model is run using $Q_{flume,20}$ applied to the original bed (Geometry 1) to obtain the bed shear stress field.

(4) The bed geometry is modified according to that shear stress field to yield Geometry 2; (the technique for the bed modification is described just afterwards).

(5) The field tests are then evaluated to determine the Q_{flume} that yielded a cumulative 50 grams sediment mass loss ($Q_{flume,50}$), which is associated with 500 cm^3 volume eroded; the median value from all the tests is selected.

(6) The CFD model is run using $Q_{flume,50}$ applied to Geometry 2 to obtain the shear stress field.

(7) The bed geometry is modified according to that shear stress field to obtain Geometry 3.

(8) The process is repeated to obtain all the desired geometries.

Erosion of the bed to a specified volume eroded using the calculated shear stress field is based on the erosion formulation chosen. In this case the Ariathurai-Partheniades formulation is used:

$$E = k_d(\tau_b - \tau_c)^a \qquad \text{(C1)}$$

The value of τ_c is not dependent on the morphodynamic considerations described above; its value is determined using the procedure described in the main body of the report that involves only the initial bed geometry. The typical value of τ_c = 0.14 Pa determined from the field tests is used for the quasi-morphodynamic simulations. The value of the exponent a is generally taken to be equal to 1 in the absence of specific information to indicate otherwise. Therefore the value of a = 1 is used for the quasi-morphodynamic analysis. Eq. (C1) can be written using previously defined variables and the specified parameter values as:

$$\frac{D_{er}}{t_2 - t_1} = \begin{Bmatrix} 0 & \text{if } \tau_b \leq 0.14 \\ k_d(\tau_b - 0.14) & \text{if} \tau_b > 0.14 \end{Bmatrix} \qquad \text{(C2)}$$

For a true morphodynamic model, the time step (t_2 – t_1) should be small during active erosion. For the quasi-morphodynamic case, it is necessary to relax this requirement and evaluate the larger time step required to modify the bed between the starting and ending geometries specified by the representative values selected for the bed volume eroded. Inherent in this assumption is that the shear stress field does not change during the erosion process between the starting and ending bed geometries and that the sediment properties do not change with depth. From Eq. (C2), it follows that:

$$D_{er} = \begin{cases} 0 & \text{if } \tau_b \leq 0.14 \\ k_d \Delta t(\tau_b - 0.14) & \text{if} \tau_b > 0.14 \end{cases} \tag{C3}$$

$$V_{er} = \frac{M_{sed}}{\rho_{sed,bulk}} = \int D_{er} dA \tag{C4}$$

$$\frac{M_{sed}}{\rho_{sed,bulk}} = k_d \Delta t \int^{EA} (\tau_b - 0.14) dA \tag{C5}$$

where the "EA" on the upper limit of the integral indicates integration only over the erosion area (the portion of the bed where $\tau_b > 0.14$). M_{sed} indicates the net sediment mass eroded in the Δt interval under consideration as opposed to the cumulative mass eroded. Using the shear stress distribution from the CFD simulation, the integral can be approximated as a summation over the discrete grid cell areas. The unknown $k_d \Delta t$ is then simply calculated algebraically since all other variables in Eq. (C5) are known. Once $k_d \Delta t$ is calculated, each grid cell of the bed can be modified per Eq. (C3), which specifies that the depth eroded is linearly dependent on the excess shear stress. Note that this is a general solution to yield typical bed geometries representative of different stages of erosion and is not intended to determine or otherwise utilize actual values of $k_d \Delta t$ from the experiments; k_d and Δt vary between sample sites, and the former value is still undetermined.

Additional elaboration on the details of implementing Eq. (C3) to modify successive bed geometries is warranted. The initial erosion geometries are characterized by a scour that begins at the upstream end of the erosion segment of the flume. Subsequent simulations generally yield a peak in the bed shear stress field where the flow first impinges on the bed at the downstream end of the scour hole, which tends to cause the scour hole to expand downstream in successive geometries. Downstream of the first bed shear stress peak, the shear stress field generally had an oscillating character, associated with the complex dynamics of the flow downstream of the impingement point. This shear stress field is valid for an instant in time and the scour would be concentrated in the high shear stress regions. However, such concentration of scour for a prolonged period of time in an oscillating shear stress field is not realistic, as it would subsequently expose nearby areas experiencing less scour to the direct action of the flow. This would be explicitly resolved if Δt was very small and geometry was modified continually. However for the large Δt associated with the quasi-morphodynamic approach, the effect requires special consideration. To mitigate the effect of localized bed shear stress concentrations, the boundary shear stress field was smoothed before implementing the geometric modification per Eq. (C3) to avoid an unrealistically spiky bed surface geometry. The smoothing of the boundary shear stress surface was implemented by calculating average values in the longitudinal direction over the grid cells 1.5 cm upstream and 1.5 cm downstream of each cell. The smoothing of the shear stress field is effectively intended to represent a time average over the large Δt value under consideration. After calculating the new bed geometry surface, any unrealistic spikiness was smoothed in the same manner as the smoothing of the boundary shear stress surface; in other words, the running mean z value was applied to each cell as calculated from the original z values in a 3-cm long window in the longitudinal direction throughout the domain.

The representative sequence of flows to obtain the specified bed geometries used in the quasi-morphodynamic approach is illustrated in Figure B1.

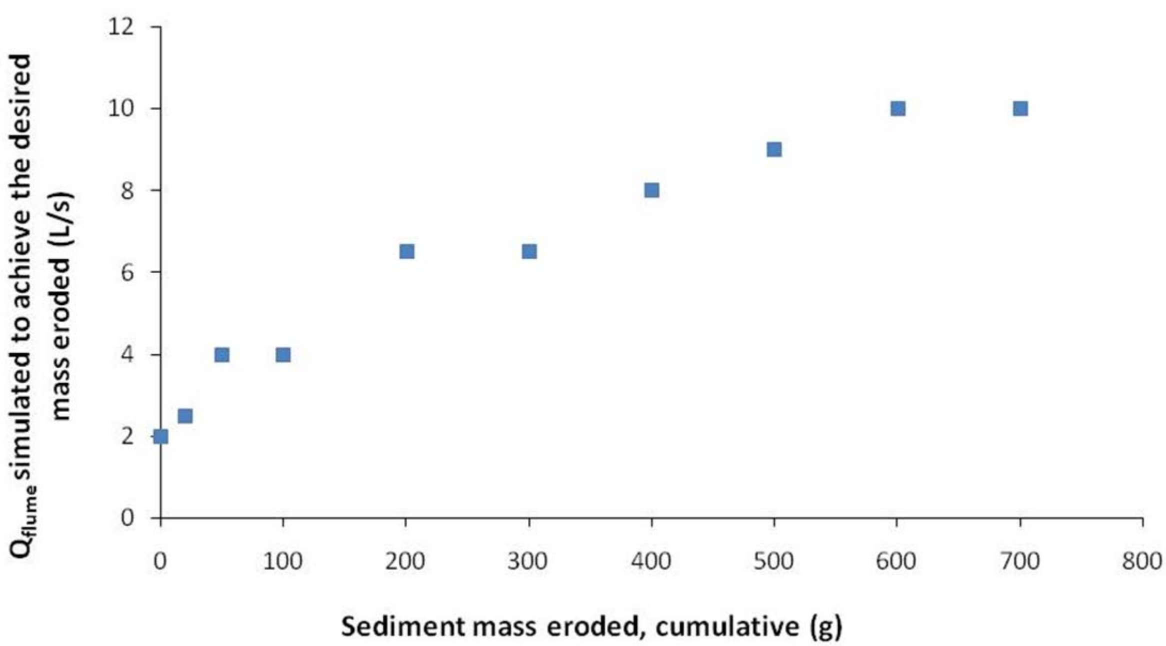

Figure B1: The sequence of flows simulated to achieve the representative bed geometries specified by the cumulative eroded bed volume.

The representative bed geometries obtained are illustrated in Figures B2 through B11.

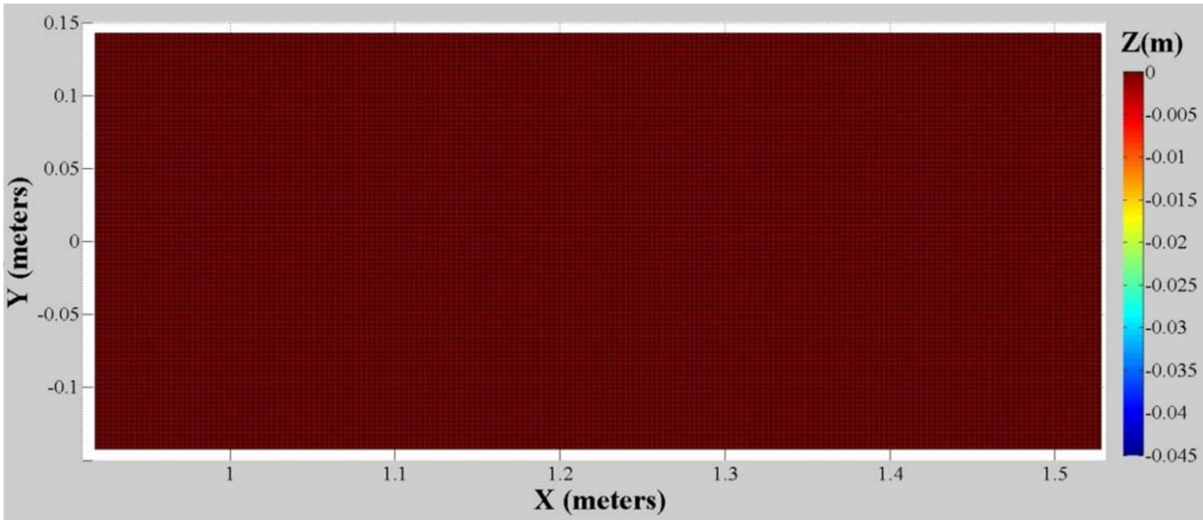

Figure B2: Geometry 1, 0 cm^3 cumulative bed erosion (initial condition)

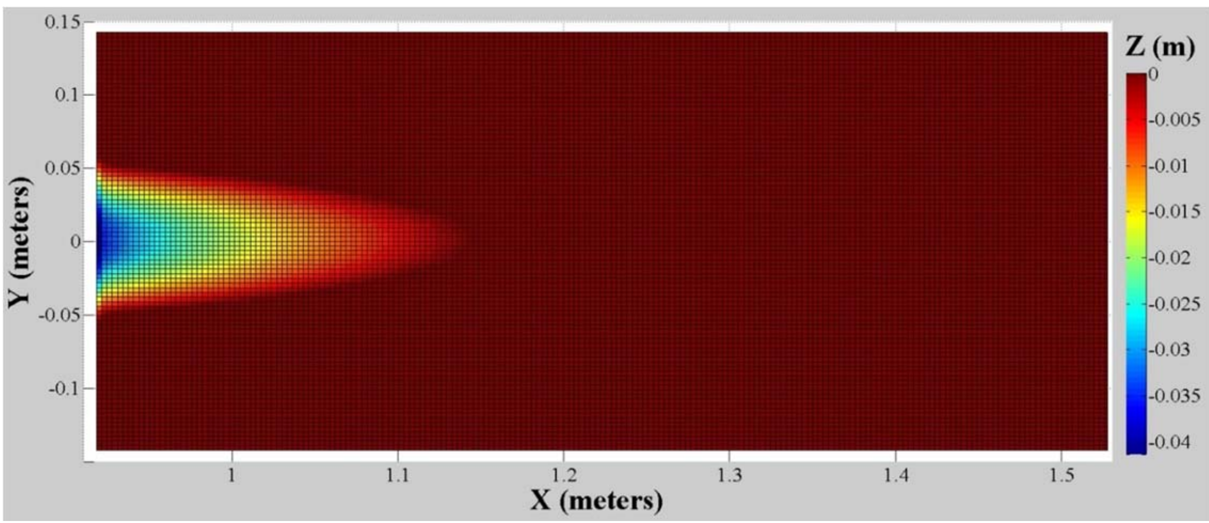

Figure B3: Geometry 2, 200 cm^3 cumulative bed erosion

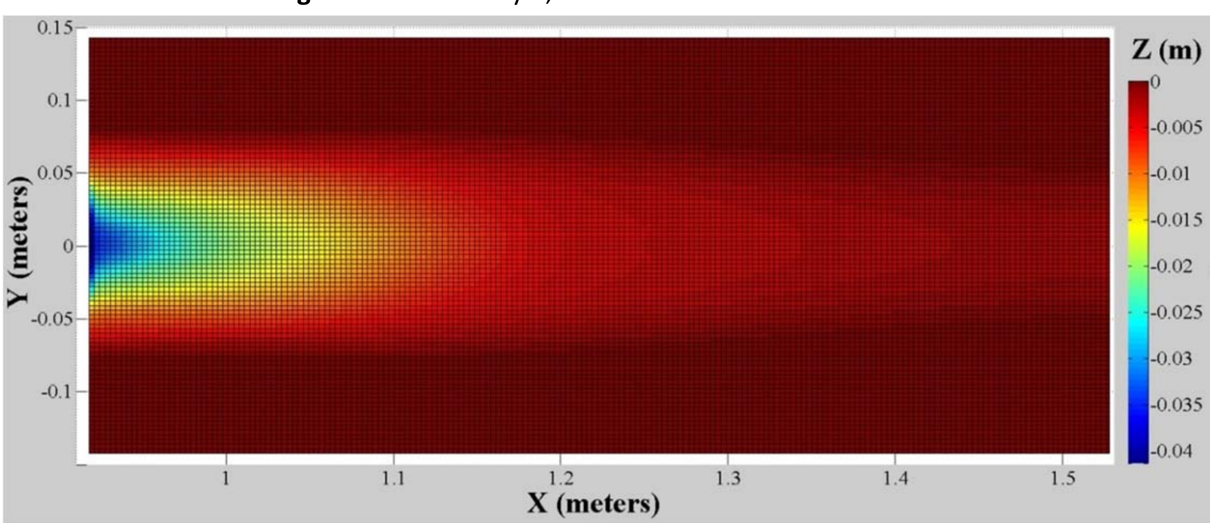

Figure B4: Geometry 3, 500 cm^3 cumulative bed erosion

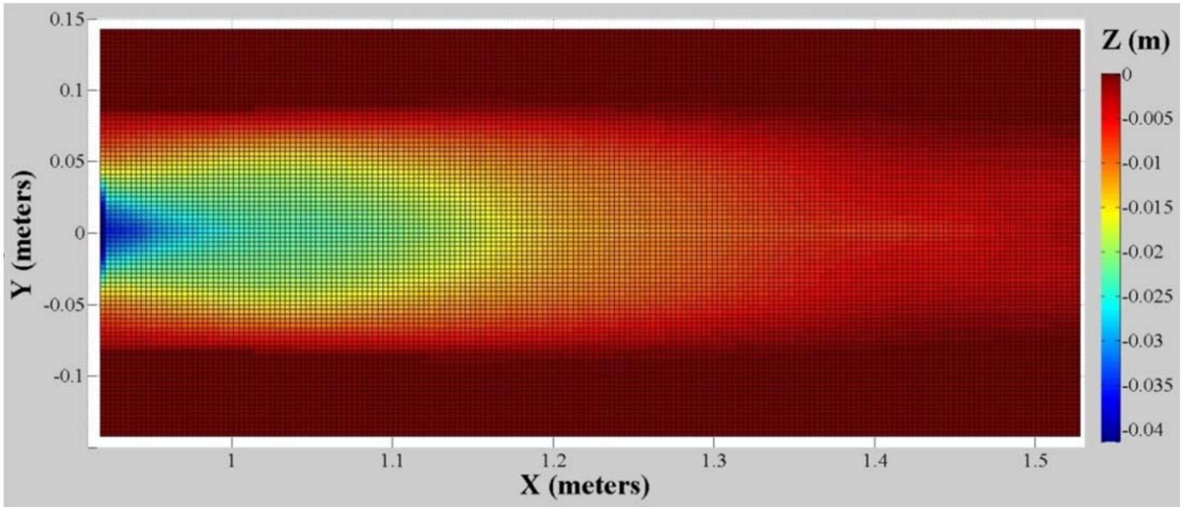

Figure B5: Geometry 4, 1000 cm^3 cumulative bed erosion

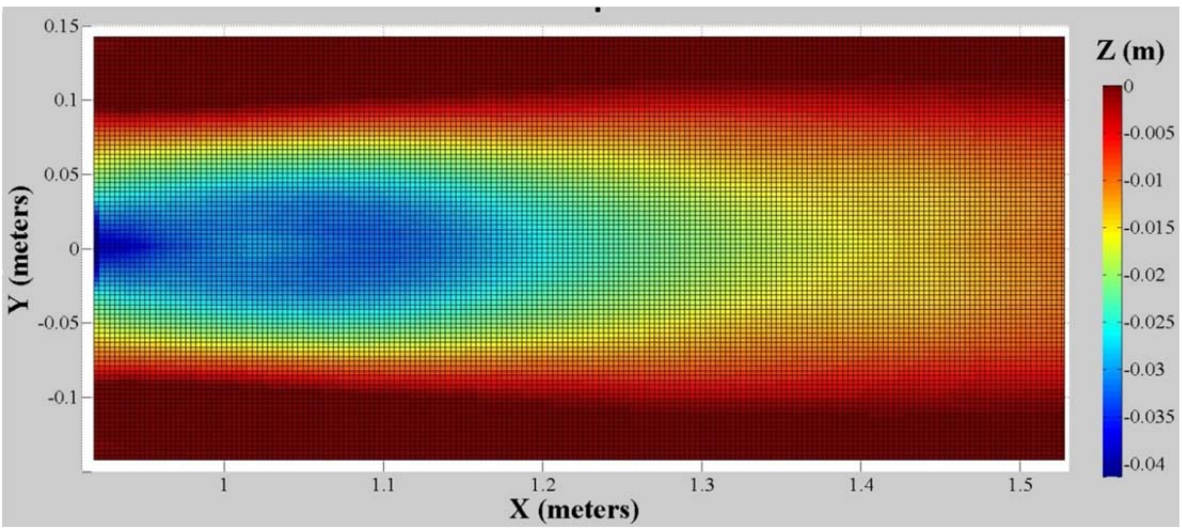

Figure B6: Geometry 5, 2000 cm^3 cumulative bed erosion

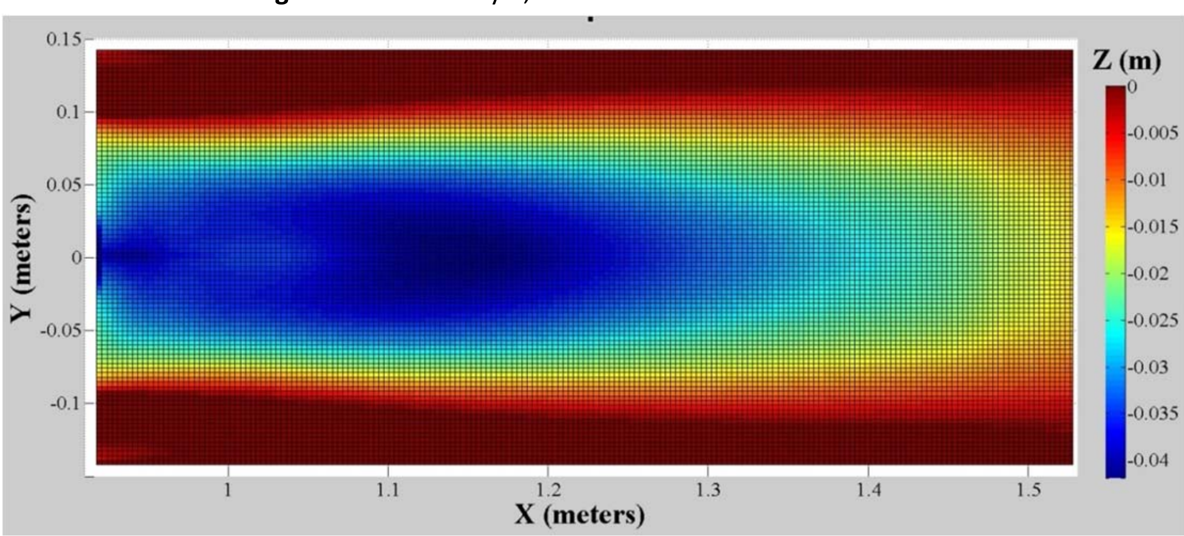

Figure B7: Geometry 6, 3000 cm^3 cumulative bed erosion

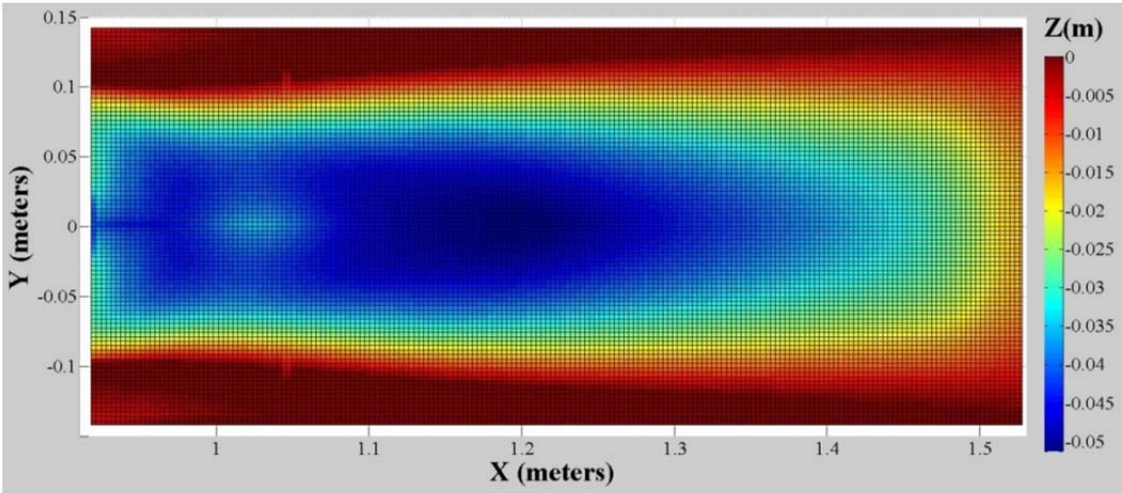

Figure B8: Geometry 7, 4000 cm^3 cumulative bed erosion

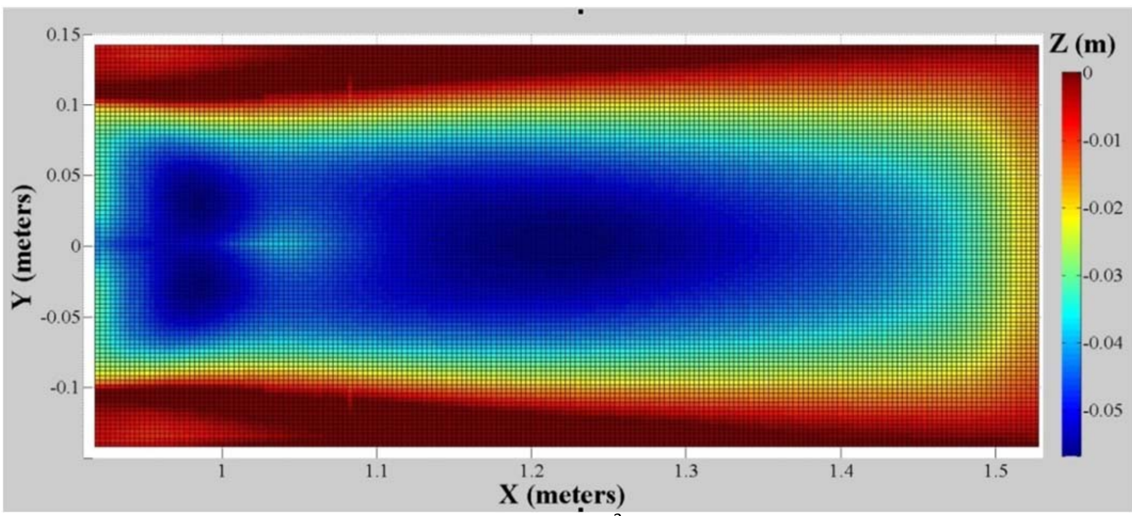

Figure B9: Geometry 8, 5000 cm^3 cumulative bed erosion

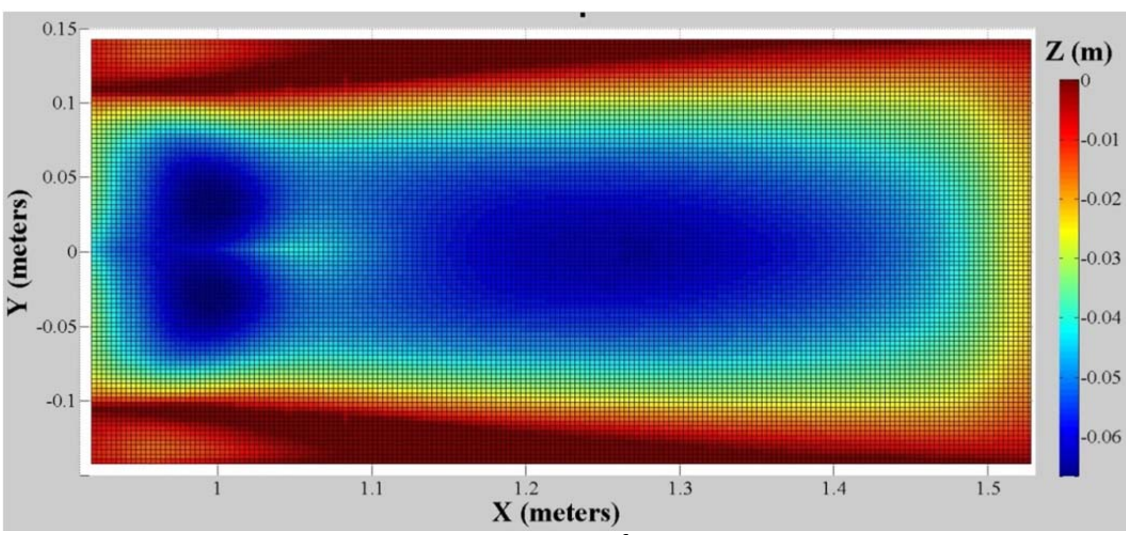

Figure B10: Geometry 9, 6000 cm^3 cumulative bed erosion

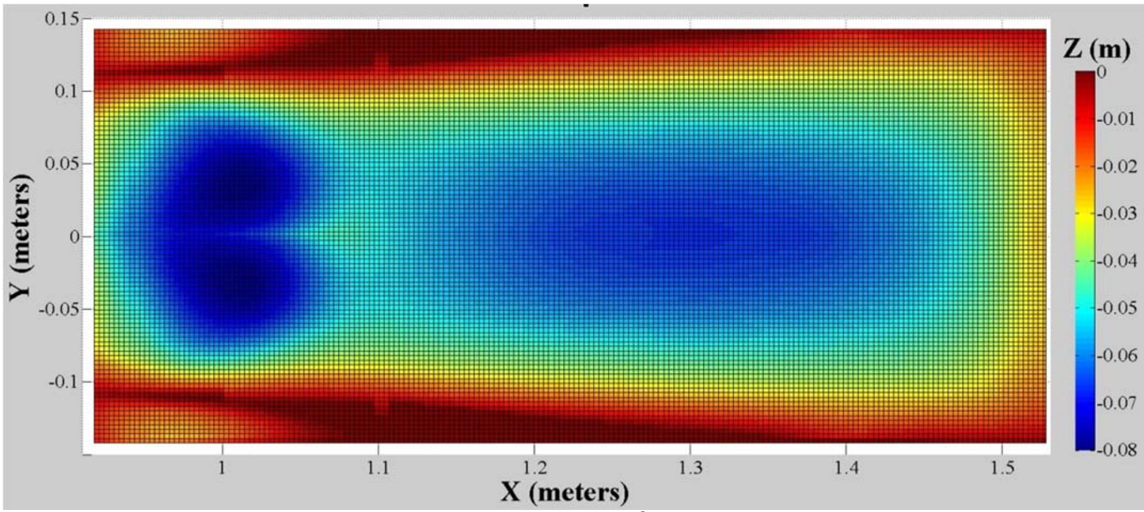

Figure B11: Geometry 10, 7000 cm^3 cumulative bed erosion

For each of the representative bed geometries illustrated in Figures B2 through B11, a range of flows were simulated using the CFD model. In general, the full range of flow rates were simulated for each geometry, even when a particular geometry only occurred in the field under a limited set of flow conditions. The flow rates simulated with the CFD model for Geometry 1 through 5 were as follows, with all values expressed in L/s: 0.3, 0.5, 1.0, 1.5, 1.75, 2.0, 2.5, 3.0, 4.0, 5.0, 6.5, 8.0, 10.0, 11.5. The flow rates simulated with the CFD model for Geometry 6 through 10 were as follows, with all values expressed in L/s: 2.0, 3.0, 4.0, 5.0, 6.0, 7.0, 8.0, 9.0, 10.0, 11.5.

Using the results of the CFD simulations, the variables A_{er} and $(\tau_b - \tau_c)$ can be obtained as a function of the following: Q_{flume}, the bed geometry (as determined by the cumulative bed erosion volume) at the time under consideration, and the determined value of τ_c at the sample site. A single characteristic value of $(\tau_b - \tau_c)$ to represent the distribution is desired. This is calculated as an area-weighted average of the excess shear stress distribution $(\tau_b - \tau_c)$ over the erosion area:

$$(\tau_b - \tau_c)_R = \frac{1}{A_{er}} \int^{EA} (\tau_b - \tau_c)\, dA \qquad \text{(C6)}$$

The subscript "R" indicates the representative value of the excess shear stress distribution within in the erosion area; and "EA" on the integral limit indicates integration only over the portion of the bed where $\tau_b > \tau_c$. The integral in Eq. (C6) is approximated as the summation over the discrete areas represented by the grid cells in the model. Figures B12 and B13 below illustrate values of A_{er} and $(\tau_b - \tau_c)_R$ obtained from the CFD results for [Q_{flume} = 4 L/s and τ_c = 0.14 Pa] and [Q_{flume} = 8 L/s and τ_c = 0.14 Pa], respectively.

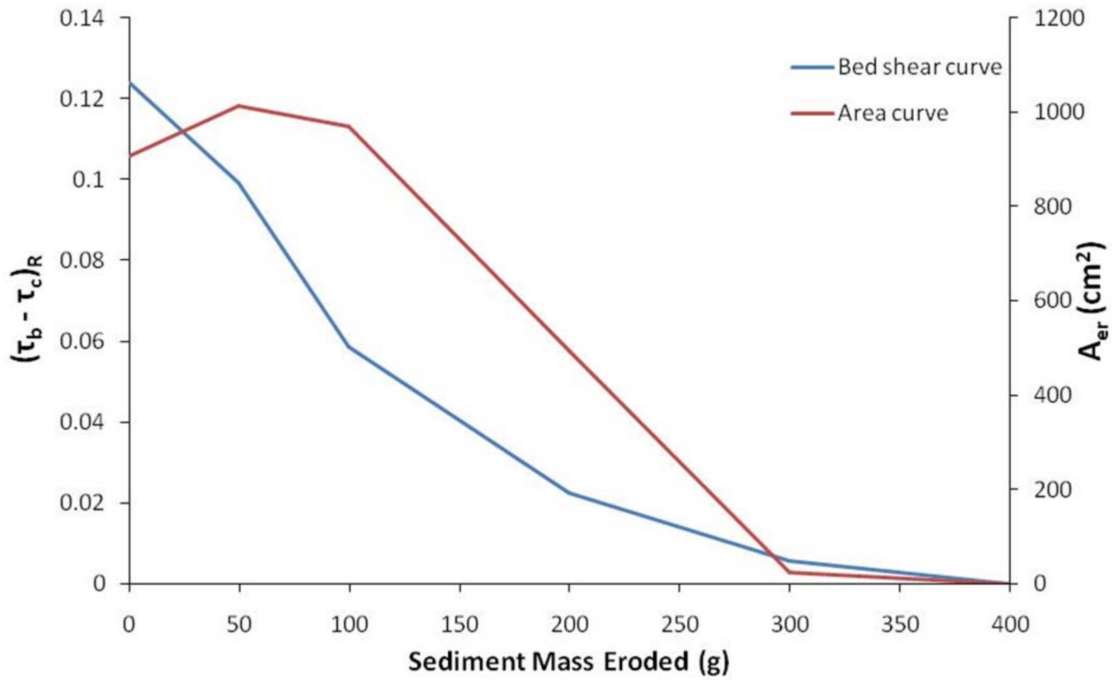

Figure B12: Example illustrating the influence of bed geometry on the bed shear stress field; the example shows the calculated results with Q_{flume} = 4 L/s and τ_c= 0.14 Pa.

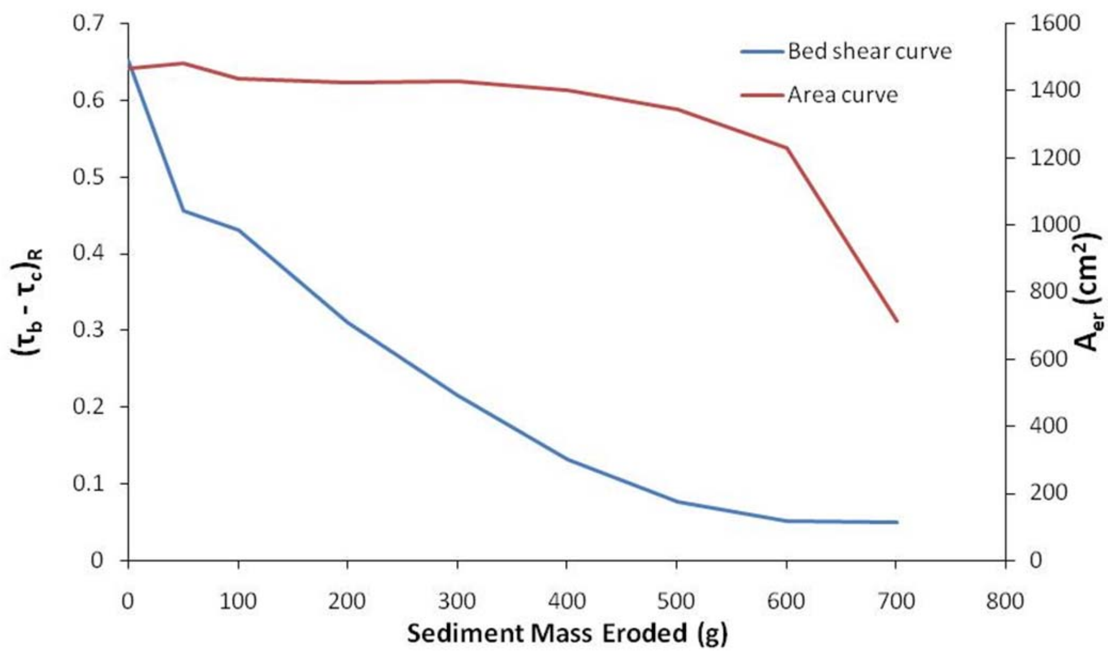

Figure B13: Example illustrating the influence of bed geometry on the bed shear stress field; the example shows the calculated results with Q_{flume} = 8 L/s and τ_c= 0.14 Pa.

The results used to generate the curves illustrated in Figures B12 and B13 can be utilized to determine the appropriate values of A_{er} and $(\tau_b - \tau_c)_R$ at any instant of time during the field experiment as the geometry changes under a single value of Q_{flume}. Per the same logic of obtaining a single value of M_{sed} for a Q_{flume} interval, the analysis also should yield a single value of A_{er} and $(\tau_b - \tau_c)_R$ to relate to the Q_{flume} flow interval. At any instant in time during the test, the cumulative bed erosion volume is known; and it is thus possible to interpolate values of A_{er} and $(\tau_b - \tau_c)_R$ from curves such as Figures B12 and B13. While it would be possible to integrate these values over time to obtain a representative value, for simplicity, the chosen approach is to evaluate the cumulative sediment mass loss exactly half way between the starting condition of the interval and the end condition of the interval. With a value of cumulative mass loss at this half-way position, values of A_{er} and $(\tau_b - \tau_c)_R$ are readily interpolated from the results that yielded Figures B12 and B13.

The curves that form Figures B12 and B13 can be thought of as slices of a three-dimensional surface, where the flow rate Q_{flume} constitutes the third dimension. Each surface is associated with a particular value of τ_c. Therefore a family of three-dimensional surfaces exists associated with the various τ_c values under consideration. The three-dimensional surfaces associated with different values of τ_c are separate but similar, given the narrow range of τ_c observed from the field data. Interpolations along the surfaces were necessary, when for example a Q_{flume} from an experiment did not correspond exactly to a Q_{flume} simulated with the CFD model. In all cases, interpolations along the three-dimensional surfaces were linear interpolations.

Appendix D

Field data in tabular format

Site ID	Q (L/s)	$\tau_{b,R}$ (Pa)	Δt (sec.)	M_{sed} (g)	$\rho_{sed,bulk}$ (g/cm^3)	E (m/s)
2	2	0.0489	475	3.398	0.434	9.55E-08
	2.25	0.0582	355	1.302	0.434	4.90E-08
	2.5	0.0676	420	4.725	0.434	1.50E-07
	2.75	0.0814	420	4.217	0.434	1.34E-07
	3	0.0952	540	14.696	0.434	3.63E-07
	3.25	0.1129	420	10.791	0.434	3.43E-07
	3.5	0.1305	300	8.29	0.434	3.69E-07
	3.85	0.1552	300	7.039	0.434	3.13E-07
	4.2	0.1846	360	25.627	0.434	9.50E-07
	4.55	0.2174	600	9.809	0.434	2.18E-07
	4.9	0.2503	360	11.425	0.434	4.24E-07
	5.25	0.2913	480	15.186	0.434	4.22E-07
	5.75	0.3544	400	26.528	0.434	8.85E-07
3	0.4	0.0045	300	0.304	0.241	2.41E-08
	0.5	0.0061	300	0.686	0.241	5.45E-08
	0.6	0.0080	1200	6.715	0.241	1.33E-07
	0.75	0.0109	480	3.444	0.241	1.71E-07
	0.9	0.0137	420	6.743	0.241	3.82E-07
	1.1	0.0184	420	5.158	0.241	2.93E-07
	1.3	0.0240	720	18.997	0.241	6.28E-07
	1.5	0.0295	480	8.885	0.241	4.41E-07
	1.75	0.0383	540	17.871	0.241	7.88E-07
	2	0.0489	360	13.74	0.241	9.09E-07
	2.35	0.0620	420	28.027	0.241	1.59E-06
	2.7	0.0786	480	26.83	0.241	1.33E-06
	3	0.0952	420	36.099	0.241	2.05E-06
	3.3	0.1164	360	37.066	0.241	2.45E-06
	3.7	0.1446	300	32.668	0.241	2.59E-06
	4.1	0.1752	540	66.472	0.241	2.93E-06
	4.5	0.2127	360	73.9	0.241	4.89E-06
	5	0.2597	300	43.923	0.241	3.49E-06
	5.5	0.3228	300	72.154	0.241	5.73E-06
	6	0.3860	495	89.042	0.241	4.28E-06
4	2	0.0489	480	0.689	0.257	3.21E-08
	2.25	0.0582	720	6.189	0.257	1.92E-07
	2.5	0.0676	840	7.544	0.257	2.01E-07
	2.75	0.0814	360	1.938	0.257	1.20E-07
	3	0.0952	300	1.192	0.257	8.88E-08
	3.4	0.1235	900	19.839	0.257	4.92E-07
	3.8	0.1517	360	3.569	0.257	2.21E-07
	4.25	0.1893	780	19.398	0.257	5.56E-07
	4.75	0.2362	600	16.144	0.257	6.01E-07
	5.25	0.2913	1020	66.181	0.257	1.45E-06
	5.75	0.3544	600	38.489	0.257	1.43E-06
	7	0.5238	1140	132.353	0.257	2.59E-06
	8	0.6731	300	33.96	0.257	2.53E-06
	9	0.8590	420	66.761	0.257	3.55E-06

4	10	1.0448	430	75.046	0.257	3.90E-06
5A	2.25	0.0582	840	4.291	0.321	9.14E-08
	2.75	0.0814	840	13.861	0.321	2.95E-07
	3	0.0952	720	19.652	0.321	4.88E-07
	3.75	0.1482	420	18.326	0.321	7.80E-07
	4.5	0.2127	600	47.7	0.321	1.42E-06
	5.25	0.2913	480	73.799	0.321	2.75E-06
	6	0.3860	420	83.038	0.321	3.54E-06
	7	0.5238	540	107.534	0.321	3.56E-06
	8	0.6731	360	73.601	0.321	3.66E-06
	9	0.8590	300	80.939	0.321	4.83E-06
	10	1.0448	480	132.541	0.321	4.94E-06
	11.5	1.3898	540	141.24	0.321	4.68E-06
5B	2.25	0.0582	180	0.121	0.321	1.20E-08
	2.75	0.0814	540	52.882	0.321	1.75E-06
	3	0.0952	540	25.156	0.321	8.33E-07
	3.75	0.1482	300	4.084	0.321	2.43E-07
	4.5	0.2127	360	7.717	0.321	3.83E-07
	5.25	0.2913	480	17.227	0.321	6.42E-07
	6	0.3860	660	25.767	0.321	6.98E-07
	7	0.5238	600	106.681	0.321	3.18E-06
	8	0.6731	540	174.464	0.321	5.78E-06
	10	1.0448	780	379.312	0.321	8.70E-06
6A	1	0.0156	360	0.112	0.257	6.95E-09
	1.4	0.0267	300	0.684	0.257	5.09E-08
	1.8	0.0404	540	5.113	0.257	2.12E-07
	2.25	0.0582	360	6.694	0.257	4.15E-07
	2.75	0.0814	720	24.19	0.257	7.50E-07
	3.5	0.1305	720	51.787	0.257	1.61E-06
	4.25	0.1893	660	69.761	0.257	2.36E-06
	5	0.2597	420	55.417	0.257	2.95E-06
	6	0.3860	600	72.992	0.257	2.72E-06
	7	0.5238	660	63.935	0.257	2.16E-06
	8	0.6731	660	137.704	0.257	4.66E-06
	9	0.8590	265	104.188	0.257	8.78E-06
6B	1.8	0.040	480	2.575	0.257	1.20E-07
	3	0.095	300	16.485	0.257	1.23E-06
	5	0.260	300	47.424	0.257	3.53E-06
	7	0.524	720	168.013	0.257	5.21E-06
	9	0.859	480	545.195	0.257	2.54E-05
	11	1.275	900	430.464	0.257	1.07E-05